

# Report of the Working Group on Diffractive Physics and Color Coherence

**Conveners:** Michael Albrow<sup>a</sup>, Andrew Brandt<sup>b</sup>, Alfred Mueller<sup>c</sup>, Carl Schmidt<sup>d</sup>

<sup>a</sup>Fermi National Accelerator Laboratory, Batavia, IL, 60510

<sup>b</sup>University of Texas, Arlington, TX 76019

<sup>c</sup>Columbia University, New York, NY 10027

<sup>d</sup>Michigan State University, East Lansing, MI 48824

## INTRODUCTION AND OVERVIEW

1. **Introduction to Diffractive Physics at Run II**, M. Albrow, A. Brandt, A. Mueller, C. Schmidt.

## RUN I HARD DIFFRACTION AND DIFFRACTIVE PARTON DENSITIES

2. **Diffractive parton densities**, K. Goulianos.
3. **CDF results on double diffraction**, M. Convery.
4. **Diffractive dijets at CDF**, K. Hatakeyama.
5. **DØ Rapidity Gap Studies**, A. Brandt.
6. **QCD analysis of the diffractive structure functions measured at HERA and factorisation breaking at Tevatron**, C. Royon.
7. **Diffractive heavy flavor production at CDF**, A. Solodsky.
8. **Diffractively produced charm final states in  $pp$  interactions at 800 GeV/c**, M. Wang.

## CENTRAL RAPIDITY GAPS

9. **Cost of Survival for Large Rapidity Gaps**, E. Levin.
10. **Is BFKL ruled out by the Tevatron gaps between jets data?**, B. Cox.
11. **Interjet Energy and Color Flow**, G. Sterman.
12. **Color Evaporation Induced Rapidity Gaps**, E. Gregores.
13. **Monte Carlo simulation of color singlet exchange between jets**, R. Engel and J. Ranft.

14. **Hard color coherent phenomena**, M. Strikman.

## DOUBLE POMERON PHYSICS

15. **Double Pomeron Physics in Run II**, J. Pumplin.
16. **Higgs and Heavy Quarks Diffractive Production**, E. Levin.
17. **Diffractive Production of Glueballs**, D. Kharzeev.
18. **Glueballs and Exclusive Hadron Production at the Tevatron**, M. Albrow.

## BFKL PHYSICS

19. **A determination of pomeron intercepts at colliders**, R. Peschanski and C. Royon.
20. **BFKL Monte Carlo for Dijet Production at Hadron Colliders**, L. Orr.

## PLANS FOR RUN II

21. **Run 2 plans for hard diffraction studies in CDF**, K. Goulianos.
22. **The DØ Forward Proton Detector**, A. Brandt.

# Introduction to Diffractive Physics at Run II

**Conveners:** Michael Albrow<sup>a</sup>, Andrew Brandt<sup>b</sup>, Alfred Mueller<sup>c</sup>, Carl Schmidt<sup>d</sup>

<sup>a</sup>Fermi National Accelerator Laboratory, Batavia, IL, 60510

<sup>b</sup>University of Texas, Arlington, TX 76019

<sup>c</sup>Columbia University, New York, NY 10027

<sup>d</sup>Michigan State University, East Lansing, MI 48824

## 1. Diffraction

The word “diffraction” covers a rather large class of events at colliders and fixed target machines. The central thread in all the processes one calls diffractive is a rapidity gap (where no particles are produced) which is large enough to guarantee that no flavor or color quantum numbers are exchanged between the colliding particles. Thus, for example at a proton-antiproton collider the reaction  $p + \bar{p} \rightarrow p^* + \bar{p}^*$  is diffractive if the particles (or jets) making up the  $p^*$  and the particles (or jets) making up the  $\bar{p}^*$  are separated by a rapidity gap  $\Delta Y$  which is large enough to guarantee that the flavor and color quantum numbers of  $p^*$  are the same as  $p$  and those of  $\bar{p}^*$  the same as  $\bar{p}$ .  $\Delta Y \geq 3$  is a common criterion for such a gap size. The physics being studied varies considerably according to the type of diffraction and so we separate our discussion into (somewhat arbitrary) categories and attempt to highlight the physics issues in each of these categories. The emphasis here is physics at Fermilab, but there are often complementary reactions at HERA. The contrast and comparison between diffraction at these two colliders yields much more insight than the study of diffraction at either collider in isolation.

## 2. Soft Diffraction

Regge Theory gives a good description of two-body and quasi-two-body reactions, including diffraction, at ISR energies and below. This Regge picture continues to describe total and elastic cross sections through collider energies. However, it is known from studies of elastic and total cross sections of proton-proton and proton-antiproton scattering that the unitarity limit (blackness) has been reached for central impact parameter collisions. It is then somewhat of a mystery why the simple Regge pole picture, a picture only valid far from unitarity limits, works so well for total and elastic scattering. Soft diffraction adds a new piece of

information here. Although the Regge pole picture fits the total and elastic cross sections at collider energies it does not work for diffraction [1,2]. The growth in the diffraction cross section is much less rapid through the collider energy region than predicted by fits at ISR energies and below. This fits nicely with the picture that central collisions are unitarity saturating but become weaker with increasing impact parameter. Let’s see qualitatively how this looks.

A high energy proton is a state having many degrees of freedom which are built out of quarks and gluons. Schematically one may write

$$|\psi_{\text{proton}}\rangle = \sum_i |\psi_i\rangle c_i \quad (1)$$

where  $i$  labels a state in terms of the fundamental degrees of freedom and where  $\sum_i |c_i|^2 = 1$ . From studying elastic and total cross sections we know that  $S(b)|\psi_{\text{proton}}\rangle$  is small when  $b$ , the impact parameter, is small where  $S$  is the S-matrix for elastic reactions. This means that  $S(b)|\psi_i\rangle$  is small at central impact parameters for all  $i$  having non-negligible  $c_i$ . This in turn gives equal inelastic and elastic cross sections because the T-matrix defined by

$$T(b) = i(1 - S(b)) \quad (2)$$

becomes equal to  $i$  at small impact parameters. Diffraction occurs when  $S(b)|\psi_i\rangle$  is zero for some configurations,  $i$ , and far from zero for other configurations. In such a case the “shadow” of the inelastic collisions is not just the proton state but a wide variety of other states as well, that is diffractive states. Below ISR energies the proton is not black at any impact parameter and the shadow of these inelastic events is both elastic scattering and diffractive production. Here Regge theory works well. As one goes through the ISR region and into collider energies, central impact parameter collisions are becoming black and these regions contribute more strongly to elastic scattering

and give much less diffraction than at lower energies. Diffraction comes from those impact parameters where the S-matrix is changing from strong to relatively weak interactions. The Regge picture (pomeron exchange) now does not work because a single pomeron cannot properly describe a region where  $S \approx 0$ . In Regge language one needs multiple pomeron exchange for small impact parameter collisions and this considerably complicates the whole Regge picture and robs it of much of its predictive power.

Thus we qualitatively understand the behavior of the soft diffractive cross section. Attempts to make this explanation more quantitative are hampered by the lack of control over nonperturbative QCD, but there are interesting phenomenological attempts in terms of multiple pomeron exchange [8] (absorption) and a suggestion that the “pomeron flux” may in some sense need to be renormalized as one reaches unitarity limits [1,2].

### 3. Hard Diffraction

We have seen that soft diffraction comes about at impact parameters corresponding to the transition from the region where  $S = 0$  to the region where  $S = 1$ . This should also be the case for hard diffraction at Fermilab, while new elements come into diffraction at HERA, partly because a virtual photon is weakly interacting, and partly because a virtual photon is not quite a “state.”

The motivation for looking at hard diffraction is clear. Unbiased hard interactions probe the parton structure of the proton and tell how many quarks and gluons are in a proton. In hard diffraction one probes the quark and gluon structure of diffraction itself. This is often described in a picturesque language as saying that hard diffraction studies the quark and gluon distribution of the pomeron [2–4] In a typical Fermilab diffractive reaction

$$\text{proton}(p) + \text{antiproton}(\bar{p}) \rightarrow \text{proton}(p') + X$$

with a large rapidity gap between  $p'$  and  $X$  one often pictures the process as  $p \rightarrow p' + \text{pomeron}$  followed by the reaction

$$\text{pomeron}(p - p') + \text{antiproton}(\bar{p}) \rightarrow X.$$

If there are jets in  $X$  then this reaction can be used to study the parton structure of the pomeron and the antiproton in a standard way. This picture is a little suspect because we have already seen that in low impact parameter reaction a single pomeron does not dominate diffractive reactions. Also it is far from clear in what sense a pomeron can be treated as an incoming state. Nevertheless, it is clear that hard diffraction

does study what partons are involved in diffractive reactions, and one may consider the whole description in terms of the structure of the pomeron as simply a picturesque language for describing the quark and gluon structure of diffraction. Similar hard diffraction can be studied at HERA [5] with the reaction

$$\text{proton}(p) + \text{photon}(Q) \rightarrow \text{proton}(p') + X$$

with, again, a rapidity gap between  $p'$  and the particles making up  $X$ .

Comparing hard diffraction at Fermilab and HERA gives a disagreement between the pomeron structure function of about an order of magnitude [3]. This is strong evidence for factorization breaking with HERA distributions much larger than the corresponding Fermilab ones. This result is not unexpected, and the cause is the same as that leading to the slowing of the growth of soft diffraction. Namely the pomeron is not really a universal object. In pomeron language there should be many pomeron exchanges occurring at Fermilab because unitarity bounds are being reached. The hard part of the reaction then does measure properties of this exchange. At HERA the exchange is much simpler because deep inelastic scattering is a point-like probe and it is this probe itself which is one of the scatterers initiating the reaction. Also in deep inelastic scattering one can view the virtual photon as turning into a quark-antiquark pair before the scattering. This quark-antiquark pair then scatters on the proton and both elastic and diffractive scattering of this pair will be counted as diffractive events in deep inelastic scattering. Thus there is no suppression of diffraction of HERA events at central impact parameter in contrast to what happens at Fermilab.

The nature of diffraction at HERA and at Fermilab is fundamentally different. In neither case have theorists been able to frame the discussion in sharp enough terms to make good use of the large amount of data which is already available and that which can be expected in Run II. Thus in the case of Fermilab it is certainly true that hard diffraction tells us something about the partonic structure of diffraction. But, to what extent are we probing the diffraction that occurs in soft processes at Fermilab, and to what extent is the hard process creating or modifying the diffraction? That is, what properties of diffraction are universal? Similar issues hold at HERA where one might say that large  $Q^2$  diffraction is determining a particular event rather than measuring any particular property of a universal quantity, the pomeron.

In fact it may be that the focus on viewing diffractive hard scattering as probing a preexisting object is misleading. In particular another point of view has proved very successful in understanding and correlat-

ing diffraction and small- $x$  structure functions in a low to moderate  $Q^2$  regime at HERA. In this picture one chooses a frame where the virtual photon breaks up into a quark-antiquark pair before the scattering. Then the process is quark-antiquark pair scattering on a proton. If the scattering is inelastic then the process contributes to the inelastic part of  $F_2$ . If the scattering is elastic then the process contributes to the diffractive part of  $F_2$ . Thus, here, hard diffraction is the shadow of inelastic events. A rather simple model proposed by Goelec-Biernat and Wüsthoff incorporates unitarity limits (saturation) for the small- $x$  scattering of moderate spatial-sized quark-antiquark pairs along with the probability that a photon will breakup into a pair of a certain size. This model comfortably describes moderate  $Q^2$  deep inelastic scattering,  $F_2$ , and diffraction in a semiquantitative way which matches well with theoretical ideas of saturation and dense gluon systems. It is a great challenge to theorists to invent a comparably well-motivated model to deal with hard diffraction at Fermilab.

#### 4. Rapidity Gaps Between Jets

There is a special class of diffractive events which have been pioneered at Fermilab in which one looks for events with a sizeable rapidity gap and where there is a hard jet on either side of the gap. For a gap size  $\Delta Y \geq 3$  such events constitute about 1% of all two-jet events at Fermilab and about 10% of all two-jet events at HERA.

There is a good QCD motivation for studying such events. The basic hard process is elastic quark-antiquark (or gluon-gluon) scattering at large momentum transfer and at large rapidity. This seems a good place to measure the BFKL pomeron. However, for the rapidity gap to be present it is also necessary that the spectator parts of the colliding proton and antiproton not produce particles in the rapidity gap. The probability that the latter happens is called the “survival probability” of the gap and is estimated to be about 10% at Fermilab [8]. From the BFKL pomeron point of view the most unfortunate part of the data is the fact that the percentage of gap events decreases when one goes from a center of mass energy of 630 GeV to 1800 GeV. At Fermilab the 1800 GeV runs should be predominately gluon jets while at 630 GeV quarks should dominate the hard scattering. The BFKL contribution (at comparable rapidity gaps) to the gap fraction should be enhanced for hard gluon scattering by a factor of  $(\frac{N_c}{C_F})^2 = (\frac{9}{4})^2$  as compared to hard quark scattering. Thus we might expect the gap fraction to grow as one goes from 630 GeV to 1800 GeV while in fact the gap fraction decreases by a factor of 2.

What has gone wrong [9]? The most likely problem is that the survival probability also has an energy dependence [8] and that the survival probability is decreasing between 630 and 1800 GeV. It may be that there are still important contributions from secondary trajectories and that the BFKL pomeron is not dominating the hard scattering. Oderda and Sterman [10] have a variant on rapidity gaps where one requires less than a certain amount of transverse energy be emitted in the gap. This allows the QCD calculation, including color non-singlet exchanges, to be done reliably, but it does not eliminate the difficult survival probability questions. It would be interesting to analyze the data in the Oderda-Sterman way to see if the survival probabilities become significantly larger, and even more importantly, to see if the survival probability becomes energy independent.

There is a very simple picture, the “color evaporation” picture, which qualitatively describes the data [11,12]. Here one takes the hard scattering scattering to be given by a single hard gluon exchange. For example in  $p + \bar{p} \rightarrow QX + \bar{Q}Y$  one views the  $X$  as the remnant of  $p$  after the quark  $Q$  is taken out and  $Y$  the remnant of  $\bar{p}$  after  $\bar{Q}$  is taken out.  $Q$  and  $\bar{Q}$  are the (in this case quark) jets being measured. Thus  $X$  is a  $\mathfrak{3} \times \mathfrak{3}$  representation of color  $SU(3)$  while  $Q$ ,  $\bar{Q}$ , and  $Y$  are  $\mathfrak{3}$ ,  $\mathfrak{3}^*$ , and  $\mathfrak{3}^* \times \mathfrak{3}^*$  representations respectively. The final state color singlet structure is then formed just by counting the ways in which the color representations can be combined into singlets. For example,  $Q$  and  $X$  have 27 different color states of which only one of them is a singlet. It is necessary to take this singlet in order to have a color singlet state on one side of the rapidity gap. These simple counting rules give reasonable numbers for the gap fractions and predict a decreasing gap fraction as one goes from 630 GeV to 1800 GeV because of the color counting change when  $Q$  and  $\bar{Q}$  are replaced by gluons.

The color evaporation model is an interesting picture and may be a good hint about how the dynamics is working. However, without a stronger underlying QCD framework it will remain an intriguing curiosity. It is an important challenge to see if a QCD dynamical framework can be developed which leads to something like the color evaporation model.

#### 5. BFKL Searches

There has been an important activity at Fermilab, at HERA and at LEP trying to measure the BFKL pomeron intercept. In the Fermilab analysis the reaction is

$$\text{proton}(p) + \text{antiproton}(\bar{p}) \rightarrow \text{jet}(k_1) + \text{jet}(k_2) + X$$

where  $k_{1\perp}$  and  $k_{2\perp}$  are greater than 20 GeV, and where  $k_1/p = x_1$  and  $k_2/\bar{p} = x_2$  are fixed to be the same at 630 and 1800 GeV. If one takes the ratio

$$R = \frac{\sigma_{2jet}(1800)}{\sigma_{2jet}(630)}$$

then BFKL predicts

$$R = \sqrt{\frac{\Delta Y(630)}{\Delta Y(1800)}} \exp\{(\alpha_P - 1)[\Delta Y(1800) - \Delta Y(630)]\}.$$

$\Delta Y$  is the rapidity interval between the two jets, but this is a purely inclusive measurement so there are no survival probability worries. At HERA one of the jets is replaced by the virtual photon and a similar formula holds. At LEP one simply measures the energy dependence of virtual photon-virtual photon scattering. Each of the accelerators have strong and weak points. The LEP analysis is certainly the cleanest, but so far there is a marginal amount of data. The Fermilab DØ experiment has very robust jets but  $\Delta Y(630)$  is only about 2.4 and one may worry that this is not yet large enough for BFKL dominance. At HERA the jets have a rather small  $k_{\perp}$  and the worry is that the jet cross section has not been properly identified.

Perhaps the surprising result [18] is that both Fermilab and HERA suggest that  $\alpha_P$  is near 1.5, close to the leading order BFKL calculation. The present theoretical prejudice is that  $\alpha_P$  will likely turn out to be nearer 1.25-1.3 when, and if, the dust settles over attempts to give a reliable answer for the higher order corrections. What is perhaps even more striking is that the BFKL evolution seems to be so prominent in this inclusive reaction while it appears to be completely masked by other effects in the more exclusive rapidity gap analysis.

Monte Carlo calculations [19] incorporating BFKL evolution suggest that BFKL effects should be suppressed by various kinematic and non-asymptotic effects. Is there another explanation of the strong small  $x$  growth seen in the Fermilab dijet data and the HERA forward jet data, or are the Monte Carlos over-compensating non-leading factors as perhaps the next-to-leading analytic calculations are doing? Much remains to be understood.

## 6. Run II Diffraction Prospects

Improved understanding of this new field of hard diffraction, requires new detectors for tagging and measuring scattered protons. In Ref [3], new results from a short data taking period with the CDF Roman pot spectrometer, show some of the possibilities of this new sub-detector. In Run II, this detector will be available for the whole run, and will be more fully exploited.

The CDF Run II plans, including addition of new forward calorimeters and gap veto counters are outlined in Ref. [20].

DØ is in the process of installing a new Forward Proton Detector (FPD) (see Ref. [21]). This sub-detector consists of nine independent spectrometers which will maximize the acceptance for scattered protons *and* anti-protons. The FPD will be fully integrated into the DØ triggering and data acquisition systems and will provide unprecedented samples of hard diffractive events of all types.

Double pomeron exchange is the most intriguing process that can be studied with these new detectors [14], and there were many talks on this subject at the workshop [22]. In this process both the incoming proton and anti-proton are scattered but remain intact, and a massive central system may be produced. At the Tevatron objects with a mass of more than 100 GeV could be produced. With both arms instrumented it would be possible to measure both the proton and anti-proton using the FPD, and jets (for example) using the central calorimeter. This allows the kinematics of the event to be fully determined.

In addition, CDF can expand on its “gap+track” double pomeron results in Run I, where they tag an anti-proton and a gap. Although, these events are not gold-plated like the DØ double-tagged events, the acceptance penalty of tagging with both proton and anti-proton is avoided, and are thus the data sample is larger. DØ, of course can study both types of events, and combine the results to gain a deeper understanding of this process. Both collaborations will also be able to exploit double gap events as done by DØ in Run I [4], which will be especially valuable for rare events.

Measurement of hard double pomeron exchange would help determine the pomeron structure and provide unique information on the pomeron flux. Double pomeron exchange would have a normalization proportional to the square of the flux factor, unlike other hard diffractive processes. In addition, this process has been proposed as a trigger for Higgs production at the LHC, with optimistic assumptions [15], it might be possible to observe a handful of Higgs events via this mechanism during Tevatron Run II [17]. While this may be unlikely, these would be spectacular events with only the decay products of the Higgs in the central detector, and a proton and an anti-proton in the forward pot spectrometers. In any case, knowledge gained at the Tevatron would indicate if this approach is worth pursuing at the LHC.

Double pomeron interactions are also an ideal place to look for glueball production (bound states of gluons) and states with exotic quantum numbers, and the clean event topologies would make them easier to detect [14,

16,17].

In conclusion, the Run II outlook for hard diffraction and related topics appears to be quite bright and will require the best efforts of the experimental collaborations along with a recently invigorated theoretical community to finally unravel the mysterious pomeron.

## REFERENCES

1. M. Convery, "CDF results on double diffraction".
2. K. Goulianos, "Diffractive parton densities".
3. K. Hatakeyama, "Diffractive dijets at CDF".
4. A. Brandt, "DØ Rapidity Gap Studies".
5. C. Royon, "QCD analysis of the diffractive structure functions measured at HERA and factorization breaking at Tevatron".
6. A. Solodsky, "Diffractive heavy flavor production at CDF".
7. M. Wang, "Diffractively produced charm final states in pp interactions at 800 GeV/c".
8. E. Levin, "Cost of Survival for Large Rapidity Gaps".
9. B. Cox, "Is BFKL ruled out by the Tevatron gaps between jets data?".
10. G. Sterman, "Interjet Energy and Color Flow".
11. E. Gregores, "Color Evaporation Induced Rapidity Gaps".
12. R. Engel and J. Ranft, "Monte Carlo simulation of color singlet exchange between jets".
13. M. Strikman, "Hard color coherent phenomena".
14. J. Pumplin, "Double Pomeron Physics in Run II".
15. E. Levin, "Higgs and Heavy Quarks Diffractive Production".
16. D. Kharzeev, "Diffractive Production of Glueballs".
17. M. Albrow, "Glueballs and Exclusive Hadron Production at the Tevatron".
18. R. Peschanski and C. Royon, "A determination of pomeron intercepts at colliders".
19. L. Orr, "BFKL Monte Carlo for Dijet Production at Hadron Colliders".
20. K. Goulianos, "Run 2 plans for hard diffraction studies in CDF".
21. A. Brandt, "The DØ Forward Proton Detector".
22. Working Group VI Web page,  
<http://www.pa.msu.edu/~schmidt/soft.html>.

# Diffractive Parton Densities

K. GOULIANOS, The Rockefeller University, 1230 York Avenue, New York, NY 10021, USA.

We present a phenomenological model of hard diffraction in which the structure of the Pomeron is derived from the structure of the parent hadron. Predictions for diffractive deep inelastic scattering are compared with data.

The inclusive and diffractive deep inelastic scattering (DIS) cross sections are proportional to the corresponding  $F_2$  structure functions of the proton,

$$\begin{aligned} \text{Inclusive DIS} & \quad \frac{d^2\sigma}{dx dQ^2} \propto \frac{F_2^h(x, Q^2)}{x} \\ \text{Diffractive DIS} & \quad \frac{d^3\sigma}{d\xi dx dQ^2} \propto \frac{F_2^{D(3)}(\xi, x, Q^2)}{x} \end{aligned} \quad \text{where}$$

$h$  and  $D(3)$  indicate, respectively, a *hard* structure function (at scale  $Q^2$ ) and a 3-variable diffractive structure function (integrated over  $t$ ). The latter depends not only on the hard scale  $Q^2$ , but also on the *soft* scale,  $\langle M_T \rangle \sim 1$  GeV, which is the relevant scale for the formation of the gap.

The only marker of the rapidity gap is the variable  $\xi$ . We therefore postulate that the rapidity gap probability is proportional to the *soft* parton density at  $\xi$  and write the DDIS (diffractive DIS) cross section as

$$\frac{d^3\sigma}{d\xi dx dQ^2} \propto \frac{F_2^h(x, Q^2)}{x} \times \frac{F_2^s(\xi)}{\xi} \otimes \xi\text{-norm}$$

where the symbolic notation “ $\otimes \xi$ -norm” is used to indicate that the  $\xi$  probability is normalized. Since  $x = \beta\xi$ , the normalization over all available  $\xi$  values involves not only  $F_2^s$  but also  $F_2^h$ , breaking down factorization. It is therefore prudent to write the DDIS cross section in terms of  $\beta$  instead of  $x$ , so that the dependence of  $F_2^h$  on  $\xi$  is shown explicitly:

$$\frac{d^3\sigma}{d\xi d\beta dQ^2} \propto \frac{1}{\beta} \left[ F_2^h(\beta\xi, Q^2) \times \frac{F_2^s(\xi)}{\xi} \otimes \xi\text{-norm} \right]$$

The term in the brackets represents the DDIS structure function  $F_2^{D(3)}(\xi, \beta, Q^2)$ .

In the next step, we seek guidance from the scaling behavior of the soft single-diffractive (sd) differential cross section [1,2],

$$\frac{d\sigma_{sd}}{dM^2} \propto \frac{1}{(M^2)^{1+\epsilon}} \quad (\text{no } s\text{-dependence!})$$

which in terms of  $\xi$  takes the form

$$\frac{d\sigma_{sd}}{d\xi} \propto \underbrace{\frac{1}{s^{2\epsilon}} \frac{1}{\xi^{1+2\epsilon}}}_{\text{gap probability}} \times (s')^\epsilon$$

where  $s' \equiv M^2$  is the  $s$ -value of the diffractive sub-system. Noting that  $\xi$  is related to the associated rapidity gap by  $\Delta Y = \ln \frac{1}{\xi}$ , and that the integral  $\int_{(s_0/s)}^1 \frac{1}{s^{2\epsilon}} \frac{d\xi}{\xi^{1+2\epsilon}} = \text{constant}$ , the above equation may be viewed as representing the product of the total cross section at the sub-system energy multiplied by a *normalized* rapidity gap probability. In analogy with this experimentally established behavior, we factorize  $F_2^{D(3)}(\xi, \beta, Q^2)$  into  $F_2^h(\beta, Q^2)$ , the sub-energy DIS cross section, times a normalized gap probability:

$$F_2^{D(3)}(\xi, \beta, Q^2) = P_{gap}(\xi, \beta, Q^2) \times F_2^h(\beta, Q^2)$$

The gap probability is therefore given by

$$P_{gap}(\xi, \beta, Q^2) = F_2^h(\beta\xi, Q^2) \times \frac{F_2^s(\xi)}{\xi} \times N(s, \beta, Q^2)$$

The normalization factor,  $N(s, \beta, Q^2)$ , is obtained from the following equation, using  $\xi_{min} = Q^2/s$ ,

$$N^{-1}(s, \beta, Q^2) = \frac{1}{f_q} \int_{\xi_{min}}^1 F_2^h(\beta\xi, Q^2) \times \frac{F_2^s(\xi)}{\xi} d\xi$$

$f_q$  is the quark fraction of the hard structure and is used here because only quarks participate in DIS.

At small  $x$  ( $\leq \sim 0.1$ ), the structure functions  $F_2^h$  and  $F_2^s$  are represented well by the power law expressions [3]  $F_2^h(x, Q^2) = A^h/x^{\lambda_h(Q^2)}$  and  $F_2^s(\xi) = A^s/\xi^{\lambda_s}$ . Using these forms we obtain

$$N^{-1}(s, \beta, Q^2) = \frac{1}{f_q} \left[ \frac{A^h}{\beta^{\lambda_h}} \frac{A^s}{\lambda_h + \lambda_s} \left( \frac{\beta s}{Q^2} \right)^{\lambda_h + \lambda_s} \right]$$

$$F_2^{D(3)}(\xi, \beta, Q^2) = \frac{1}{\xi^{1+\lambda_h+\lambda_s}} \times f_q(\lambda_h + \lambda_s) \left( \frac{Q^2}{\beta s} \right)^{\lambda_h + \lambda_s} \times \frac{A^h}{\beta^{\lambda_h}}$$

Since in DDIS  $x$  is always smaller than  $\xi$ , the above form of  $F_2^{D(3)}$ , derived for small  $x$ , should be valid for all  $x$  when  $\xi$  is small; it should also be valid for all  $\beta (= x/\xi)$ . We therefore expect  $F_2^{D(3)}$  to have the following  $\xi$  and  $\beta$  dependence at small  $\xi$ :

$$F_2^{D(3)}(\xi, \beta, Q^2)|_{\beta, Q^2} \propto \frac{1}{\xi^{1+n}} \quad n = \lambda_h(Q^2) + \lambda_s$$

$$F_2^{D(3)}(\xi, \beta, Q^2)|_{\xi, Q^2} \propto \frac{1}{\beta^m} \quad m = 2\lambda_h(Q^2) + \lambda_s$$

The HERA (non-diffractive) DIS measurements [3] yield  $\lambda_s \approx 0.1$ , which is in agreement with the value of  $\epsilon = \alpha(0) - 1 = 0.104$  [4], where  $\alpha(0)$  is the intercept of the Pomeron trajectory at  $t=0$ . In the  $Q^2$  range of 10-50  $\text{GeV}^2$ , where the DDIS data are concentrated, these measurements yield  $\lambda_h \approx 0.3$ . Using these values we obtain  $n = 0.4$  and  $m = 0.7$ . We therefore expect

$$\text{Prediction: } F_2^{D(3)} \propto \frac{1}{\xi^{1.4}} \times \frac{1}{\beta^{0.7}}$$

We observe the following features:

### Factorization

Our prediction exhibits factorization between  $\xi$  and  $\beta$ , in agreement with HERA results at small  $\xi$ .

### $\xi$ -dependence

In the Regge framework, the  $\xi$ -dependence of  $F_2^{D(3)}$  is expected to have the ‘‘Pomeron flux’’ form  $\sim 1/\xi^{1+n}$  with  $n = 2\epsilon = 0.2$ , independent of  $Q^2$ . In the  $Q^2$  range of 10-50  $\text{GeV}^2$ , the HERA experiments find that  $n$  is  $\approx 0.4$  and has a small  $Q^2$  dependence, in agreement with our prediction of  $n = \lambda_h(Q^2) + \lambda_s$ .

### $\beta$ -dependence

The predicted form  $1/\beta^m$  for  $F_2^{D(3)}$  is valid in the region of (fixed) small  $\xi$  and high  $Q^2$ , where the  $x$ -distribution of  $F_2(x, Q^2)$  has the form  $A^h/x^{\lambda_h(Q^2)}$ . As there are no data points at strictly fixed  $\xi$ , we have selected the following set of five points at  $Q^2 = 45 \text{ GeV}^2$  and  $\xi \approx 0.01$  from Ref. [5] with which to compare the measured values of  $F_2^{D(3)}$  with our prediction:

$\beta$	$x$	$\xi = x/\beta$	$\xi \cdot F_2^{D(3)} \pm \text{stat} \pm \text{syst}$
0.10	0.00133	0.0133	$0.0384 \pm 0.0066 \pm 0.0030$
0.20	0.00237	0.0118	$0.0406 \pm 0.0061 \pm 0.0026$
0.40	0.00421	0.0105	$0.0215 \pm 0.0046 \pm 0.0016$
0.65	0.00750	0.0115	$0.0240 \pm 0.0054 \pm 0.0026$
0.90	0.00750	0.0083	$0.0088 \pm 0.0041 \pm 0.0005$

The following parameters are used in the calculation of  $F_2^{D(3)}$ :  $\sqrt{s} = 280 \text{ GeV}$ ,  $\xi = 0.01$ ,  $Q^2 = 45 \text{ GeV}^2$ ,  $\lambda_s = 0.1$ ,  $\lambda_h = 0.3$ ,  $f_q = 0.4$  [7], and  $A^h = 0.2$ ; the latter was evaluated from  $F_2(Q^2 = 50, x = 0.00133) = 1.46$  [6] assuming a  $\frac{A^h}{x^{0.3}}$  dependence. In figure 1, our prediction for  $\xi \cdot F_2^{D(3)}(\beta)$  versus  $\beta$  is compared with the data. The observed agreement both in shape and normalization is satisfactory, particularly since no free parameters are used in the calculation.

## REFERENCES

1. K. Goulianos, Phys. Lett. **B358**, 379 (1995); **B363**, 268 (1995).

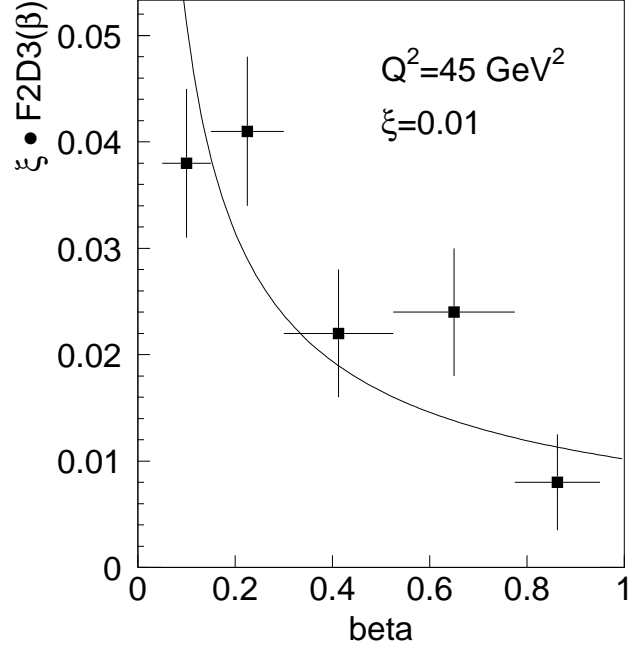


Figure 1. Predicted  $\beta$  dependence of  $\xi \times F_2^{D(3)}(\xi, \beta, Q^2)$  for  $\xi = 0.01$  and  $Q^2 = 45 \text{ GeV}^2$  (solid curve) compared with measured values (points) obtained from Ref. [5]

2. K. Goulianos and J. Montanha, Phys. Rev. **D 59**, 114017 (1999).
3. ZEUS Collaboration, *ZEUS Results on the Measurement and Phenomenology of  $F_2$  at Low  $x$  and Low  $Q^2$*  (Fig. 7), contribution to ICHEP98, Vancouver, Canada.
4. R.J.M. Covolan, J. Montanha and K. Goulianos, Phys. Lett. **B 389**, 176 (1996).
5. C. Adloff *et al.*, H1 Collaboration, Z. Phys. **C 76**, 613 (1997).
6. T. Ahmed *et al.*, H1 Collaboration, Nuc. Phys. **B 439**, 471 (1995).
7. T. Affolder *et al.*, CDF Collaboration, *Observation of Diffractive Beauty Production at the Fermilab Tevatron*, to be published in Phys. Rev. Letters.

# CDF Results on Double Diffraction

M. E. Convery <sup>a</sup>

<sup>a</sup>The Rockefeller University, 1230 York Avenue, New York, NY 10021, USA

The double-diffractive cross section is measured for  $\bar{p}p$  interactions which produce a central rapidity gap with width  $\Delta\eta > 3$  at  $\sqrt{s} = 1800$  and 630 GeV. Comparisons are made to predictions from Regge theory based on the triple Pomeron amplitude and factorization and to previous measurements.

Double-diffractive (DD) events are characterized by the exchange of a color singlet with the quantum numbers of the vacuum, the Pomeron, causing both incident hadrons to dissociate. The dissociated hadrons produce diffractive mass clusters along their initial direction, while, since the exchanged object does not radiate as, for example, a colored object would, the region in between the clusters is empty of particles.

Hard double diffraction (Fig. 1a) has previously been studied in events with rapidity gaps between jets. The fraction of dijet events with  $1.8 < |\eta^{jet1,jet2}| < 3.5$ ,  $\eta^{jet1}\eta^{jet2} < 0$ , and  $E_T^{jet1,jet2} > 20$  GeV at  $\sqrt{s} = 1800$  GeV due to color singlet exchange (CSE) was found to be [1]

$$R_{JJ}(1800) = [1.13 \pm 0.12(stat) \pm 0.11(syst)]\%,$$

and for jets with  $E_T^{jet1,jet2} > 8$  GeV at  $\sqrt{s} = 630$  GeV [2]

$$R_{JJ}(630) = [2.7 \pm 0.7(stat) \pm 0.6(syst)]\%,$$

so that the CSE fraction at 630 GeV is greater than that at 1800 GeV by a factor of

$$R(630)/R(1800) = 2.4 \pm 0.7(stat) \pm 0.6(syst).$$

The distribution of the CSE fraction as a function of the rapidity separation between the jets was seen to drop as the jets reached the edges of the acceptance. No dependence was observed of the CSE fraction on mean dijet  $E_T$  or on jet  $x$ , determined from the  $E_T$  and  $\eta$  of the jets as  $x_i = e^{|\eta_i|} E_T^i / \sqrt{s}$ .

We have studied soft double diffraction (Fig. 1b) by looking for central rapidity gaps in minimum-bias events which have hits in the Beam-Beam Counters (BBC's). We looked for gaps which overlap  $\eta = 0$  rather than the largest gap anywhere in the detector because the latter method is more likely to be biased by inefficiencies in the calorimeters. The  $\eta$  of the track or calorimeter tower above a given threshold with the smallest  $|\eta|$  for  $\eta > 0$  ( $\eta < 0$ ) is defined to be  $\eta_{max(min)}$ . Events with the lowest- $|\eta|$  particle in the BBC,  $3.2 < |\eta| < 5.9$ , are assigned  $|\eta_{max(min)}| \equiv 3.3$ . The data

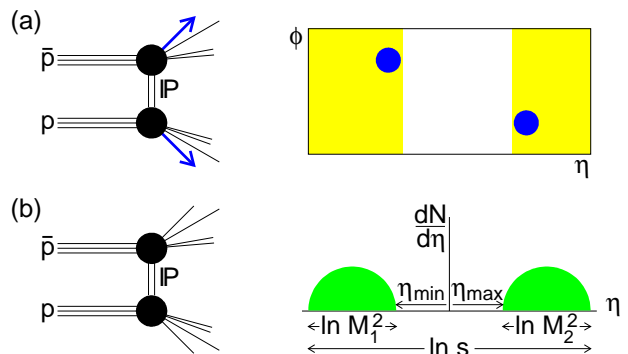


Figure 1. A double-diffractive interaction in which a Pomeron ( $IP$ ) is exchanged in a  $\bar{p}p$  collision at center-of-mass energy  $\sqrt{s}$ , (a) with a hard scattering producing jets on opposite sides of a rapidity gap, and (b) producing diffractive masses  $M_1$  and  $M_2$  separated by a rapidity gap of width  $\eta_{max} - \eta_{min}$ .

are compared to non-diffractive (ND), single-diffractive (SD), and DD Monte Carlo (MC) simulated events as a function of  $\eta_{max}$  and  $-\eta_{min}$  (not shown). Structure due to different thresholds and efficiencies in the calorimeter is visible, e.g., at the interface between the plug and forward calorimeters at  $\eta \sim 2.4$ .

Figure 2 shows histograms of the data and MC as a function of  $\Delta\eta^0 = \eta_{max} - \eta_{min}$ . The SD contribution is fixed by known cross sections and the fraction of events passing the BBC trigger in the MC. The ND and DD contributions are determined as follows. The DD and non-DD MC distributions are normalized to give the number of events observed in the data in the region  $\Delta\eta^0 < 0.8$  (dominantly ND) and  $\Delta\eta^0 > 3$  (dominantly DD). The DD MC uses the differential cross sections from Regge theory based on the triple Pomeron amplitude and factorization. The agreement between data and MC seen in Fig. 2 shows that Regge theory appears to correctly predict the mass dependence, as was also observed by the H1 collaboration [3]. Note that the fluctuations in the  $\Delta\eta^0$  distribution are due to structure in the calorimeter and are followed closely

by the MC because of careful calibrations derived to match MC particle  $p_T$ 's to observed calorimeter  $E_T$ 's.

We find cross sections at  $\sqrt{s} = 1800$  (630) GeV by measuring  $\sigma_{DD}\mathcal{A}$ , where  $\mathcal{A}$  is the detector acceptance for triggering on diffractive mass clusters. Preliminary calculations from MC yield  $\mathcal{A} = (48.7 \pm 8.4)\%$  [(61.4  $\pm$  6.8)%], and

$$\sigma_{DD}(\sqrt{s} = 1800 \text{ GeV}, \Delta\eta^0 \geq 3) = 4.71 \pm 0.02(\text{stat})_{-0.90}^{+0.92}(\text{syst}) \text{ mb},$$

$$\sigma_{DD}(\sqrt{s} = 630 \text{ GeV}, \Delta\eta^0 \geq 3) = 4.32 \pm 0.01(\text{stat})_{-0.76}^{+0.54}(\text{syst}) \text{ mb}.$$

The cross sections for all gaps of width  $\Delta y > 2.3$ , corresponding to the SD coherence limit of  $\xi < 0.1$ , can be obtained by extrapolation using the differential cross section shape from Regge theory, and are greater by a factor of 1.72 (1.67) at  $\sqrt{s} = 1800$  (630) GeV. The resulting cross sections are shown in Fig. 3 along with results from UA5 [4] and other cross sections at lower energies [5,6], most of which were derived from exclusive measurements using factorization relations. The DD cross sections measured by CDF are an order of magnitude smaller than what is predicted using Regge theory, but are in general agreement with the renormalized gap model [7],

The improved plug calorimeters and proposed mini-plug detectors for CDF in Run II will allow a better measurement of the DD cross section and hard DD dijet production, including better resolution of gaps and jets out to  $\eta \approx 5.5$ .

## REFERENCES

1. F. Abe *et al.*, (CDF Collaboration), Phys. Rev. Lett. **80**, 1156 (1998).
2. F. Abe *et al.*, (CDF Collaboration), Phys. Rev. Lett. **81**, 5278 (1998).
3. C. Adloff *et al.*, (H1 Collaboration), Z. Phys. C **74**, 221 (1997).
4. R. E. Ansorge *et al.*, (UA5 Collaboration), Z. Phys. C **33**, 175 (1986).
5. C. Conta *et al.*, Nucl. Phys. B **175**, 97 (1980).
6. A. Givernaud *et al.*, Nucl. Phys. B **152**, 189 (1979) and references therein.
7. K. Goulios, Phys. Lett. B **358**, 379 (1995).

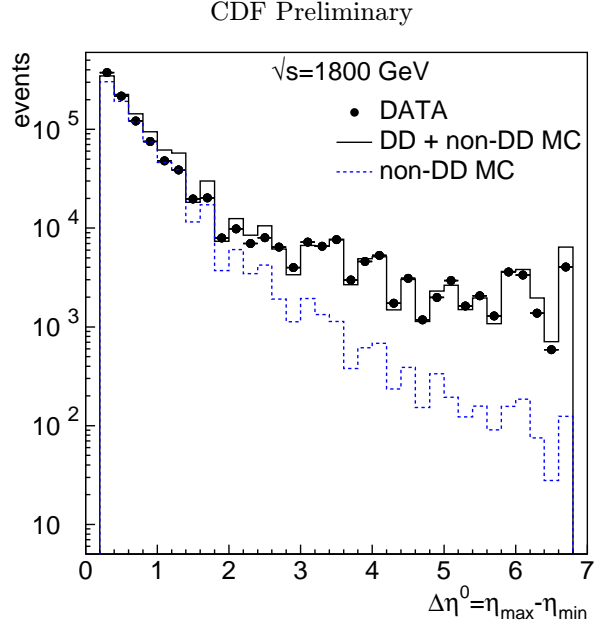


Figure 2. The number of events as a function of  $\Delta\eta^0 = \eta_{max} - \eta_{min}$  for 1800 GeV data, and for DD + non-DD and only non-DD MC-generated events.

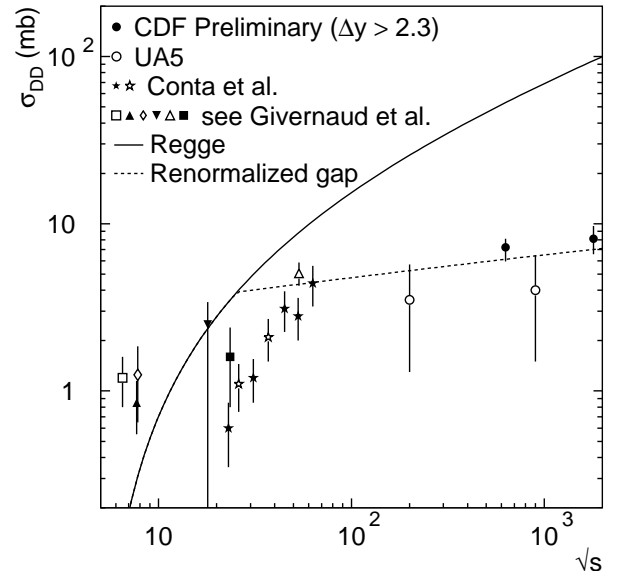


Figure 3. The total DD cross section versus  $\sqrt{s}$  compared with predictions from standard Regge theory based on the triple-Pomeron amplitude and factorization (dashed curve) and from the renormalized gap model (solid curve).

# Diffractive Dijets at CDF

Ken-ichi Hatakeyama<sup>a</sup>

<sup>a</sup>The Rockefeller University, 1230 York Avenue, New York, NY 10021, USA

We report results obtained from a study of Roman Pot triggered events with a leading antiproton of beam momentum fraction  $0.905 < x_F < 0.975$  and 4-momentum transfer squared  $|t| < 3 \text{ GeV}^2$ , produced in  $\bar{p}p$  collisions at  $\sqrt{s} = 1800 \text{ GeV}$ . Using events which contain two jets with transverse energy  $E_T^{jet} > 7 \text{ GeV}$ , the diffractive structure function of the antiproton is evaluated and compared with expectations based on results obtained at HERA.

We have studied diffractive dijet events produced in  $\bar{p}p$  collisions, which are characterized by two jets with high transverse energy and a leading (anti)proton accompanied by a rapidity gap. The rapidity gap, defined as a region of pseudorapidity devoid of particles, is associated with the exchange of a Pomeron ( $\mathbb{P}$ ), which is a color-singlet state with vacuum quantum numbers. In this framework, diffractive dijet events produced in  $\bar{p}p$  collisions can be expressed as,  $\bar{p} + p \rightarrow [\bar{p}' + \mathbb{P}] + p \rightarrow \bar{p}' + \text{Jet}_1 + \text{Jet}_2 + X$ .

Previously, the CDF collaboration studied diffractive  $W$ -boson, dijet and  $b\bar{b}$  productions [1,2]. In these analyses, diffractive production is tagged by the requirement of a forward rapidity gap. The observed rates of diffractive  $W$ -boson, dijet and  $b\bar{b}$  productions were found to be significantly lower than predictions based on factorization, while such models describe well the diffractive DIS and photoproduction data obtained at HERA [3,4]. The breakdown of factorization observed in the rate comparisons raises the question of whether the  $\beta$ -distribution is also process dependent, where  $\beta$  is the momentum fraction of the struck parton in the Pomeron. In this analysis, we measure the diffractive structure function of the antiproton, and compare it with expectations based on the diffractive parton densities obtained in diffractive DIS experiments at HERA [4].

The diffractive data used in this analysis were collected by triggering an antiproton detected in three Roman Pot (RP) spectrometers. The beam momentum fraction  $x_F = 1 - \xi$  and the four momentum squared  $t$  of the detected antiproton were reconstructed from the  $X$ - $Y$  RP track position, the position of the event vertex, and the machine transport matrix. The non-diffractive (ND) data were collected with a minimum bias (MB) trigger which required a coincidence of hits on two beam-beam counters (BBC). From these two data samples, we select diffractive and ND dijet events with two jets of  $E_T > 7 \text{ GeV}$ .

Figs. 1(a) and 1(b) show the RP acceptance and a logo plot of the inclusive diffractive event sample as a

function of  $\xi$  and  $t$ , respectively. The fraction of dijet events in the inclusive diffractive events is shown as a function of  $\xi$  in Fig. 1(c) and  $t$  in Fig. 1(d). The fraction is found to increase linearly with increasing  $\xi$ , but no significant  $t$  dependence is observed, in agreement with the UA8 result [5] which showed a flat  $t$  dependence in the region  $0.9 < |t| < 2.3$ . The jet  $E_T$  distributions fall faster with  $E_T$  in the diffractive events than in the ND. The diffractive dijets are boosted away from the leading antiproton in  $\eta$ , and are more back-to-back in  $\phi$  than the ND.

In leading order QCD, the cross section ratio,  $R(x)$ , of the diffractive to ND dijet productions represents the ratio of the diffractive to ND effective structure functions defined as  $F_{JJ}^{(D)}(x) = x\{g^{(D)}(x) + \frac{4}{9}\sum_i[q_i^{(D)}(x) + \bar{q}_i^{(D)}(x)]\}$ . Thus, the diffractive structure may be obtained by multiplying the “known” ND structure by  $R(x)$ . The  $x$ , the momentum fraction of struck parton in the antiproton, is evaluated from the jets (including a third jet if  $E_T^{jet3} > 5 \text{ GeV}$ ) as,  $x = \sum_{i=1,2(3)} E_T^{(i)} e^{-\eta^{(i)}} / (2p_0^{\bar{p}})$ . Fig. 2 shows the ratio  $R(x)$  of the diffractive dijet events to the ND dijet events for six  $\xi$  bins of width  $\Delta\xi = 0.01$ , where the two data samples are normalized to the same luminosity. The distributions are fitted well by the form  $R(x) = R_0(x/0.0065)^{-r}$ , with similar slopes for all  $\xi$  bins in the region  $10^{-3} < x < 0.5\xi_{min}$ .

The diffractive structure function can be determined by multiplying the measured  $R(x)$  by the known ND structure function. By changing the variable from  $x$  to  $\beta (= x/\xi)$ , we obtain the diffractive structure function  $F_{JJ}^D(\beta)$ , shown in Fig. 3. This structure function is compared to that extracted by the H1 collaboration from diffractive DIS measurements using a QCD analysis [4]. The dashed (dotted) line in Fig. 3 is obtained from H1 diffractive parton densities derived with fit 2 (fit 3), scaled down by a factor of 20. The measured diffractive structure function does not agree with expectations from the H1 results both in normalization and shape. Summed over all  $\beta$ , the discrepancy in nor-

malization is about a factor of 10, in general agreement with predictions based on the renormalized Pomeron flux model [6].

In Run 2, the Roman Pot spectrometers will be placed closer to the antiproton beam, which will enable us to extend our measurement to lower  $\xi$  values. In addition, the improved plug calorimeters, two proposed miniplug calorimeters and a set of beam shower counters (BSC) to tag forward rapidity gaps will provide the basis for improved studies in hard diffraction.

## REFERENCES

1. F. Abe *et al.*, Phys. Rev. Lett. **78**, 2698 (1997); **79**, 2636 (1997)
2. F. Affolder *et al.*, FERMILAB-PUB-99/229-E. Submitted to Phys. Rev. Lett. Aug. 7, 1999.
3. M. Derrick *et al.*, Z. Phys. **C 68**, 569 (1995); Phys. Lett. **B 356**, 129 (1995).
4. C. Adloff *et al.*, Z. Phys. **C 76**, 613 (1997); Eur. Phys. J. **C 6**, 421 (1999).
5. A. Brandt *et al.* Phys. Lett. **B 298**, 417 (1992).
6. K. Goulianos, Phys. Lett. **B 356**, 379 (1995); **B 363**, 268 (1995).

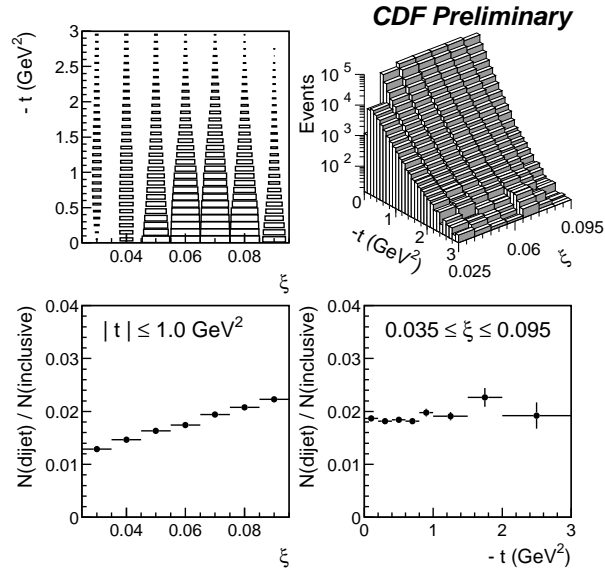


Figure 1. Distributions versus  $\xi$  and  $t$ : (a) Roman Pot acceptance; (b) inclusive diffractive event sample; (c) ratio of dijet to inclusive diffractive events versus  $\xi$  and (d) versus  $t$ .

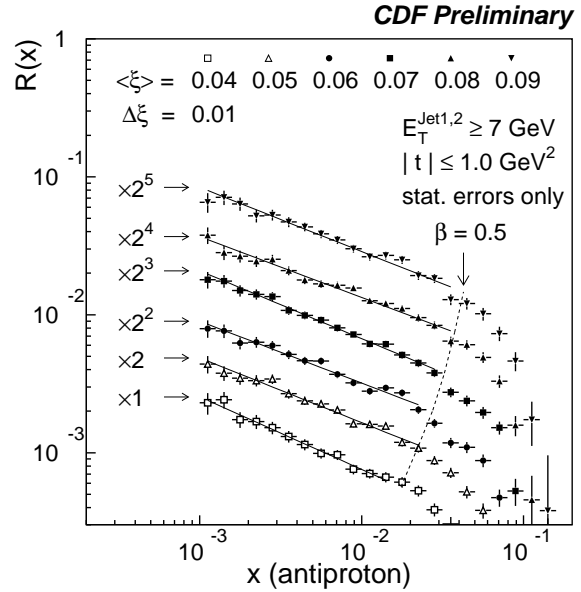


Figure 2. Ratio of diffractive to non-diffractive dijet event rates as a function of  $x$  (momentum fraction of struck parton in antiproton). The solid lines are fits to the form  $R(x) = R_0(x/0.0065)^{-r}$  for  $\beta < 0.5$ , where  $\beta = x/\xi_{min}$ .

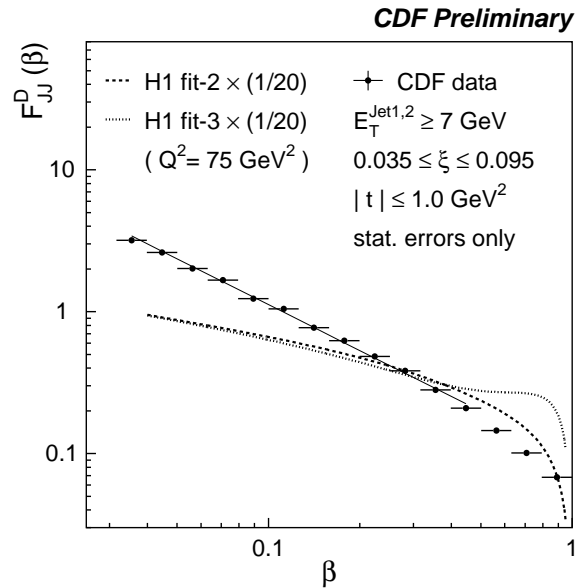


Figure 3. The  $\beta$  distribution from the data (points) and fit (solid line), compared with expectations from the diffractive parton densities of the proton from H1 fit 2 (dashed) and fit 3 (dotted) scaled down by a factor of 20.

# DØ Rapidity Gap Studies

Andrew Brandt (DØ Collaboration)<sup>a</sup>

<sup>a</sup>University of Texas at Arlington, P.O. Box 19059, Arlington, TX 76019

DØ Run I Rapidity Gap studies are briefly described.

## 1. Hard Diffraction Introduction

Inelastic diffractive collisions are responsible for 10–15% of the  $\bar{p}p$  total cross section and have been described by Regge theory through the exchange of a pomeron. Diffractive events are characterized by the absence of significant hadronic particle activity over a large region of rapidity or pseudorapidity. This empty region is called a rapidity gap and can be used as an experimental signature for diffraction. Recent interest in diffraction has centered on the possible partonic nature of the pomeron in the framework of quantum chromodynamics (QCD), as suggested by Ingelman and Schlein [1]. Hard single diffraction (HSD), which combines diffraction and a hard scatter (such as jet or  $W$ -boson production), can be used to study the properties of the pomeron.

The pomeron's partonic nature was first inferred by the UA8 experiment [2]. Recent analyses of diffractive jet production [3–5] and diffractive  $W$ -boson production [6] are consistent with a predominantly hard gluonic pomeron, but measured rates at the Fermilab Tevatron are several times lower than predictions based on data from the DESY  $ep$  collider HERA [7].

Current analyses in DØ on diffractive  $W$ -boson exchange, double pomeron exchange (central jets with a forward and a backward rapidity gap), and diffractive jet production all attempt to provide new insight into the nature of the pomeron and diffractive interactions. Here we present new measurements from the most mature of these analyses, diffractive jet production.

## 2. Diffractive Jet Production

In the DØ detector [8], jets are measured with the uranium/liquid-argon calorimeters using a fixed-cone algorithm. The jets are corrected using standard DØ routines for jet-energy scale [9], except that there is no subtraction of energy from spectator parton interactions, since these are unlikely for diffractive events. To identify rapidity gaps, we measure the number of tiles containing a signal in the LØ forward scintillator arrays ( $n_{LØ}$ ), and towers ( $\Delta\eta \times \Delta\phi = 0.1 \times 0.1$ ) above threshold in the calorimeters ( $n_{CAL}$ ).

For  $\sqrt{s} = 630$  and 1800 GeV, we use triggers which required at least two jets with transverse energy  $E_T > 12$  or 15 GeV to study the dependence of the gap fraction on jet location. The forward jet triggers required the two leading jets to both have  $\eta > 1.6$  (or  $\eta < -1.6$ ), while the central jet triggers had an offline requirement of  $|\eta| < 1.0$ . The events in the final data samples all have a single  $\bar{p}p$  interaction requirement, a vertex position within 50 cm of the center of the interaction region, and two leading jets that satisfy standard quality criteria [10].

The  $n_{LØ}$  versus  $n_{CAL}$  distributions are shown in Fig. 1. For forward jet events, these quantities are defined by the  $\eta$  region on the side opposite the two leading jets, while for central jet events they are defined by the forward  $\eta$  interval that has the lower multiplicity. The distributions display a peak at zero multiplicity ( $n_{CAL} = n_{LØ} = 0$ ), in qualitative agreement with expectations for a diffractive component in the data.

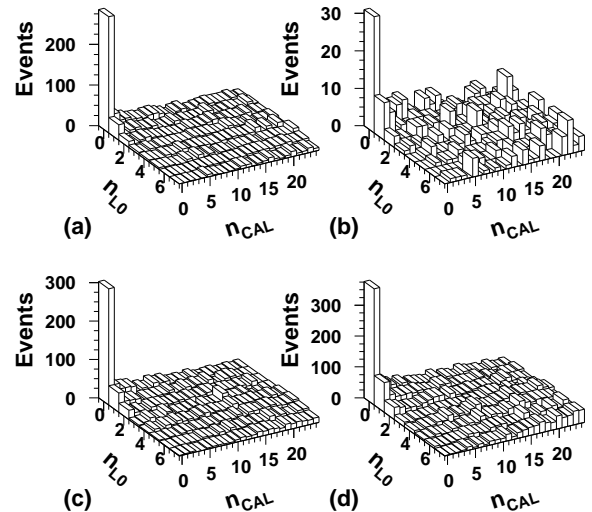


Figure 1. Multiplicity distributions at  $\sqrt{s} = 1800$  GeV for (a) forward and (b) central jet events, and at  $\sqrt{s} = 630$  GeV for (c) forward and (d) central jet events.

Table 1

The measured and predicted gap fractions and their ratios.

Gap Fractions					
Sample	Data	Hard Gluon	Flat Gluon	Soft Gluon	Quark
1800 GeV $ \eta  > 1.6$	$(0.65 \pm 0.04)\%$	$(2.2 \pm 0.3)\%$	$(2.2 \pm 0.3)\%$	$(1.4 \pm 0.2)\%$	$(0.79 \pm 0.12)\%$
1800 GeV $ \eta  < 1.0$	$(0.22 \pm 0.05)\%$	$(2.5 \pm 0.4)\%$	$(3.5 \pm 0.5)\%$	$(0.05 \pm 0.01)\%$	$(0.49 \pm 0.06)\%$
630 GeV $ \eta  > 1.6$	$(1.19 \pm 0.08)\%$	$(3.9 \pm 0.9)\%$	$(3.1 \pm 0.8)\%$	$(1.9 \pm 0.4)\%$	$(2.2 \pm 0.5)\%$
630 GeV $ \eta  < 1.0$	$(0.90 \pm 0.06)\%$	$(5.2 \pm 0.7)\%$	$(6.3 \pm 0.9)\%$	$(0.14 \pm 0.04)\%$	$(1.6 \pm 0.2)\%$
Ratios of Gap Fractions					
630/1800 $ \eta  > 1.6$	$1.8 \pm 0.2$	$1.7 \pm 0.4$	$1.4 \pm 0.3$	$1.4 \pm 0.3$	$2.7 \pm 0.6$
630/1800 $ \eta  < 1.0$	$4.1 \pm 0.9$	$2.1 \pm 0.4$	$1.8 \pm 0.3$	$3.1 \pm 1.1$	$3.2 \pm 0.5$
1800 $ \eta  > 1.6/ \eta  < 1.0$	$3.0 \pm 0.7$	$0.88 \pm 0.18$	$0.64 \pm 0.12$	$30. \pm 8.$	$1.6 \pm 0.3$
630 $ \eta  > 1.6/ \eta  < 1.0$	$1.3 \pm 0.1$	$0.75 \pm 0.16$	$0.48 \pm 0.12$	$13. \pm 4.$	$1.4 \pm 0.3$

The gap fraction is extracted from a two-dimensional fit to the lego plot of  $n_{L\emptyset}$  versus  $n_{CAL}$ . Table 1 shows the gap fractions obtained for the four event samples. Uncertainties are dominated by those on the fit parameters. Table 1 shows that the gap fractions at  $\sqrt{s} = 630$  GeV are larger than gap fractions at  $\sqrt{s} = 1800$  GeV and that gap fractions for forward jets are larger than for central jets. Table 1 also lists predicted gap fractions for several possible pomeron structure functions.

We compare the data to Monte Carlo (MC) simulations using the hard diffractive event generator POMPYT [11]. In POMPYT, a pomeron is emitted from the proton with a certain probability (called the flux factor [1]), and has a structure functions  $s(\beta)$ , where  $\beta$  is the fractional momentum of the pomeron carried by the hard parton. We used the standard Donnachie-Landshoff flux factor [12] in this analysis and compare our data to several typical structure function choices. In each case, the gap fraction is defined as the cross section for jet events with a rapidity gap based on POMPYT divided by the jet cross section from PYTHIA [13]. Many uncertainties, such as the choice of proton parton densities, cancel in the ratio. The MC values are corrected for diffractive events that fail the gap selection criteria.

Monte Carlo gap fractions are shown in Table 1. The systematic uncertainties are dominated by the difference in energy scale between data and MC. We observe that rates for harder gluon structures are far higher than supported by data, while the quark structure is in reasonable agreement with the data. The quark structure, however, has previously been shown to predict an excessive rate of diffractive  $W$ -Bosons [6].

A hard gluonic pomeron is capable of describing previous measurements [3–6], if combined with a flux factor that decreases with increasing  $\sqrt{s}$  [14]. The ratios of gap fractions shown in the lower half of Table 1 provide new information, since the flux factor cancels for the same  $\sqrt{s}$ , and dependence on the flux

factor is reduced for different  $\sqrt{s}$ . The ratios for jets with  $|\eta| > 1.6$  to jets with  $|\eta| < 1.0$  show clear disagreement between the data and predictions for a hard-gluon pomeron structure, despite this cancellation. A gluon-dominated pomeron containing both soft and hard components, combined with a reduced flux factor, could describe all the data samples.

## REFERENCES

1. G. Ingelman and P. Schlein, Phys. Lett. B **152**, 256 (1985).
2. A. Brandt *et al.* (UA8 Collaboration), Phys. Lett. B **297**, 417 (1992).
3. F. Abe *et al.* (CDF Collaboration), Phys. Rev. Lett. **79**, 2636 (1997).
4. J. Breitweg *et al.* (ZEUS Collaboration), Eur. Phys. J. **C5**, 41 (1998) and references therein.
5. C. Adloff *et al.* (H1 Collaboration), Eur. Phys. J. **C6**, 421 (1999).
6. F. Abe *et al.* (CDF Collaboration), Phys. Rev. Lett. **78**, 2698 (1997).
7. L. Alvero, J.C. Collins, J. Terron and J. Whitmore, Phys. Rev. D **59**, 74022 (1999).
8. S. Abachi *et al.* (DØ Collaboration), Nucl. Instrum. Methods Phys. Res. A **338**, 185 (1994).
9. B. Abbott *et al.* (DØ Collaboration), Nucl. Instrum. Methods Phys. Res. A **424**, 352 (1999).
10. B. Abbott *et al.* (DØ Collaboration), Phys. Rev. Lett. **82**, 2451 (1999).
11. P. Bruni and G. Ingelman, DESY 93-187, 1993 (unpublished). We used a modified version of 2.6.
12. A. Donnachie and P.V. Landshoff, Nucl. Phys. B **303**, 634 (1988).
13. H.-U. Bengtsson and T. Sjöstrand, Comp. Phys. Comm. **46**, 43 (1987); T. Sjöstrand, CERN-TH.6488/92. We used version 5.7.
14. K. Goulianos, Phys. Lett. B **358**, 379 (1995).

# QCD Analysis of the Diffractive Structure Functions Measured at HERA and Factorization Breaking at the Tevatron

C. Royon <sup>a</sup>

<sup>a</sup>DAPNIA/SPP, Commissariat à l'Énergie Atomique, Saclay,  
F-91191 Gif-sur-Yvette Cedex

The 1994 data published by the H1 collaboration are compared with models based on Regge phenomenology. The  $x_{\mathcal{P}}$  dependence of the data can be described in a model based on the exchange of a dominant diffractive (pomeron) trajectory with additional sub-leading reggeon contributions. The dynamics of the Pomeron structure is studied within the framework of perturbative QCD and new parton distributions are obtained. These parton distributions will allow a direct test of factorization breaking at Tevatron.

## 1. Regge parameterization

The 1994 data are first investigated in the framework of a Regge phenomenological model [1]. The 1994 data are subjected to a fit in which a single factorizable trajectory ( $\mathcal{P}$ ) is exchanged such that:

$$F_2^{D(3)}(Q^2, \beta, x_{\mathcal{P}}) = f_{\mathcal{P}/p}(x_{\mathcal{P}}) F_2^{\mathcal{P}}(Q^2, \beta). \quad (1)$$

In this parameterization,  $F_2^{\mathcal{P}}$  can be interpreted as the structure function of the pomeron [4]. The value of  $F_2^{\mathcal{P}}$  is treated as a free parameter at each point in  $\beta$  and  $Q^2$ . The pomeron flux takes a Regge form with a linear trajectory  $\alpha_{\mathcal{P}}(t) = \alpha_{\mathcal{P}}(0) + \alpha'_{\mathcal{P}} t$ , such that

$$f_{\mathcal{P}/p}(x_{\mathcal{P}}) = \int_{t_{cut}}^{t_{min}} \frac{e^{B_{\mathcal{P}} t}}{x_{\mathcal{P}}^{2\alpha_{\mathcal{P}}(t)-1}} dt, \quad (2)$$

where  $|t_{min}|$  is the minimum kinematically allowed value of  $|t|$  and  $t_{cut} = -1 \text{ GeV}^2$  is the limit of the measurement. The value of  $\alpha_{\mathcal{P}}(0)$  is a free parameter and  $B_{\mathcal{P}}$  and  $\alpha'_{\mathcal{P}}$  are taken from hadron-hadron data [1]. The fit with a single trajectory does not give a good description of the data in the same way as it is observed at  $Q^2 = 0$  [2] that secondary trajectories in addition to the pomeron are required to describe diffractive  $ep$  data.

A much better fit is obtained when both a leading ( $\mathcal{P}$ ) and a sub-leading ( $\mathcal{R}$ ) trajectory are considered in the same way as in formula (1), where the values of  $F_2^{\mathcal{P}}$  and  $F_2^{\mathcal{R}}$  are treated as free parameters at each point in  $\beta$  and  $Q^2$ ,  $\alpha_{\mathcal{P}}(0)$  and  $\alpha_{\mathcal{R}}(0)$  being two free parameters. The flux factor for the secondary trajectory takes the same form as equation (2), with  $B_{\mathcal{R}}$ , and  $\alpha'_{\mathcal{R}}$  again taken from hadron-hadron data [1]. This fit yields to the following value of  $\alpha_{\mathcal{P}}(0) = 1.203 \pm 0.020 \text{ (stat.)} \pm 0.013 \text{ (syst.)}^{+0.030}_{-0.035} \text{ (model)}$  [1] and is significantly larger than values extracted from soft hadronic data ( $\alpha_{\mathcal{P}} \sim 1.08$ ). The quality of the fit is similar if interference between the two trajectories is introduced.

## 2. QCD fits and the structure of the Pomeron

It has been suggested that the  $Q^2$  evolution of the Pomeron structure function may be understood in terms of parton dynamics from perturbative QCD where parton densities are evolved according to DGLAP [3] equations [4,1], using the GRV parameterization for  $F_2^{\mathcal{R}}$  [5].

For the pomeron, a quark flavor singlet distribution ( $zS_q(z, Q^2) = u + \bar{u} + d + \bar{d} + s + \bar{s}$ ) and a gluon distribution ( $zG(z, Q^2)$ ) are parameterized in terms of coefficients  $C_j^{(S)}$  and  $C_j^{(G)}$  at  $Q_0^2 = 3 \text{ GeV}^2$  such that :

$$zS(z, Q^2 = Q_0^2) \left[ \sum_{j=1}^n C_j^{(S)} \cdot P_j(2z-1) \right]^2 \cdot e^{\frac{a}{z-1}} \quad (3)$$

$$zG(z, Q^2 = Q_0^2) \left[ \sum_{j=1}^n C_j^{(G)} \cdot P_j(2z-1) \right]^2 \cdot e^{\frac{a}{z-1}} \quad (4)$$

where  $z = x_{i/\mathcal{P}}$  is the fractional momentum of the pomeron carried by the struck parton,  $P_j(\zeta)$  is the  $j^{\text{th}}$  member in a set of Chebyshev polynomials, which are chosen such that  $P_1 = 1$ ,  $P_2 = \zeta$  and  $P_{j+1}(\zeta) = 2\zeta P_j(\zeta) - P_{j-1}(\zeta)$ . Some details about the fits can be found in Reference [7].

A sum of  $n = 3$  orthonormal polynomials is used so that the input distributions are free to adopt a large range of forms for a given number of parameters. The exponential factor is needed to ensure a correct convergence close to  $z=1$ .

The trajectory intercepts are fixed to  $\alpha_{\mathcal{P}} = 1.20$  and  $\alpha_{\mathcal{R}} = 0.62$ . Only data points of H1 with  $\beta \leq 0.65$ ,  $M_X > 2 \text{ GeV}$  and  $y \leq 0.45$  are included in the fit in order to avoid large higher twist effects and the region that may be most strongly affected by a non zero value of  $R$ , the longitudinal to transverse cross-section ratio.

### 3. Results of the QCD fits

The resulting parton densities of the Pomeron are presented in figure 1. As it was noticed in the 1994  $F_2^D$  paper [1], we find two possible fits quoted here as fit 1 and fit 2. Each fit shows a large gluonic content. The quark contribution is quite similar for both fits, but the gluon distribution tends to be quite different at high values of  $z$ . This can be easily explained as no data above  $z = 0.65$  are included in the fits. Thus there is no constraint from the data at high  $z$ . The quark densities is on the contrary more constrained in this region with the DGLAP evolution. Both fits show similar  $\chi^2$  (the  $\chi^2$  per degree of freedom is about 1.2)\*. Adding the 1995 data points into the fits also allows to get a better constraint on initial parton densities at  $Q_0^2 = 3 \text{ GeV}^2$  compared to the fits performed with 1994 data points alone. For the gluon density presented in figure 1, we have determined that  $\frac{\delta G}{G} \simeq 25\%$  for  $z$  below 0.6.

The result of the fit is presented in figure 2 together with the experimental values for 1994 data points ; we see on this figure the good agreement of the QCD prediction and the data points, which supports the validity of description of the Pomeron in terms of partons following a QCD dynamics.

We have also tried to extend the QCD fits to lower  $Q^2$  (below  $3 \text{ GeV}^2$ ) using the 1995  $F_2^D$  measurement. The  $\chi^2$  of the fit turns out to increase ( $\chi^2/ndf = 1.6$ , adding 35 low  $Q^2$  points to the 171 points) [8]. This can be illustrated in figure 2 of Reference [8] where changes of slopes of scaling violations for  $Q^2$  below and above  $3 \text{ GeV}^2$  can be seen. It may indicate that breaking of perturbative QCD has already occurred in this region.

The idea would then to use these parton distributions and to compare with the measurements at Tevatron in order to study factorization breaking. The roman pots which will be available in the D0 experiment at Run II will allow a direct comparison with the results obtained from the HERA parton distributions. It will be possible to know where factorization breaking takes place at Tevatron, e.g. is it at low or high  $\beta$ ?

### 4. Acknowledgments

The results described in the present contribution come from a fruitful collaboration with H. Jung and L. Schoeffel.

\*Fit 2 is a bit disfavored compared to fit 1 (its  $\chi^2$  by degree of freedom is 1.3 compared to 1.2 for fit 1) and is quite instable: changing a little the parameters modifies the gluon distribution at high  $z$ .

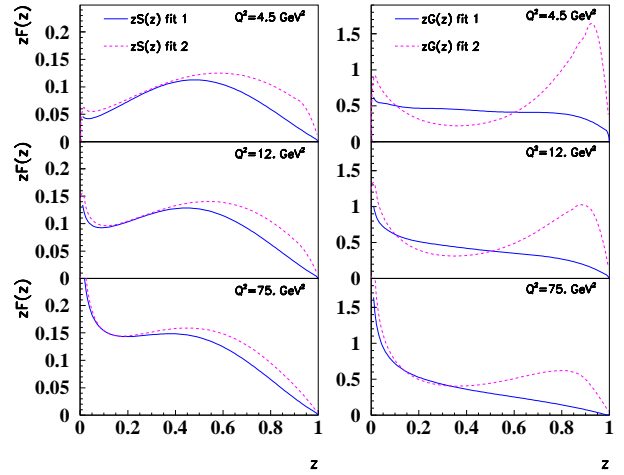


Figure 1. Quark flavor singlet ( $zS$ , left) and gluon ( $zG$ , right) distributions of the pomeron deduced as a function of  $z$ , the fractional momentum of the pomeron carried by the struck parton, from the fit on 1994 data points with  $Q^2 \geq 4 \text{ GeV}^2$ . Two possible fits labelled as fit 1 and fit 2 are found ( $\chi^2/ndf = 1.2$  for fit 1, and  $\chi^2/ndf = 1.3$  for fit 2 with statistical errors only).

### REFERENCES

1. H1 Collab., C.Adloff et al., Z. Phys. C76 (1997) 613.
2. H1 Collab., C. Adloff et al., Z. Phys. C74 (1997) 221.
3. G.Altarelli, G.Parisi, Nucl. Phys. B126 (1977) 298. V.N.Gribov, L.N. Lipatov, Sov. J. Nucl. Phys. 15 (1972) 438 and 675.
4. G. Ingelman, P. Schlein, Phys. Lett. B152 (1985) 256.
5. M. Glück, E. Reya, A. Vogt, Z. Phys. C53 (1992) 651.
6. V.S.Fadin, E.A.Kuraev, L.N.Lipatov Phys. Lett. B60 (1975) 50. I.I.Balitsky, L.N.Lipatov, Sov. J. Nucl. Phys. 28 (1978) 822.
7. L.Schoeffel, N.I.M.A423 (1999) 439.
8. C.Royon for the H1 collaboration, talk given at the DIS99 conference, Zeuthen (Allemagne), 19-23/04/99, preprint hep-ph/9908216

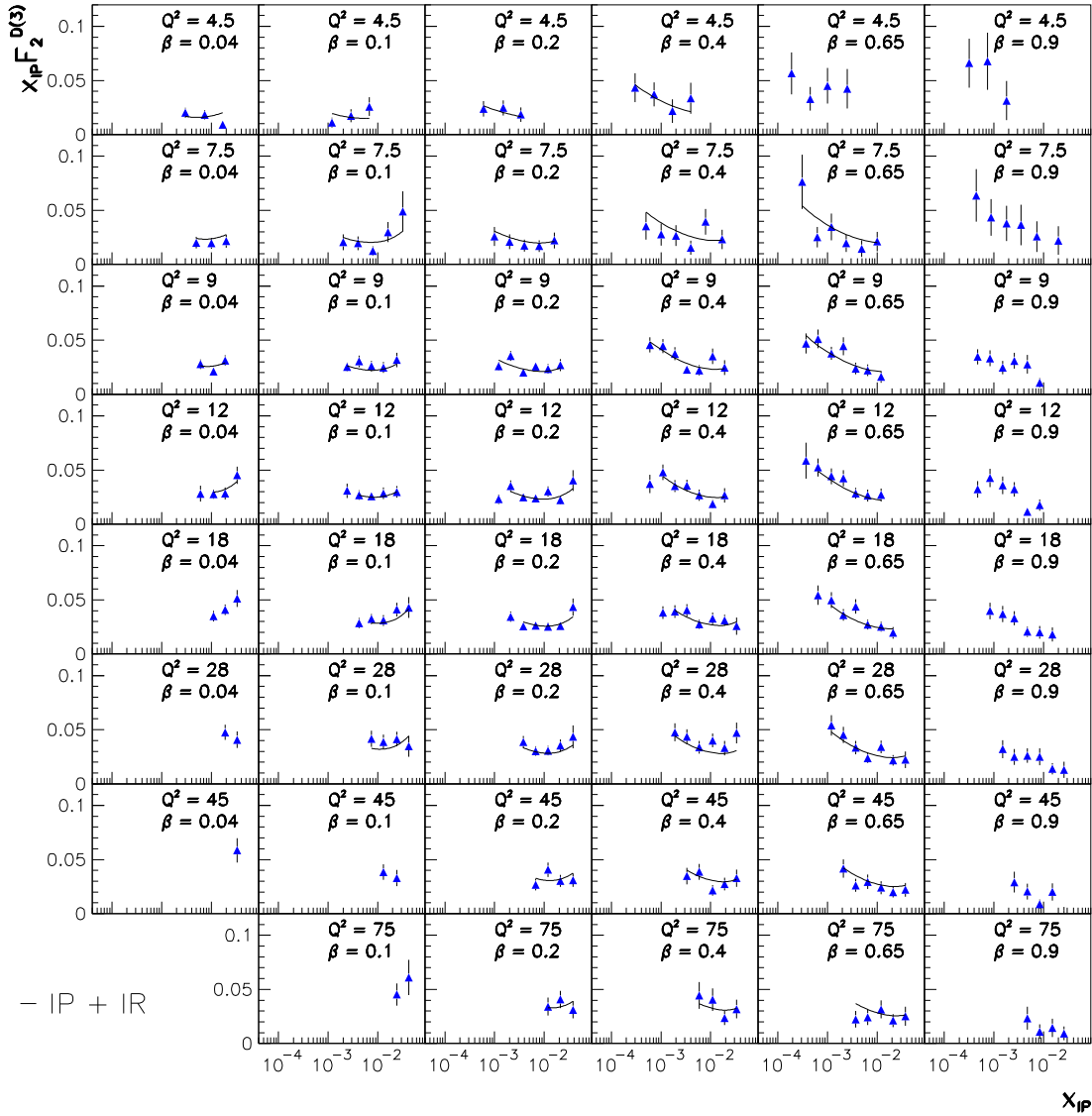


Figure 2. The H1 data points on  $x_P F_2^{D(3)}$  (1994) are shown with the result of the QCD fit described in the text; the result of the fit is drawn only in bins included in the minimization procedure.

# Diffractive Heavy Flavor Production at CDF

Andrei Solodsky <sup>a</sup>

<sup>a</sup>The Rockefeller University, 1230 York Avenue, New York, NY 10021

We report results of diffractive production of heavy flavors, charm and beauty, from CDF.

We extended our studies of diffractive processes to diffractive heavy flavor production, charm and beauty, to probe directly the gluon content of the pomeron. Our diffractive beauty [1] production measurement is based on identifying a high transverse momentum electron with  $E_T > 9.5$  GeV and  $|\eta| < 1.1$ , from the semi-leptonic  $b$ -quark decay, produced in single diffraction dissociation,  $p + \bar{p} \rightarrow p/\bar{p} + b(\rightarrow e + X') + X$ . Each event is required to have a jet consisting of at least two tracks in addition to the electron candidate.

First, we extract a diffractive signal from the obtained event sample and then estimate the  $b$ -quark fraction separately in the diffractive and total event samples.

As in our diffractive dijet[2] and W [3] analyses, the diffractive signal is extracted by counting BBC hits,  $N_{BBC}$ , and adjacent forward calorimeter towers,  $N_{CAL}$ , with  $E > 1.5$  GeV. Figure 1(a) shows the correlation between  $N_{BBC}$  and  $N_{CAL}$  for both the positive and negative  $\eta$  sides of the detector, i.e. two entries per event. The (0,0) bin contains 100 events. We evaluate the non-diffractive content of the (0,0) bin from the distribution of events along the diagonal of Fig. 1(a), with  $N_{BBC} = N_{CAL}$ , shown in Fig. 1(b) by extrapolating a fit to the data of bins (2,2) to (9,9) to bin (0,0). This yields  $24.4 \pm 5.5$  non-diffractive background events in the (0,0) bin.

Figures 1(c) and 1(d) show the electron  $E_T$  and  $\eta$  distribution, respectively, for the diffractive (points) and total (histogram) event samples. In Fig. 1(d), the sign of  $\eta$  of diffractive events with a gap at positive  $\eta$  was changed, so that the gap always appears at negative  $\eta$ . While the  $E_T$  spectra show no significant difference, the diffractive  $\eta$  distribution is shifted away from the gap relative to the symmetric distribution of the total event sample, in agreement with the single diffraction event topology.

In addition to events from  $b$ -quark decays, the data contain events from charm decays and background. The background is mainly due to electrons from residual photon conversions and to hadrons faking electrons.

We use two methods to extract the fraction of beauty events in the data. In the first method, we fit the electron momentum component perpendicular to the

jet axis,  $p_T^{e/jet}$ , which depends on the mass of the parent quark, with the sum of four templates: photon conversions, fake electrons from hadrons, charm and beauty. This fit yields a beauty fraction of  $(42.9 \pm 0.4)\%$  [ $(38 \pm 14)\%$ ] for the total [diffractive] event sample. The second method uses the impact parameter of the electron track, which is defined as the minimum distance between the primary vertex and the electron track in the  $r - \phi$  plane and depends on both the mass and the lifetime of the parent quark. A fit to the impact parameter distribution using four templates, as above, yields  $(47.7 \pm 0.4)\%$  [ $(38 \pm 14)\%$ ] for our two data samples.

The average of the results of both methods yields  $73371 \pm 485(stat) \pm 7774(syst)$  [ $44.4 \pm 10.2(stat) \pm 4.7(syst)$ ] beauty events for the total [diffractive] event sample. The difference between the results of the two methods is assigned as systematic uncertainty. After subtracting the 24% non-diffractive background estimated from the fit in Fig. 1(b), there remain  $33 \pm 10(stat) \pm 5(syst)$  diffractive beauty events. Correcting the diffractive event yield for single-vertex selection cut efficiency ( $0.26 \pm 0.01$ ), and for the detector live-time acceptance ( $0.77 \pm 0.07$ ) due to noise or beam associated background, we obtain  $165 \pm 50(stat) \pm 29(syst)$  diffractive beauty events.

The diffractive to total  $b$ -quark production ratio obtained from the above numbers is  $R_{bb}^{gap} = [0.23 \pm 0.07(stat) \pm 0.05(syst)]\%$ . The rapidity gap acceptance for events generated using POMPYT Monte Carlo with a flat pomeron structure, which is favored by HERA measurements [4,5], and a gluon to quark ratio of  $0.7 \pm 0.2$ , as reported in ref. 3, is found to be  $0.37 \pm 0.02$ . Dividing  $R_{bb}^{gap}$  by this value yields a diffractive to total production ratio of

$$R_{\bar{b}b} = [0.62 \pm 0.19(stat) \pm 0.14(syst)]\% \quad (\xi < 0.1).$$

POMPYT with the standard pomeron flux and a flat (hard) pomeron structure consisting of purely gluons or quarks yields  $R_{\bar{b}b}$  of 10.4%(11.6%) and 0.92%(1.02%), respectively. The ratio  $D$  of the measured  $R_{\bar{b}b}$  fraction to that predicted by POMPYT depends on the gluon fraction  $f_g$  of the pomeron. This dependence is shown in Fig. 2, where  $D$  is plotted as a function of  $f_g$  along with published results from ZEUS

and CDF measurements [2,3]. For each measurement the two curves show the  $1\sigma$  bounds. The black cross and shaded ellipse represent the best fit and  $1\sigma$  contour of a least square two-parameter fit to the three CDF results. The fit yielded  $D_{CDF} = 0.19 \pm 0.04$  and  $f_g^{CDF} = 0.54^{+0.16}_{-0.14}$ , in agreement with the results we obtained from the  $W$  and dijet rates, namely  $D = 0.18 \pm 0.04$  and  $f_g = 0.7 \pm 0.2$  [2]. The value of  $D_{CDF}$  is significantly smaller than the ZEUS result. The discrepancy between the HERA and Tevatron  $D$ -values represents a breakdown of factorization. The observed discrepancy is in general agreement with predictions based on the renormalized pomeron flux model [6].

We also searched for diffractive  $J/\psi$  production in a sample of central ( $|\eta| < 1.1$ ) dimuons. For  $J/\psi$  reconstruction we required a pair of opposite charge muons with  $p_T > 2$  GeV/ $c$  and invariant mass close to the  $J/\psi$  mass. The technique we used to extract the diffractive signal is identical to that used in our previous studies. Preliminary results of this analysis, before correcting for the gap acceptance  $A$ , give a ratio of diffractive to non-diffractive  $J/\psi$  production of

$$R_{J/\psi} \times A = [0.36 \pm 0.07]\%.$$

In spite of the fact that all diffractive processes studied at CDF are differently sensitive to the quark and gluon content of the pomeron, the obtained ratios of diffractive to non-diffractive production are all of the same order of magnitude,  $\sim 1\%$ . This indicates that the structure of the pomeron probed in single diffraction events is not very different from the structure of the proton.

## REFERENCES

1. T. Affolder *et al.*, submitted to Phys. Rev. Lett.
2. F. Abe *et al.*, Phys. Rev. Lett. **79**, 2636 (1997).
3. F. Abe *et al.*, Phys. Rev. Lett. **78**, 2698 (1997).
4. M. Derrick *et al.*, Z. Phys. **C 68**, 569 (1995); Phys. Lett. **B 356**, 129, (1995); *Eur. Phys. J. A* **6**, 43 (1999).
5. T. Ahmed *et al.*, Phys. Lett. **B 348**, 681, (1995); C. Adloff *et al.*, Z. Phys. **C 76**, 613 (1997).
6. K. Goulianos, Phys. Lett. **B 358**, 379, (1995); **B 363**, 268 (1995).

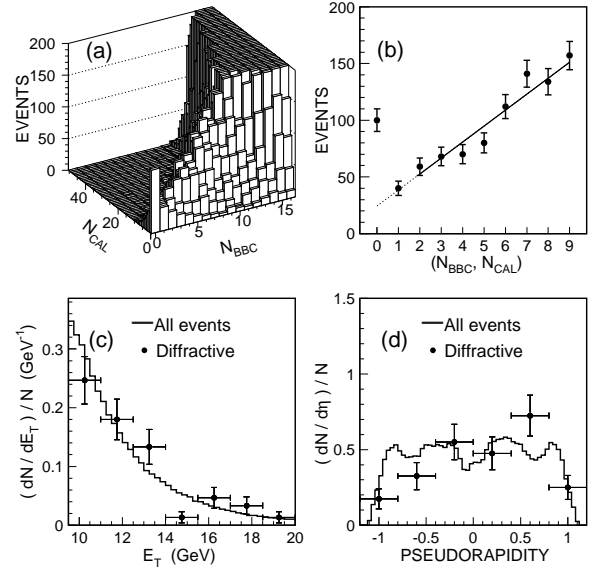


Figure 1. (a) Beam-beam counter multiplicity,  $N_{BBC}$ , versus forward calorimeter tower multiplicity,  $N_{CAL}$ ; (b) multiplicity distribution along the diagonal with  $N_{BBC} = N_{CAL}$  in the plot in (a); (c) electron  $p_T$  and (d) pseudorapidity for the diffractive (points) and total (histogram) event samples.

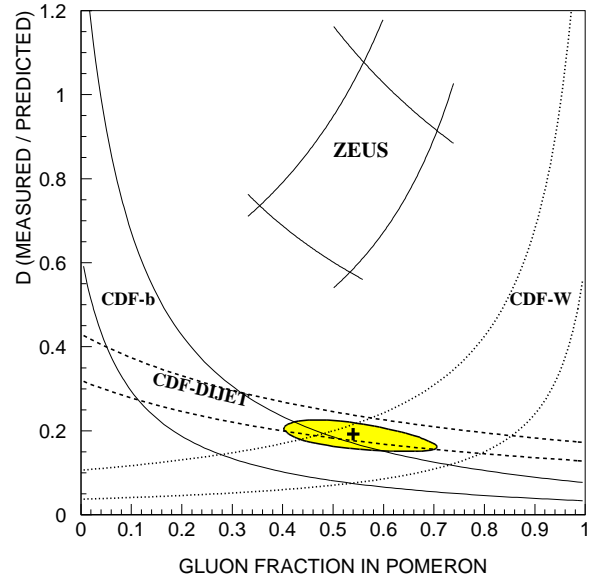


Figure 2. The ratio  $D$  of measured to predicted diffractive rates as a function of the gluon content of the pomeron.

# Diffractively Produced Charm Final States in $pp$ Interactions at 800 GeV/c

M.H.L.S. Wang<sup>a,e</sup>, M.C. Berisso<sup>a</sup>, D.C. Christian<sup>b</sup>, J. Félix<sup>c</sup>, A. Gara<sup>d</sup>, E. Gottschalk<sup>b</sup>, G. Gutiérrez<sup>b</sup>, E.P. Hartouni<sup>e</sup>, B.C. Knapp<sup>d</sup>, M.N. Kreisler<sup>a,e</sup>, S. Lee<sup>a</sup>, K. Markianos<sup>a</sup>, G. Moreno<sup>c</sup>, M.A. Reyes<sup>c</sup>, M. Sosa<sup>c</sup>, A. Wehmann<sup>b</sup>, D. Wesson<sup>a</sup>

<sup>a</sup>University of Massachusetts, Amherst, Massachusetts 01003, USA

<sup>b</sup>Fermilab, Batavia, Illinois 60510, USA

<sup>c</sup>Universidad de Guanajuato, León, Guanajuato, México

<sup>d</sup>Columbia University, Nevis Laboratories, Irvington, New York 10533, USA

<sup>e</sup>Lawrence Livermore National Laboratory, Livermore, California 94551, USA

We report the observation of charm final states produced by the diffractive dissociation reaction  $pp \rightarrow pX$  at a c.m. energy of  $\sqrt{s} = 40$  GeV. Signals are observed for the decay modes  $D^{*+} \rightarrow D^0(K^-\pi^+)\pi^+$  and  $D^{*-} \rightarrow \overline{D^0}(K^+\pi^-)\pi^-$ . Our results are based on analysis of data representing over 50% of the 5.5 billion events acquired by experiment E690 in the Fermilab fixed target run of 1991.

## 1. Experiment

Experiment E690 was a fixed target experiment that investigated diffractive  $pp$  interactions using an 800 GeV/c proton beam incident on a fixed liquid hydrogen target. The E690 detector was made up of a beam spectrometer system and a multi-particle spectrometer. The beam spectrometer system consisted of two separate spectrometers— an incoming beam spectrometer which detected the incident beam proton and an outgoing beam spectrometer which measured the forward or scattered beam proton. Together they allowed measurement of the momentum difference between the beam proton and the fast, outgoing proton. The multi-particle spectrometer, on the other hand, which was made up of 6 drift chambers, a time-of-flight (TOF) system and a Cerenkov counter for particle identification, measured the particles produced by the interaction of the beam proton in the  $LH_2$  target.

During the run, events were written to tape when they met the following requirements:

1. An incident beam proton in the incoming beam spectrometer.
2. A fast proton in the outgoing beam spectrometer.
3. At least one extra charged track in the main spectrometer.

By the end of the fixed target run in 1991, E690 had acquired about 5.5 billion events meeting these requirements. The number of events used for this analysis was about 2.8 billion events, representing over half of the entire data sample.

## 2. Charm selection

In the search for diffractive charm, the charm decay mode  $D^* \rightarrow D^0(K\pi)\pi$  was used due to its low  $Q$  value (where  $Q = M(K\pi\pi) - M(K\pi) - M(\pi)$ ) which provided a valuable signature for reducing combinatorial backgrounds. The following criteria were used to select charm candidates from the E690 data sample:

1. At least 3 tracks with the appropriate charges to form a  $K\pi\pi$  invariant mass combination.
2. Track assigned as the  $K$  from the  $D^0$  decay must have Cerenkov identification consistent with a  $K$ .
3. Track assigned as the  $\pi$  from the  $D^0$  decay must have Cerenkov identification consistent with a  $\pi$ .
4.  $1.810 \text{ GeV}/c^2 < M(K\pi\pi) < 2.210 \text{ GeV}/c^2$ .
5.  $|Q - .00583 \text{ GeV}/c^2| < .0005 \text{ GeV}/c^2$ .
6. Only for the  $D^{*+}$ : TOF identification for slow  $\pi$  from the  $D^*$  decay consistent with a  $\pi$ .

## 3. Results

Applying all of these cuts to the 2.8 billion events used for this analysis resulted in 446 events for the  $D^{*+}$  and 4,916 events (without the TOF requirement for the slow  $\pi$ ) for the  $D^{*-}$ . Fitting a Gaussian plus a linear background to the invariant  $K\pi\pi$  mass distributions of the events meeting these requirements provided an estimate of 45 events for the  $D^{*+}$  and 157 events for the  $D^{*-}$ . To select diffractive events, the

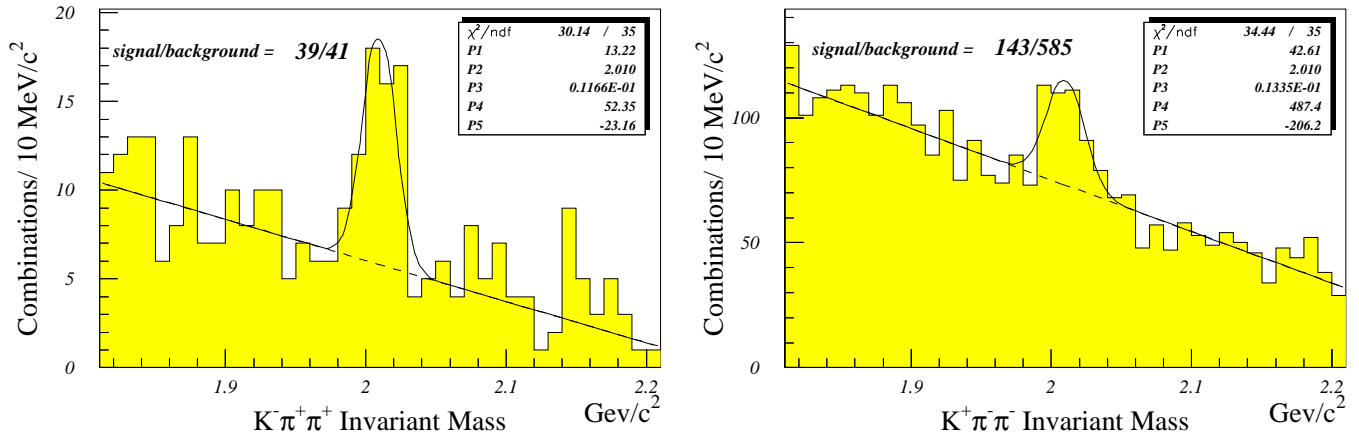


Figure 1. Invariant  $K\pi\pi$  mass distributions for  $D^{*+}$  and  $D^{*-}$  events meeting the coherence condition,  $x_F > 0.85$ , fitted to a Gaussian plus a linear background

coherence condition [1] was imposed requiring the  $x_F$  of the fast, outgoing proton to be greater than 0.85. With this additional requirement, fits to the  $K\pi\pi$  mass distributions shown in Figure 1 yielded 39 events for the  $D^{*+}$  and 143 events for the  $D^{*-}$ . A plot of the rapidity  $y$  (where  $y = \frac{1}{2} \ln(\frac{E+P_L}{E-P_L})$ ) is shown in Figure 2 for the  $D^{*+}$ , the scattered proton, and the  $Y$  system where  $Y$  represents all the particles in the  $X$  system excluding the  $D^*$  in a single diffractive reaction of the type  $pp \rightarrow p_{fast} X(D^* Y)$ . This plot shows a rapidity gap of nearly 5 units between the  $D^*$  and the fast, outgoing proton  $p_{fast}$  which is characteristic of a single diffractive interaction.

#### 4. Conclusion

In conclusion, after analyzing over half of the entire E690 data sample, we observe signals of 39 events in the  $D^{*+} \rightarrow \overline{D^0}(K^-\pi^+)\pi^+$  channel and 143 events in the  $D^{*-} \rightarrow \overline{D^0}(K^+\pi^-\pi^0)\pi^-$  channel meeting the coherence condition of  $x_F > 0.85$  for the fast, outgoing proton. To our knowledge this is the first observation of open charm production in single diffractive  $pp$  interactions. A search conducted by a previous experiment, FNAL E653, found no evidence for diffractively produced charm in  $p - Si$  interactions [2] resulting in an upper limit of  $\sigma_{diff}(c\bar{c}) < 26 \mu b$  for  $p - Si$ . If we assume that the dependence of the cross section  $\sigma$  on the atomic weight  $A$  goes like  $\sigma \propto A^{2/3}$ , this upper limit translates to  $\sigma_{diff}(c\bar{c}) < 2.8 \mu b$  in the case of  $pp$  interactions at 800 GeV/c. Preliminary cross section estimates based on the E690 results using some crude assumptions and models yielded figures consistent with this upper limit.

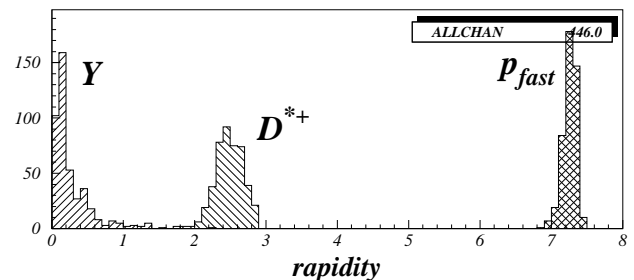


Figure 2. Rapidity plot of the  $D^*$ ,  $Y$  system, and  $p_{fast}$  for  $D^{*+} \rightarrow D^0(K^-\pi^+)\pi^+$  events

#### REFERENCES

1. K. Goulios, Phys. Rep. 101 (1983) 170.
2. K. Kodama et al., Phys. Lett. B 316 (1993) 188.

# Cost of Survival for Large Rapidity Gaps

Eugene Levin <sup>a b</sup>

<sup>a</sup> HEP Department, School of Physics, Tel Aviv University, Tel Aviv 69978, ISRAEL

<sup>b</sup> Physics Department, Brookhaven National Laboratory, Upton, NY 11973 - 5000, USA

In this note we report on calculations of the survival probability of the large rapidity gap (LRG) processes and its energy behaviour.

## 1. INTRODUCTION

In this note we consider the reaction

$$p + p \longrightarrow \quad (1)$$

$X_1 + jet_1(y_1, p_{1,t} \ll \mu) + [LRG] + jet_2(p_{2,t} \ll \mu) + X_2$ , where LRG denotes the large rapidity gap between produced particles and  $X$  corresponds to a system of hadrons with masses much smaller than the total energy.

The story of LRG processes started from Refs. [1–3], where it was noticed that these processes give us a unique way to measure high energy asymptotic at short distances. Indeed, at first sight the experimental observable

$$f_{gap} = \frac{\sigma(\text{ dijet production with LRG })}{\sigma_{inclusive}(\text{ dijet production })} \quad (2)$$

is directly related to the so called “hard” Pomeron exchange. However, this is not the case and the factor ( survival probability  $\langle |S|^2 \rangle$  appears between the “hard” Pomeron exchange and the experimental observable.

$$f_{gap} = \frac{\sigma(\text{LRG})}{\sigma(\text{INCL})} = \langle S^2 \rangle \frac{\text{Diagram with Pomeron (P) and Gluon (G) exchange}}{\text{Diagram with Gluon (G) exchange}}$$

The diagram consists of two parts. The top part shows two sets of blue lines representing partons. Between them is a red wavy line labeled 'P' (Pomeron). The bottom part shows two sets of blue lines representing partons. Between them is a red wavy line labeled 'G' (Gluon). Both parts have a vertical line on the right side with a superscript '2' at the top, indicating a squared amplitude.

Actually, this factor  $\langle |S|^2 \rangle$  is a product of two survival probabilities

$$\langle |S|^2 \rangle = \quad (3)$$

$\langle |S_{bremsstrahlung}(\Delta y = |y_1 - y_2|)^2 \rangle \times \langle |S_{spectators}(s)|^2 \rangle$  which have different meanings.

1.  $\langle |S_{bremsstrahlung}|^2 \rangle$  is probability that the LRG will not be filled by emission of bremsstrahlung gluons from partons, taking part in the “hard” interaction ( see fig 1-a). This factor is certainly important and has been calculated in pQCD in Refs. [4,5,10]. We are not going to discuss it here;
2.  $\langle |S_{spectator}|^2 \rangle$  is related to probability that every parton with  $x_i > x_1$  will have no inelastic interaction with any parton with  $x < x_2$  ( see fig. 1-b). The situation with our knowledge of this survival probability is the main goal of this paper.

## 2. Q & A

**Q:** Have we developed a theory for  $\langle |S_{spectators}|^2 \rangle$ ?

**A:** No, there are only models on the market (see Refs. [6–10]).

**Q:** Can we give a reliable estimates for the value of  $\langle |S_{spectator}|^2 \rangle$ ?

**A:** No, we have only rough estimates based on the Eikonal - type models.

**Q:** Can we give a reliable estimates for the energy behaviour of  $\langle |S_{spectator}|^2 \rangle$ ?

**A:** No, but we understood that  $\langle |S_{spectator}|^2 \rangle$  could steeply decreases with energy.

**Q:** Why are you talking about  $\langle |S_{spectator}|^2 \rangle$  if you can do nothing ?

**A:** Because dealing with models we learned what questions we should ask experimentalists to improve our estimate and what problems we need to solve theoretically to provide reliable estimates.

## 3. EIKONAL-TYPE MODELS

### 3.1. Eikonal model

In eikonal model we assumed that the correct degrees of freedom at high energies are hadrons, and, therefore, the scattering amplitude is diagonal in the hadron basis. Practically, it means [6] that we assume that

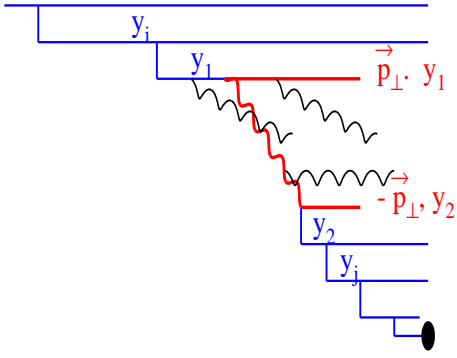


Fig.1-a

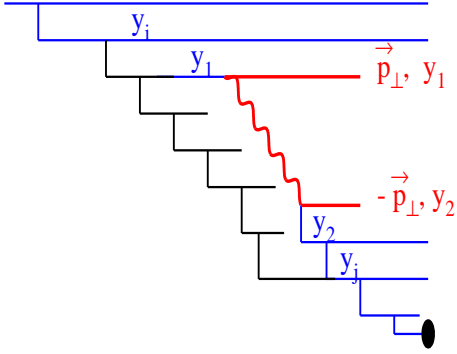


Fig. 1 -b

Figure 1. *Two sources of survival probability: (a) emission of gluons from the partons taking parts in “hard” interaction and (b) emission due to “soft” interaction of spectator quarks (partons).*

the ratio  $\sigma^{SD}/\sigma^{el} \ll 1$ . In this model the unitarity constraint looks simple, namely,

$$\text{Im}a_{el}(s, b) = |a_{el}(s, b)|^2 + G_{in}(s, b), \quad (4)$$

which has solution in terms of arbitrary real function - opacity  $\Omega(s, b)$ :

$$a_{el} = i \left[ 1 - e^{-\frac{\Omega(s, b)}{2}} \right]; \quad (5)$$

$$G_{in}(s, b) = 1 - e^{-\Omega(s, b)}; \quad (6)$$

$$\Omega(s, b) = \nu(s) e^{-\frac{b^2}{R^2(s)}}; \quad (7)$$

where Eq. (7) is Pomeron-like parameterization that has been used for numerical estimates. The formula

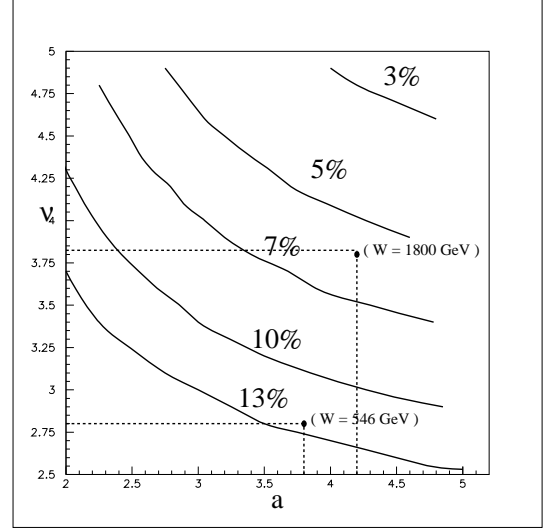


Figure 2. *Survival probability in the eikonal model.*

for survival probability looks as [3] [6]

$$\langle |S|^2 \rangle = \frac{\int d^2b e^{-\frac{b^2}{R_H^2}} e^{-\Omega(s, b)}}{\int d^2b e^{-\frac{b^2}{R_H^2}}} \quad (8)$$

where  $R_H^2$  is radius for the hard processes. In Ref. [6] the values of  $R_H^2$  and  $R^2(s)$  were discussed in details. The main observation is that the experimental value of the ration  $\sigma^{el}/\sigma_{tot}$  depends only on the value of  $\nu$ . This gives us a way to find the value of  $\nu$  directly from the experimental data. The result is plotted in Fig.2 and shows both the small value of the survival probability and its sharp energy dependence.

### 3.2. Three channel model.

The assumption that  $\sigma^{SD}/\sigma^{el} \ll 1$  is in contradiction with the experimental data, therefore, it is interesting to generalize the eikonal model to include processes of the diffractive dissociation. It was done in Ref.[7], where the rich diffractive final state was described by one wave function orthogonal to the hadron

$$\Psi_{hadron} = \alpha \Psi_1 + \beta \Psi_2; \quad \Psi_D = -\beta \Psi_1 + \alpha \Psi_2, \quad (9)$$

where  $\alpha^2 + \beta^2 = 1$ . The scattering amplitude is diagonal with respect functions  $\Psi_{1,2}$  and we used Eq. (5)-Eq. (7) -type parameterization to describe it. The result of our calculation is given in Fig.3.

#### 4. CONCLUSIONS

The experimentally observed value of the survival probability appear naturally in these two models.

The parameters that have been used are in agreement with the more detailed fit of the experimental data.

It turns out that the scale of  $\langle |S_{spectator}|^2 \rangle$  is given by ratios  $R_{el} = \frac{\sigma_{el}}{\sigma_{tot}}$ ,  $R_{SD} = \frac{\sigma_{SD}}{\sigma_{tot}}$  and  $R_{DD} = \frac{\sigma_{DD}}{\sigma_{tot}}$ , but not the ratio  $R_D = \frac{\sigma_{el} + \sigma_{SD} + \sigma_{DD}}{\sigma_{tot}}$ , which does not show any energy dependence.

The further measurement all ratios mentioned above will specify the model and will provide a better predictions for the survival probability. For example, new data on  $R_{DD}$  [11] will specify the value of  $\beta$  which will lead to more definite predictions for  $\langle |S_{spectator}|^2 \rangle$  (see Fig. 3).

#### Acknowledgements:

I am very grateful to A. Gotsman and U. Maor for encouraging optimism and their permanent efforts in hard business of survival of LRG.

#### REFERENCES

1. Yu.L. Dokshitser, V. Khoze and S.I. Troyan, Sov. J. Nucl. Phys. 46 (1987) 116.
2. Yu.L. Dokshitser, V.A. Khoze and T. Sjostrand, Phys. Lett. B274 (1992) 116.
3. J.D. Bjorken, Phys. Rev. D45 (1992) 4077; D47 (1993) 101.
4. A.D. Martin, M.G. Ryskin and V.A. Khoze, Phys. Rev. D56 (1997) 5867; Phys. Lett. B401 (1997) 330.
5. G. Oderda and G. Sterman, Phys. Rev. Lett. 81 (1998) 359; Talk at ISMD'99, Providence, RI, 9-13 Aug 1999, hep-ph/9910414;
6. E. Gotsman, E. Levin and U. Maor, Phys. Rev. D48 (1993) 2097; Nucl. Phys. B493 (1997) 354; Phys. Lett. B438 (1998) 229.
7. E. Gotsman, E. Levin and U. Maor, Phys. Rev. D60 (1999) 094011; Phys. Lett. B438 (1998) B452 (1999) 387, B438 (1998) 229.
8. R.S. Fletcher, Phys. Rev. D48 (1993) 5162; Phys. Lett. B320 (1994) 373.
9. A. Rostovtsev and M.G. Ryskin, Phys. Lett. B390 (1997) 375).
10. E. Levin, A.D. Martin and M.G. Ryskin. J. Phys. G25 (1999) 1507.
11. K. Goulios, talk at this WS.

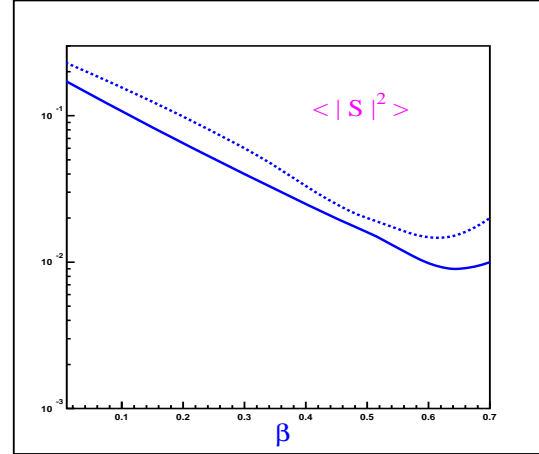


Fig.3-a

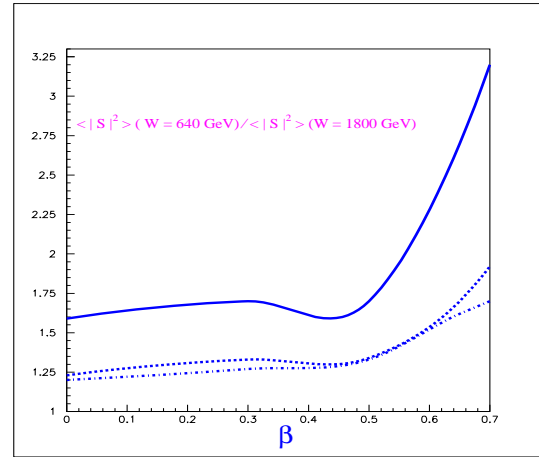


Fig. 3-b

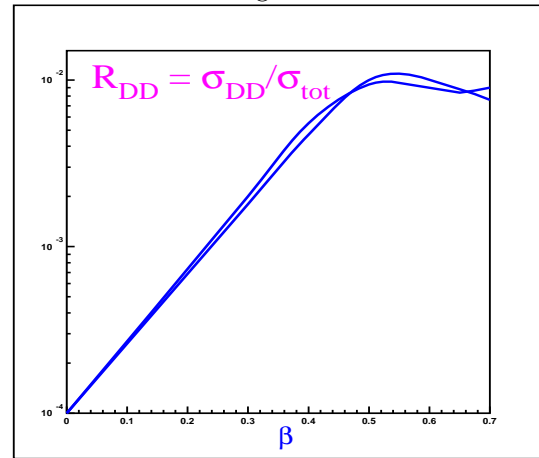


Fig. 3-c

Figure 3. The value of survival probability (Fig.3-a), its energy dependence (Fig.3-b) and prediction for the ratio of double diffraction dissociation to the total cross section (Fig.3-c) versus  $\beta$ .

# Is BFKL ruled out by the Tevatron Gaps between Jets Data?

B.E. Cox, J.R. Forshaw<sup>a</sup> and L. Lönnblad<sup>b</sup>

<sup>a</sup>Department of Physics and Astronomy, University of Manchester, Manchester, M13 9PL, England.

<sup>b</sup>Dept. of Theoretical Physics 2, Sölvegatan 14A, S-223 62 Lund, Sweden.

We have performed a detailed phenomenological investigation of the hard colour singlet exchange process observed at the Tevatron in events that have a large rapidity gap between outgoing jets. We include the effects of multiple interactions to obtain a prediction for the gap survival factor. Comparing the data on the fraction of gap events with the prediction from BFKL pomeron exchange we find agreement provided that a constant value of  $\alpha_s$  is used in the BFKL calculation. Moreover, the value of  $\alpha_s$  is in line with that extracted from measurements made at HERA.

## 1. Introduction

Events with large rapidity gaps in the hadronic final state and a large momentum transfer across the gap, characterized by the presence of a hard jet on each side of the gap, have been observed in both  $p\bar{p}$  collisions at the Tevatron [1–4] and in  $\gamma p$  collisions at HERA [5,6]. Such events are unexpected in standard Regge phenomenology since the cross section is predicted to fall as  $\sim s^{-\alpha|t|}$ , where  $\alpha \simeq 0.25 \text{ GeV}^{-2}$ , whilst events with  $|t| > 1000 \text{ GeV}^2$  are routinely observed at the Tevatron. Clearly some other explanation must be sought. Uniquely in diffractive physics, high- $t$  events are amenable to the use of perturbative QCD since the gap producing mechanism is squeezed to small distances [7]. Such calculations have been carried out within the leading logarithmic approximation of BFKL [8] by Mueller and Tang [9], and it is the aim of this talk to present comparisons of these calculations with the latest data from the Tevatron. The situation is greatly complicated by the possibility that rapidity gaps formed by whatever process can be destroyed by multiple interactions between spectator partons in the colliding hadrons. Detailed comparisons made and conclusions drawn from any dynamic model of high- $t$  rapidity gap formation must therefore include a careful treatment of such physics. In this analysis, we use a model implemented in the PYTHIA Monte Carlo generator to simulate the effects of multi-parton interactions.

## 2. $D\bar{O}$ data versus the BFKL pomeron

The analysis presented here was stimulated to some extent by the recent  $D\bar{O}$  measurements [2] of the fraction of dijet events containing a large rapidity gap as a function of  $E_{T2}$ , the  $E_T$  of the second hardest jet, and the rapidity difference between the two leading jets,  $\Delta\eta$ . The  $D\bar{O}$  results are shown in figure 1. Jets are

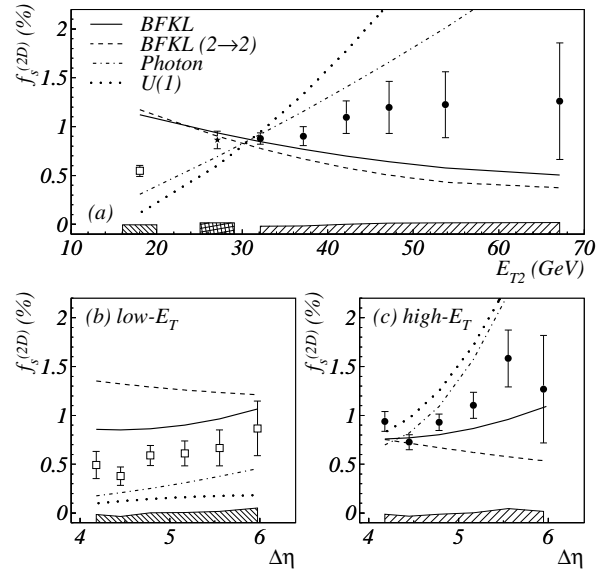


Figure 1.  $D\bar{O}$  data compared with a BFKL calculation. Plot from [2].

found using a cone algorithm [10,11] with cone radius 0.7 and the OVLIM parameter set to 0.5. The inclusive dijet sample is defined by the following cuts:

- $|\eta_1|, |\eta_2| > 1.9$ , i.e. jets are forward or backward
- $\eta_1\eta_2 < 0$ , i.e. opposite side jets
- $E_{T2} > 15 \text{ GeV}$
- $\Delta\eta > 4$ , i.e. jets are far apart in rapidity.

The sub-sample of gap events is obtained by employing the further cut that there be no particles emitted in the central region  $|\eta| < 1$  with energy greater than 300 MeV. The BFKL curve is clearly ruled out by the data. The  $D\bar{O}$  BFKL curves are based on the

calculation of Mueller and Tang implemented into the standard HERWIG 5.9 release [12,22]. In particular, the asymptotic cross-section of [9] is used; in the limit  $y \equiv \Delta\eta \gg 1$ ,

$$\frac{d\sigma(qq \rightarrow qq)}{dt} \approx (C_F \alpha_s)^4 \frac{2\pi^3}{t^2} \frac{\exp(2\omega_0 y)}{(7\alpha_s C_A \zeta(3)y)^3} \quad (1)$$

where  $\omega_0 = \omega(0) = C_A(4 \ln 2/\pi)\alpha_s$ . The  $\alpha_s^4$  in the pre-factor runs with  $-t$  according to the two-loop beta function,  $\omega_0 = 0.3$  and the  $\alpha_s$  in the denominator = 0.25. The falling of the BFKL curve with increasing  $E_{T2}$  is driven by the running of the coupling in the pre-factor since the gap fraction goes like  $\sim \alpha_s^4/\alpha_s^2$ .

### 3. Key issues

In this analysis, we choose somewhat different parameters. We also use the full Mueller Tang calculation without the asymptotic approximation. This is also available in HERWIG 5.9 [23] and is available from the authors. We choose to fix  $\alpha_s = 0.17$ . To leading logarithmic accuracy  $\alpha_s$  is simply an unknown parameter. Higher order corrections will indeed cause the coupling to run, however it is not clear how this should be done in a consistent way. In this paper we restrict ourselves to the leading logarithmic approximation and treat the coupling as a free parameter. Moreover, we are guided by recent HERA data on the double dissociation process [13] which can be described by the leading logarithmic BFKL formalism with  $\alpha_s = 0.17$ . We also note that a fixed coupling constant was needed in order to explain the high- $t$  data on  $p\bar{p}$  elastic scattering via three gluon exchange [14]. Furthermore, NLO corrections suggest a fixed value for the leading eigenvalue of the BFKL equation,  $\omega(0)$ , [15] which in turn suggests the use of a fixed coupling in the LLA kernel.

### 4. Underlying events and gap survival

As mentioned above, it is critical in any estimate of gap formation rates to take into account the possibility that gaps can be destroyed by secondary scatters, which may be perturbative or non-perturbative, between spectator partons in the colliding hadrons. Several models are available [16–18], but it would be fair to say that all are as yet in an early stage of development and are not tuned to  $p\bar{p}$  data. We choose the model as implemented in PYTHIA 6.127 [17]. Here the probability to have several parton-parton interactions in the same collision is modeled using perturbative QCD. The probability for additional interactions is not fixed but varies according to an impact-parameter picture, where central collisions are more likely to have multiple interactions. The partons in the proton are assumed

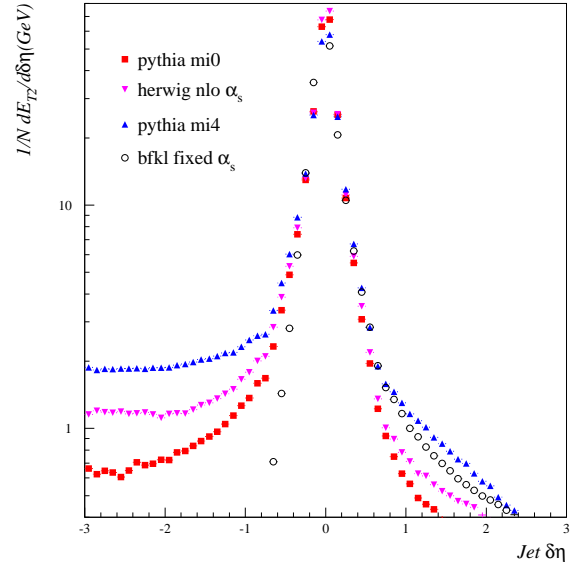


Figure 2. Jet  $\eta$  profiles

to be distributed according to a double-Gaussian as described in [19,17]. There are several parameters in this model and we have used the default setting for each.\* Our strategy is to generate high- $t$  photon exchange events (hard BFKL pomeron exchange has not been implemented in PYTHIA) with and without multiple interactions, and take the percentage change in the number of rapidity gap events, defined as in the DØ analysis, as the gap survival factor. We find that gap survival in this model is to first order independent of  $E_T^{jet}$  and  $\Delta\eta$ , i.e. it can be treated as a multiplicative factor. The gap survival factor  $\mathcal{S}$  does vary strongly with centre of mass energy, which is not unexpected since the number density of partons in the colliding hadrons, and therefore the probability of having a secondary scatter, increases with energy. In summary, we find  $\mathcal{S}(1800 \text{ GeV}) = 22\%$ ,  $\mathcal{S}(630 \text{ GeV}) = 35\%$ . Full details can be found in [20].

A key point to notice is the interplay between gap survival and underlying event: multiple interactions also give rise to the so-called jet pedestal and underlying event effects. This means that the jets measured in hadron-hadron collisions cannot be compared directly to e.g. predictions from fixed order perturbation theory. In Figure 2 we show jet profiles obtained from PYTHIA with (mi4) and without (mi0) multiple inter-

\*Setting the switch `MSTP(82)=4` in PYTHIA, with everything else default, will give the model as we have used it.

actions (and with  $|\delta\phi| < 0.7$ ). The proton remnant is at  $\delta\eta > 0$ . It is clear that multiple interactions introduce a jet pedestal of more than 1 GeV of  $E_T$  per unit rapidity. For comparison, also shown is the jet pedestal from HERWIG. We note that HERWIG predicts a greater amount of energy outside the jet cone than PYTHIA without multiple interactions. Again, a full discussion of these differences can be found in [20].

In the  $D\emptyset$  jet measurements the excess  $E_T$  from the underlying event is taken into account by correcting the jet  $E_T$  using minimum bias data. In particular, the correction is determined by looking at the  $E_T$  flow in regions away from the jets. The correction is made by subtracting approximately 1 GeV from the  $E_T$  of each reconstructed jet [21]. In particular, in the gap fraction measurement, this subtraction is performed for all jets, including those in gap events. But, requiring a large rapidity gap also selects events without multiple interactions, where the jet pedestal is absent, or at least much smaller; multiple interactions destroy gaps, and therefore a gap event *cannot have* a multiple interaction. Since jet cross sections fall faster than  $1/E_T^4$ , such a correction can decrease the measured jet rate by up to 30% for 18 GeV jets. Our contention therefore is that the jets in gap events should not be corrected for underlying event, and therefore the gap fraction should rise less steeply with  $E_T$  than in figure 1.

## 5. Gap fractions

Figures 3 and 4 show our results for the gap fractions as functions of  $\Delta\eta$  and  $E_{T2}$  respectively. The stars are the HERWIG BFKL simulation with fixed  $\alpha_s = 0.17$ , with 1 GeV subtracted from each jet in order to simulate the  $D\emptyset$  underlying event correction and the open circles are the  $D\emptyset$  data. The gap fractions are constructed using a standard PYTHIA QCD simulation without colour singlet exchange, and without multiple interactions. We have used both CTEQ2M and CTEQ3M parton distribution functions [24,25], and have found the differences to be small. Our philosophy is that the  $D\emptyset$  data have been corrected for the effects of multiple interactions in non-singlet exchange events, and we should therefore generate none, whereas we must undo the erroneous correction to the colour singlet sample. The combination of fixing  $\alpha_s$  and correcting the gap events erroneously for multiple interactions produces the rise of the gap fraction at low jet  $E_T$ . The solid circles show the gap fraction using a running  $\alpha_s$  in the BFKL sample. Even with the underlying event correction, this sample is unable to fit the data. The overall normalisation of the simulated gap fractions is multiplied by a factor of 0.6. That this is a reasonable

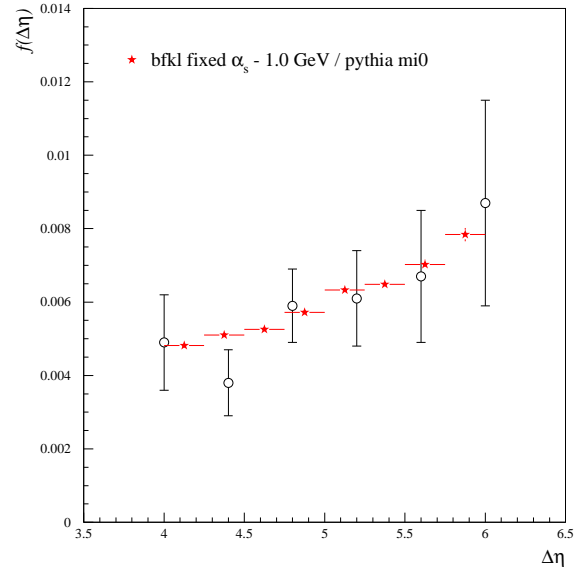


Figure 3. Gap fraction as a function of  $\Delta\eta$  compared to the  $D\emptyset$  data

thing to do can be appreciated once it is realized that our results have not been fitted to the data and that the overall normalization is acutely sensitive to the magnitude of  $\alpha_s$ . Furthermore, the overall normalization of the BFKL cross-section is uncertain since, within the leading logarithmic approximation, one does not know a priori the scale at which to evaluate the leading logarithms. Given these points, we conclude that the  $D\emptyset$  data are in agreement with the leading order BFKL result. Figure 5 shows our result for the gap fraction as a function of  $\Delta\eta \equiv 2\eta^*$  compared to the CDF data [4]. Note that CDF do not attempt to correct their jets to include the effect of an underlying event. We therefore generate the PYTHIA non-singlet sample with multiple interactions (labelled mi4), and do not perform the 1 GeV / jet subtraction from the HERWIG BFKL sample. In this plot, our theory points are obtained using a renormalization factor of unity (compared to 0.6 in the  $D\emptyset$  case). We then find reasonable agreement with the data except at the larger values of  $\eta^*$  where we are quite unable to explain a fall in the  $\eta^*$  distribution. Recall however that  $D\emptyset$  do not see a fall at large  $\Delta\eta$ . Further clarification of the situation will require an increase in statistics.

We have also computed the ratio of the gap fractions at 630 GeV and 1800 GeV. We find that, even including gap survival effects,  $R(630/1800) \sim 1$  at the

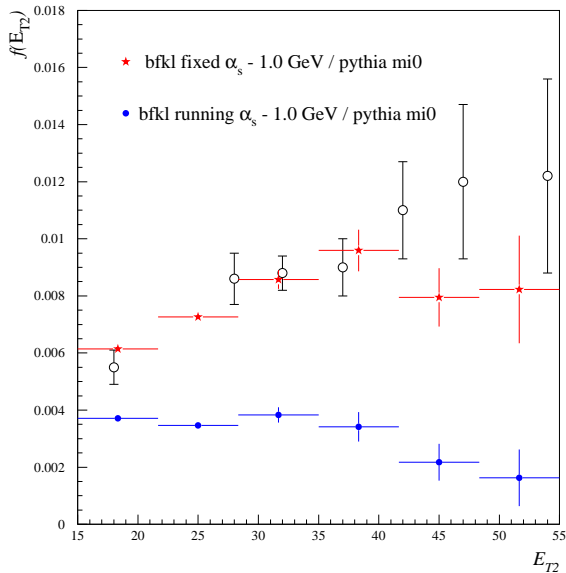


Figure 4. Gap fraction as a function of  $E_{T2}$  compared to the  $D\emptyset$  data

parton level. When hadronization effects are taken into account, however, we find that the ratio rises significantly to  $\sim 3$ , with a strong dependence on  $\Delta\eta$ .  $D\emptyset$  find  $R(630/1800) = 3.4 \pm 1.2$  [2], and CDF find  $R(630/1800) = 2.4 \pm 0.9$ . In the  $D\emptyset$  case the effect may be attributed to the different parton  $x$  ranges of the 630 GeV and 1800 GeV measurements (although we note that the CDF result is calculated at fixed  $x$ ). The restriction  $x < 1$  forces the gap and non-gap cross-sections to fall to zero at some maximum  $\Delta\eta$ ,  $\Delta\eta_{\max}$ . Now, the colour connection that exists between the jets in the non-gap sample drags the jets closer together in rapidity. This has a small effect away from  $\Delta\eta_{\max}$  (since the  $\Delta\eta$  spectrum is roughly flat) however as  $\Delta\eta \rightarrow \Delta\eta_{\max}$  it leads to a more rapid vanishing of the non-gap cross-section than occurs in the gap cross-section. This effect, combined with the fact that  $\Delta\eta_{\max}(630 \text{ GeV}) < \Delta\eta_{\max}(1800 \text{ GeV})$ , leads to an enhancement of the measured 630 GeV gap fraction at large  $\Delta\eta$  at the hadron level, and hence the larger value of  $R(630/1800)$ .

## 6. Conclusions and future possibilities

We have explicitly demonstrated that the Tevatron data on the gaps-between-jets process at both 630 GeV and 1800 GeV are in broad agreement with the predic-

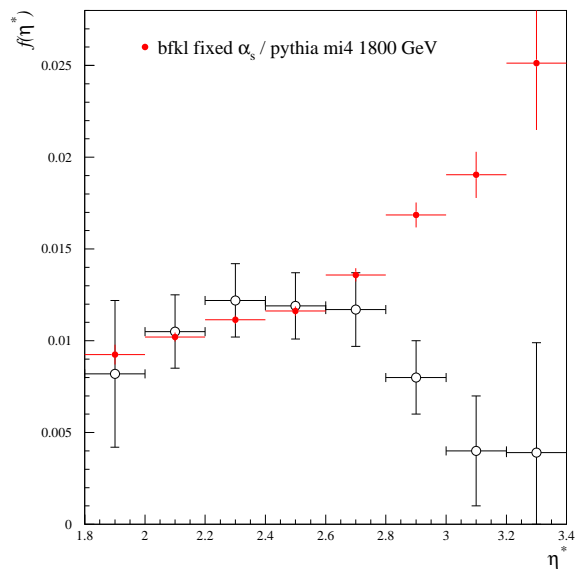


Figure 5. Gap fraction compared to the CDF data

tions obtained using the leading order BFKL formalism. However, we are not able to explain the behaviour of the CDF gap fraction at large  $\Delta\eta$ . Agreement is obtained using the same fixed value of  $\alpha_s = 0.17$  as was used to explain the recent HERA data on high- $t$  double diffraction dissociation.

Care must be taken in the interpretation of our findings, however. The BFKL formalism itself suffers from being evaluated only to leading logarithmic accuracy. The uncertainties of the overall normalization which follow will not be removed until an understanding of BFKL dynamics at non-zero  $t$  beyond the leading logarithmic approximation is achieved.

An understanding of the effects of underlying event and its impact on gap survival is crucial to the interpretation of the gaps between jets data, and indeed diffractive data as a whole.

As pointed out in [9,20], the gap fraction defined in terms of a region void of hadronic activity is not strictly infrared safe. A better observable would be to define a gap to be a region that does not contain any jets with transverse momenta above some perturbatively large scale. Work along these lines has also been performed in [26].

One major disadvantage of the gaps between jets process arises from the need to measure both jets since this limits the reach in rapidity. In [27], it was suggested to focus instead on the double dissociation sam-

ple (the gaps between jets events form a subsample of this generally much larger sample). By dropping the requirement to observe jets one not only gains in rapidity reach and statistics but also from the reduced systematics associated with this more inclusive observable.

### Acknowledgements

We should like to thank Andrew Brandt, Dino Goulianos, Mark Hayes, Mike Seymour and Torbjörn Sjöstrand for helpful discussions. This work was supported by the EU Fourth Framework Programme ‘Training and Mobility of Researchers’, Network ‘Quantum Chromodynamics and the Deep Structure of Elementary Particles’, contract FMRX-CT98-0194 (DG 12-MIHT). BC would like to thank the UK’s Particle Physics and Astronomy Research Council for support.

### REFERENCES

1. S. Abachi et al (DØ Collaboration), Phys. Rev. Lett. **72** (1994) 2332; Phys. Rev. Lett. **76** (1996) 734.
2. B. Abbott et al (DØ Collaboration), Phys. Lett. **B81** (1998) 189.
3. F. Abe et al (CDF Collaboration), Phys. Rev. Lett. **74** (1995) 855; Phys. Rev. Lett. **80** (1998) 1156.
4. F. Abe et al (CDF Collaboration), Phys. Rev. Lett. **81** (1998) 5278.
5. M. Derrick et al (ZEUS Collaboration), Phys. Lett. **B369** (1996) 55.
6. H1 Collaboration, “Rapidity gaps between jets in Photoproduction at HERA”, contribution to the International Europhysics Conference on High Energy Physics, Jerusalem, Israel (1997).
7. J.R. Forshaw and P.J. Sutton, Euro. Phys. J. **C14** (1998) 285.
8. I. Balitsky and L.N. Lipatov, Sov. J. Nucl. Phys. **28** (1978) 822.
9. A. H. Mueller and W. -K. Tang, Phys. Lett. **B284** (1992) 123.
10. S.D. Ellis, private communication to the OPAL Collaboration; D.E. Soper and H.-C. Yang, private communication to the OPAL Collaboration; L.A. del Pozo, University of Cambridge PhD thesis, RALT-002 (1993); R. Akers et al (OPAL Collaboration), Z. Phys. **C63** (1994) 197.
11. F. Abe et al (CDF Collaboration), Phys. Rev. **D45** (1992) 1448.
12. G. Marchesini et al, Comp. Phys. Comm. **67** (1992) 465.
13. H1 Collaboration, “Double Diffraction Dissociation at large  $|t|$  in Photoproduction at HERA”, contribution to the 29th International Conference on High-Energy Physics ICHEP98, Vancouver, Canada, 1998; B. E. Cox, “Double Diffraction Dissociation at large  $|t|$  from H1”, contribution to the DIS99 Workshop, Zeuthen, Germany (1999) hep-ph/9906203.
14. A. Donnachie and P. V. Landshoff, Z. Phys. **C2** (1979) 55, erratum-ibid **C2** (1979) 372; Phys. Lett. **B387** (1996) 637.
15. S. J. Brodsky et al, “The QCD Pomeron with Optimal Renormalisation”, SLAC-PUB-8037, IITAP-98-010, hep-ph/9901229.
16. E. Gotsman, E. Levin, U. Maor, Phys. Lett. **B438** (1998) 229; Phys. Rev. **D60** (1999)
17. PYTHIA version 6.127, program and manual, T. Sjöstrand, Comput. Phys. Comm. **82** (1994) 74.
18. J. M. Butterworth, J. R. Forshaw and M. H. Seymour, Zeit. für Phys. **C72** (1996) 637-646.
19. T. Sjöstrand and M. van Zijl, Phys. Rev. **D36** (1987) 2019
20. B.E.Cox, J.R. Forshaw, L.Lönnblad, JHEP10(1999)023.
21. B. Abbott et al (DØ Collaboration), Nucl. Instrum. Methods **A424** (1999) 352.
22. J. M. Butterworth, M. E. Hayes, M. H. Seymour and L. E. Sinclair, “Rapidity gaps between jets”, in the proceedings of the Workshop ‘Future Physics at HERA’, eds. G. Ingelman, A. de Roeck and R. Klanner, DESY (1996).
23. M. E. Hayes, University of Bristol PhD Thesis (1997).
24. H. L. Lai et al, Phys. Rev. **D55** (1997) 1280.
25. H. Plochow-Besch, “PDFLIB User’s Manual”, W5051 PDFLIB, 1997.07.02, CERN-PPE; Int. J. Mod. Phys. **A10** (1995) 2901.
26. G. Oderda and G. Sterman, Phys. Rev. Lett. **81**, 3591 (1998).
27. B. E. Cox and J. R. Forshaw, Phys. Lett. **B434** (1998) 133-140.

# Interjet Energy and Color Flow

George Sterman<sup>a</sup>

<sup>a</sup>C.N. Yang Institute for Theoretical Physics  
SUNY, Stony Brook, NY 11794-3840, USA

Rapidity gap events are conventionally defined by requiring no particle production in a gap region. In the case of dijet events, the distribution of energy,  $E_{\text{gap}}$ , that flows into the interjet region is calculable in perturbative QCD nearly down to  $E_{\text{gap}} = 0$ , and sheds light on the role of color exchange in hard scattering. Distributions are calculable for  $E_{\text{gap}}$  as a function of scattering angle, momentum transfer and gap width. The concept of a hard color singlet exchange is clarified.

## 1. GAPS AND COLOR FLOW

A compelling heuristic principle suggests that the exchange of gluons in a color singlet state produces little radiation even when the scattering produces jets at high  $p_T$  [1]. The correspondence has such currency that dijet gap events are routinely termed “color singlet exchange”. This insight, however, has been difficult to implement in perturbative terms. After all, gluons of any energy carry octet color charge, so that there is no unique way of defining color exchange in a finite amount of time [2]. On the other hand, it takes a very short time to radiate a hard gluon, and once radiated, it cannot be reabsorbed on the basis of soft color rearrangements at very long times.

### 1.1. Two-gluon vs. Soft Color Models

The simplest short-distance model for dijet gaps is based on two-gluon exchange [1]. In a two-gluon model, the gap is usually filled by spectator interactions, up to a “survival probability”,  $P_S$ , which may be estimated [1,3] from low- $p_T$  diffractive scattering to be of order one tenth. Denoting the probability for hard color-singlet exchange as  $f_1$ , the fraction of gap events becomes

$$f_{\text{gap}} = f_1 P_S. \quad (1)$$

If we estimate  $f_1 \sim \mathcal{O}(\alpha_s(p_T)/\pi) \sim 0.1$ , we predict gap events at the one percent level, and this is what is seen experimentally [4–7]. This analysis would lead us to expect more gap events from gluon-gluon than quark-quark scattering, because of the larger color factors in exchange graphs between gluons. This expectation was tested by comparing 630 and 1800 GeV data from the Tevatron, because at fixed  $p_T$  the role of gluon-gluon scattering increases with the overall center-of-mass energy. The proportion of gap events, however, decreased, rather than increased, with the energy.

In the soft color approach [8], normally presented as an alternative to the two-gluon model, the underlying hard scattering is treated at lowest order, which for gap

events is primarily single-gluon, color octet exchange. The gap probability is determined by counting possible color exchanges, assuming all to be equally likely, up to an overall survival factor (rather larger than 1/10). Because gluons have more color states than quarks, they are correspondingly less likely to produce gap events. The soft color model then naturally leads to fewer gap events as the energy, and hence the role of gluons, increases.

### 1.2. Energy Flow

A third approach is a perturbative QCD formalism for rapidity gaps, made possible by redefining gaps in terms of an energy flow,  $E_{\text{gap}}$ , rather than particle multiplicity [9]. The resulting cross sections can be treated via standard factorization theorems. In this formulation, if  $E_{\text{gap}} \gg \Lambda_{\text{QCD}}$  the cross section is perturbatively calculable. In addition, when  $p_T \gg E_{\text{gap}} \gg \Lambda_{\text{QCD}}$ , the gap cross sections have two perturbative scales, and logarithms in their ratio can be resummed by renormalization group methods.

Resummation in  $\ln(E_{\text{gap}}/p_T)$  allows us to probe color flow at short distances, and to generalize the concept of hard color singlet exchange.

The dijet cross section at measured  $E_{\text{gap}} \gg \Lambda_{\text{QCD}}$  falls into the class of inclusive jet cross sections that can be written in factorized form:

$$\begin{aligned} \frac{d\sigma}{dE_{\text{gap}} d\cos\hat{\theta}}(\Delta y) &= \sum_{f_A, f_B} \phi_{f_A/p} \otimes \phi_{f_B/\bar{p}} \\ &\otimes \sum_{f_C, f_D} \frac{d\hat{\sigma}^{(f)}}{dE_{\text{gap}} d\cos\hat{\theta}}(\Delta y), \quad (2) \end{aligned}$$

with the  $\phi_{f/h}$  parton distributions, evaluated at the scale of the dijet momentum transfer. The partonic cross section  $d\hat{\sigma}^{(f)}/dE_{\text{gap}} d\cos\hat{\theta}$  is a hard scattering function, starting with the Born cross section at lowest order (cf. the soft color model). The index  $f$  denotes the partonic hard scattering  $f_A + f_B \rightarrow f_C + f_D$ . The cross section depends on the dijet pair rapidity  $y_{JJ}$ , the partonic center-of-mass (c.m.) energy

squared  $\hat{s}$ , the partonic c.m. scattering angle  $\hat{\theta}$ , with  $-\frac{\hat{s}}{2}(1 - \cos \hat{\theta}) = \hat{t}$ , and  $\Delta y$ , the gap size as a rapidity interval.

## 2. INTERJET ENERGY DISTRIBUTION

To leading logarithm in  $E_{\text{gap}}/\sqrt{-\hat{t}}$ , the gap energy dependence is of the form

$$\frac{d\hat{\sigma}^{(f)}}{dE_{\text{gap}} d\cos\hat{\theta}}(\Delta y) = \sum_{\beta\gamma} \bar{\sigma}_{\beta\gamma}(\hat{\theta}) \times \frac{E_{\gamma\beta}}{E_{\text{gap}}} \left[ \ln\left(\frac{E_{\text{gap}}}{\Lambda}\right) \right]^{E_{\gamma\beta}-1} \left[ \ln\left(\frac{\sqrt{-\hat{t}}}{\Lambda}\right) \right]^{-E_{\gamma\beta}}. \quad (3)$$

In this expression,  $\beta$  and  $\gamma$  label the color exchange at short distances, contained in  $\bar{\sigma}$ , in a color tensor basis that diagonalizes a perturbative anomalous dimension matrix. The exponents  $E_{\gamma\beta}$  are given in terms of the eigenvalues,  $\lambda_\beta = (\alpha_s/\pi)\lambda_\beta^{(1)}$ , of this matrix by

$$E_{\gamma\beta}(\hat{\theta}, \Delta y) = \frac{2}{\beta_0} \left[ \lambda_{\gamma}^{(1)*} + \hat{\lambda}_{\beta}^{(1)} \right], \quad (4)$$

with  $\beta_0 = 11N_c/3 - 2n_f/3$ . The color exchange with smallest eigenvalue thus dominates the behavior of the cross section in the limit  $E_{\text{gap}}/p_T \rightarrow 0$ .

The concept of a dominant eigenvalue generalizes conventional hard singlet exchange, because the eigenvectors of the anomalous dimension matrix are linear combinations of elements in the basis of  $t$ -channel color transfers. The coefficients depend, in general, on the jet scattering angle. Eq. (3) thus leads to a detailed set of predictions for dijet data with measured interjet energy flow.

Explicit anomalous dimension eigenvalues  $\lambda_\alpha$  for quark and gluon processes may be found in Ref. [10]. The overlap of the dominant eigenvector with hard color singlet exchange grows in the direction of forward scattering for all partonic processes, so that in the Regge limit,  $-\hat{t}/\hat{s} \rightarrow 0$ ,  $\hat{t}$  fixed, the dominant color exchange becomes purely color singlet [11]. In addition, the eigenvalues for gluon-gluon scattering are larger than those for processes involving quarks. This makes it harder for gluon-gluon hard scattering to produce rapidity gaps, for much the same reasons as in the soft color model: the size of the eigenvalue  $\lambda_\alpha$  is related to the number of color states available. At low interjet energy, however, the smallest eigenvalue for quark-antiquark scattering is actually less than unity in absolute value, and produces a small upturn in the interjet energy distribution in predictions based on Eq. (3) [9]. This is the ‘‘hard singlet exchange’’ observed by CDF and D0 [4,5]. Gap events defined by vanishing particle multiplicity in the interjet region are counted

in this excess. The perturbative predictions for such events must be diluted, as usual, by corrections associated with spectator interactions, which, according to the factorization formalism, are suppressed only by powers of  $\Lambda_{\text{QCD}}/E_{\text{gap}}$ , and which therefore become important for small  $E_{\text{gap}}$ . We have in Eqs. (2)-(4), however, a set of predictions for the full range of  $E_{\text{gap}}$ .

## 3. SUMMARY

Energy flow analysis makes possible a quantitative study of radiation in interjet regions, and gives a perturbative meaning to short-distance color exchange, generalizing both the two-gluon and soft color models. On the basis of this analysis, gaps in dijet events come from a compound structure, predominantly, but not purely, singlet in the hard scattering [9,10]. Many qualitative results, including the relative suppression of dijet gaps for gluon-gluon scattering, are consistent with the successes of the soft color model. The perturbative analysis offers a systematic set of differential predictions for energy flow, as a function of momentum transfer, flavor and interjet rapidity interval.

## REFERENCES

1. J.D. Bjorken, Phys. Rev. D **47**, 101 (1993).
2. R. Oeckl and D. Zeppenfeld, Phys. Rev. D **58** 014003 (1998), hep-ph/9801257.
3. E. Gotsman, E. Levin and U. Maor, Phys. Lett. B **309**, 199 (1993); Phys. Lett. B **452** 387 (1999) hep-ph/9901416.
4. F. Abe *et al.* (CDF Collaboration) Phys. Rev. Lett. **74**, 855 (1995); Phys. Rev. Lett. **80**, 1156 (1998).
5. S. Abachi *et al.* (D0 Collaboration) Phys. Rev. Lett. **76**, 734 (1996).
6. B. Abbott *et al.* (D0 Collaboration) Phys. Lett. B **440** 189 (1998); F. Abe *et al.* (CDF Collaboration) Phys. Rev. Lett. **81** 5278 (1998).
7. M. Derrick *et al.* (ZEUS Collaboration), Phys. Lett. B **369**, 55 (1996).
8. O.J.P. Eboli, E.M. Gregores and F. Halzen, Phys. Rev. D **58** 114005 (1998).
9. G. Oderda and G. Sterman, Phys. Rev. Lett. **81** 3591 (1998), hep-ph/9806530.
10. G. Oderda, Stony Brook report ITP-SB-98-70, Mar 1999, hep-ph/9903240.
11. V. Del Duca and W.-K. Tang, Phys. Lett. B **312**, 225 (1993).

# Color Evaporation Induced Rapidity Gaps

O. J. P. Éboli<sup>a\*</sup>, E. M. Gregores<sup>a</sup>, and F. Halzen<sup>b</sup>

<sup>a</sup>Instituto de Física Teórica, Universidade Estadual Paulista  
Rua Pamplona 145, 01405–900, São Paulo – SP, Brazil

<sup>b</sup>Department of Physics, University of Wisconsin  
Madison, WI 53706, USA

We show that soft color rearrangement of final states can account for the appearance of rapidity gaps between jets. In the color evaporation model the probability to form a gap is simply determined by the color multiplicity of the final state. This model has no free parameters and reproduces all data obtained by the ZEUS, H1, DØ, and CDF collaborations.

## 1. Introduction

The inclusion of soft color interactions between the dynamical partons leads to a parameter-free calculation of the formation rate of rapidity gaps. The idea is extremely simple. A rapidity gap occurs whenever final state partons form color singlet clusters separated in rapidity. As the partons propagate within the hadronic medium, they exchange soft gluons which modify the string configuration. The probability to form a rapidity gap is then determined by the color multiplicity of the final states formed by the dynamical partons, and nothing else. All data obtained by ZEUS, H1, DØ, and CDF collaborations are reproduced when this color structure of the interactions is superimposed on the usual perturbative QCD calculation for the production of the hard jets. We pointed out [1] that this soft color mechanism is identical to the color evaporation mechanism [2] for computing the production rates of heavy quark pairs produced in color singlet onium states, like  $J/\psi$ . Moreover, we also suggested that the soft color model could provide a description for the production of rapidity gaps in hadronic collisions [1].

The success of the color evaporation model to explain the data on quarkonium production is unquestionable [3]. We showed [5] that the straightforward application of the color evaporation approach to the string picture of QCD readily explains the formation of rapidity gaps between jets at the Tevatron and HERA colliders.

## 2. Color Counting Rules

In the color evaporation scheme for calculating quarkonium production, it is assumed that all color configurations of the quark pair occur with equal probability. We propose that the same color counting applies to the final state partons in high  $E_T$  jet production. In complete analogy with quarkonium, the pro-

duction of high energy jets is a two-step process where a pair of high  $E_T$  partons is perturbatively produced at a scale  $E_T$ , and hadronize into jets at a scale of order  $\Lambda_{QCD}$  by stretching color strings between the partons and spectators. The strings subsequently hadronize. Rapidity gaps appear when a cluster of dynamical partons, *i.e.* interacting partons or spectators, form a color singlet. As before, the probability for forming a color singlet cluster is inversely proportional to its color multiplicity.

The soft color procedure is obvious in a specific example: let us calculate the gap formation probability for the subprocesses  $p\bar{p} \rightarrow Q^V \bar{Q}^V \rightarrow Q\bar{Q}XY$ , where  $Q^V$  stands for  $u$  or  $d$  valence quark, and  $X$  ( $Y$ ) is the diquark remnant of the proton (antiproton). The final state is composed of the  $X$  ( $\mathbf{3} \otimes \mathbf{3}$ ) color spectator system with rapidity  $\eta_X = +\infty$ , the  $Y$  ( $\bar{\mathbf{3}} \otimes \bar{\mathbf{3}}$ ) color spectator system with  $\eta_Y = -\infty$ , one  $\mathbf{3}$  parton  $j_1$ , and one  $\bar{\mathbf{3}}$  parton  $j_2$ . It is the basic assumption of the soft color scheme that by the time these systems hadronize, any color state is equally likely. One can form a color singlet final state between  $X$  and  $j_1$  since  $\mathbf{3} \otimes \mathbf{3} \otimes \mathbf{3} = \mathbf{10} \oplus \mathbf{8} \oplus \mathbf{8} \oplus \mathbf{1}$ , with probability  $1/27$ . Because of overall color conservation, once the system  $X \otimes j_1$  is in a color singlet, so is the system  $Y \otimes j_2$ . Moreover, to form a rapidity gap these systems ( $j_1 \otimes X$  and  $j_2 \otimes Y$ ) must not overlap in rapidity space. In this configuration, the color strings linking the remnant and the parton will not hadronize in the region between the two jets. We have thus produced two jets separated by a rapidity gap using the color counting rules which form the basis of the color evaporation scheme for calculating quarkonium production.

## 3. Rapidity Gaps at HERA

The differential cross section has two sources of gap events: color evaporation gaps ( $d\sigma_{cem}^{gap}$ ) and background gaps ( $d\sigma_{bg}^{gap}$ ). In our model, the gap cross sec-

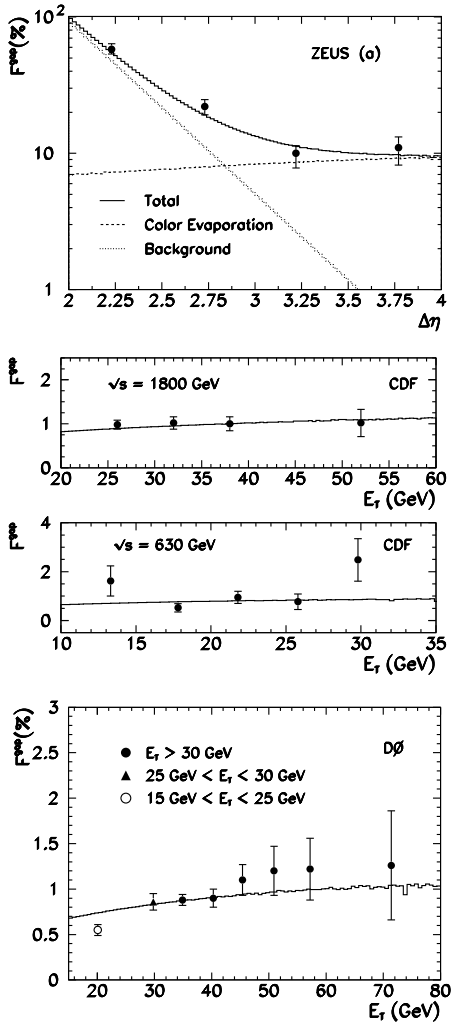


Figure 1. Frequency of events with rapidity gap between jets as a function of the gap size  $\Delta\eta$  in  $\gamma p$  collisions, and as function of the jets transverse energy in  $p\bar{p}$  collisions.

tion is the weighted sum over resolved events,  $d\sigma_{cem}^{gap} = \sum_N F_N d\sigma_{res}^N$ , with gap probability  $F_N$  for the different processes. Background gaps are formed when the region of rapidity between the jets is devoid of hadrons because of statistical fluctuation of ordinary soft particle production. Their rate should fall exponentially as the rapidity separation  $\Delta\eta$  between the jets increases. We parametrize the background gap probability as  $F_{bg}(\Delta\eta) = e^{b(2-\Delta\eta)}$ , where  $b$  is a constant. The background gap cross section is then written as  $d\sigma_{bg}^{gap} = F_{bg}(\Delta\eta)d\sigma^{jets} - d\sigma_{cem}^{gap}$ .

The gap frequency  $F^{gap}(\Delta\eta) = d\sigma^{gap}/d\sigma^{jets}$  is shown in the figure, where we depict the contributions of the color evaporation mechanism and the back-

ground.

#### 4. Rapidity Gaps at Tevatron

The color evaporation model prediction for the gap production rates in  $p\bar{p}$  collisions is analogous to the one in  $p\gamma$  interactions, with the obvious replacement of the photon by the antiproton, represented as a  $\bar{\mathbf{3}} \otimes \bar{\mathbf{3}} \otimes \bar{\mathbf{3}}$  system.

The distributions presented by CDF are normalized to unity on average. Therefore our predictions do not exhibit any free parameter to be adjusted. In the figure we compare our predictions with CDF results of the gap fraction as a function of the jets transverse energy. To compare with DØ results we assumed an *ad-hoc* survival probability of 30%.

We can also compare the ratio  $R = F_{630}^{gap}/F_{1800}^{gap}$  with the experimental result. DØ has measured this fraction for jets with  $E_T > 12$  GeV for both energies, and they found  $R = 3.4 \pm 1.2$ ; we predict  $R = 2.5 \pm 0.5$ . On the other hand, CDF measured this ratio using different values for  $E_T^{min}$  at 630 GeV and 1800 GeV; they obtained  $R = 2.0 \pm 0.9$  while we obtained  $R = 2.0 \pm 0.4$  for the same kinematical arrangement.

#### 5. Conclusion

In summary, the occurrence of rapidity gaps between hard jets can be understood by simply applying the color evaporation scheme for calculating quarkonium production to the conventional perturbative QCD calculation of the production of hard jets. The agreement between data and this model is impressive.

#### REFERENCES

1. J. Amundson, O. J. P. Éboli, E. M. Gregores, and F. Halzen, Phys. Lett. **B372**, 127 (1996).
2. H. Fritzsch, Phys. Lett. **B67**, 217 (1977); F. Halzen, Phys. Lett. **B69**, 105 (1977).
3. R. Gavai *et al.*, Int. J. Mod. Phys. **A10**, 3043 (1995); J. Amundson, O. J. P. Éboli, E. M. Gregores, and F. Halzen, Phys. Lett. **B390**, 323 (1997); O. J. P. Éboli, E. M. Gregores, and F. Halzen, Phys. Lett. **B395**, 113 (1997); *ibidem* **451**, 241 (1999); *idem*, Phys. Rev. D **60**, 117501 (1999).
4. O. J. P. Éboli, E. M. Gregores, and F. Halzen, Phys. Rev. D **58**, 114005 (1998).
5. O. J. P. Éboli, E. M. Gregores, and F. Halzen, MADPH-99-1135, Aug 1999, hep-ph/9908374.

# Monte Carlo Simulation of Color Singlet Exchange Between Jets

R. Engel<sup>a</sup> and J. Ranft<sup>b</sup>

<sup>a</sup>University of Delaware, Bartol Research Institute, Newark, DE 19716, USA

<sup>b</sup>Physics Dept. Universität Siegen, D-57068 Siegen, Germany

## 1. Introduction

Rapidity gaps between jets are an ideal configuration for searching for new-physics signatures [1]. They also provide a clean environment for testing the dynamics of perturbative QCD in Regge limit [2]. The large rapidity difference between the jets together with the transverse momentum of the two back-to-back pointing jets ensure that the center of mass energy of the hard process is much greater than its typical hard scale. In literature, alternative calculations have been proposed for such processes including the approximation of the  $n$ -gluon exchange by a BFKL pomeron [2,3] and soft color recombination (evaporation) [4,5]. Both models predict different dependences of the rapidity gap event fraction on the width of the rapidity gap and on the jet transverse momentum.

In this paper we shall calculate the experimentally observable cross section for color singlet exchange between jets using a detailed Monte Carlo simulation of both parton-parton interactions producing rapidity gaps and non-perturbative processes giving rise to the “underlying event”. We use the model PHOJET [6,7] which treats perturbative QCD effects such as hard parton-parton scattering and parton showers as well as non-perturbative effects like soft hadronic interactions. This model is based on the Dual Parton Model [8] in its two-component version [9].

## 2. Implementation of color evaporation model

To describe events with color singlet exchange between jets within the PHOJET Monte Carlo, we implement a soft color reconnection (SCR) model [4,5,10]. The simplest hard  $q$ - $q$  event, where SCR leads to a rapidity gap between two jets is an event with just one single hard valence-quark – valence-quark scattering. In normal events in the Dual Parton Model we get two color strings each being stretched between one scattered quark and the diquark of the other hadron. Large rapidity gaps are exponentially suppressed in such events. However, SCR can cause a color transfer due to the exchange of soft gluons resulting in a color configuration where the strings connect the hard scat-

tered quark and the diquark of the same hadron. These are events with might lead to hadronic final states with a large rapidity gap between two jets. In PHOJET, we use the following probabilities of color singlet exchange  $F_{qq} : F_{qg} : F_{gg} = 1/9 : 1/24 : 1/64$  [4].

In most of the hard scattering events we have a non-negligible contribution from the underlying event, mainly resulting from spectator interactions. Thus, even if a rapidity gap appears in one of the partonic collisions, the gap might be filled by hadrons produced in another parton-parton interaction. Furthermore, hard parton radiation (initial and final state radiation) can change the size of rapidity gaps considerably. Both effects are simulated in our Monte Carlo calculation which includes QCD parton showers and multiple soft and hard interactions as implemented in PHOJET. This means that the probability for the gap survival [1] is calculated in detail.

## 3. Comparison to data

Both the D0 and CDF collaborations have published data on dijet production with rapidity gaps [11–17]. In the following we will concentrate on the D0 data [14]. Further comparisons of our calculations with data can be found in [18–20].

D0 [14] uses at  $\sqrt{s} = 1800$  GeV two different triggers. With the high  $E_{\perp}$  trigger (we refer to this in short as D0-h) they find opposite side ( $\eta^{\text{jet}1} \times \eta^{\text{jet}2} < 0$ ) dijets with  $E_{\perp}^{\text{jet}1-2} > 30$  GeV and  $|\eta^{\text{jet}}| > 2$ . The pseudorapidity gap is at  $|\eta| < 1.3$ . With this the fraction of JgJ events is found to be  $R_{\text{JgJ-D0-h}} = (\text{JgJ})/(\text{JJ}) = (0.94 \pm 0.04(\text{stat}) \pm 0.12(\text{syst}))$ .

With the low  $E_{\perp}$  trigger (we refer to this in short as D0-l) they find at  $\sqrt{s} = 1800$  GeV opposite side ( $\eta^{\text{jet}1} \times \eta^{\text{jet}2} < 0$ ) dijets with  $E_{\perp}^{\text{jet}1-2} > 12$  GeV and  $|\eta^{\text{jet}}| > 2$ . The pseudorapidity gap is at  $|\eta| < 1.3$ . With this the fraction of JgJ events is found to be  $R_{\text{JgJ-D0-l}} = (\text{JgJ})/(\text{JJ}) = (0.54 \pm 0.06(\text{stat}) \pm 0.16(\text{syst}))$ . In PHOJET we find with the D0 triggers  $R_{\text{JgJ-PHOJET-D0-h}} = 1.06\%$  ,  $R_{\text{JgJ-PHOJET-D0-l}} = 0.45\%$  . Here the background JgJ events with only an accidental gap were subtracted. These PHOJET results

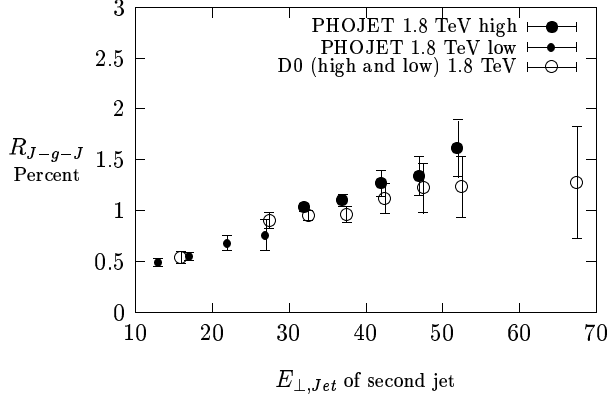


Figure 1. The change of  $R_{JgJ}$  with the  $E_{\perp}^{jet2}$  of the next to leading jet. Data from the D0 Collaboration are compared to the PHOJET results obtained with SCR.

are fully consistent with the experimental data. The same is found comparing to the 630 GeV data and to the CDF data. The change of  $R_{JgJ}$  with the  $E_{\perp}^{jet2}$  of the second leading jet was studied by the D0 Collaboration [14]. A modest rise of the color singlet fraction with  $E_{\perp}^{jet2}$  was found. In Fig. 1 we compare the PHOJET results on  $R_{JgJ}$  with these data. The PHOJET predictions exhibit a  $E_{\perp}^{jet2}$  dependence being compatible with the data. The D0 Collaboration [14] also studied for the D0-h and D0-l triggers the dependence of  $R_{JgJ}$  on  $\Delta\eta = |\eta^{jet1} - \eta^{jet2}|$ . For both triggers a slight rise of  $R_{JgJ}$  with  $\Delta\eta$  was found which is well described by the PHOJET simulations (not shown here). It is important to notice that our calculation does not only describe the rise of  $R_{JgJ}$  with  $E_{\perp}^{jet2}$  and  $\Delta\eta$ , but also reproduces the absolute sizes of  $R_{JgJ}$  without free parameters.

We also compared the pseudorapidity distributions of charged hadrons of events passing the D0-h and D0-l triggers with and without gap. The remarkable feature of this comparison is, that the opposite side jet trigger without the gap requirement selects events with much higher rapidity distribution (particle multiplicity) than typically found in minimum bias events. We interpret this in the following way. With the jet trigger events are selected with an exceptional large number of soft and hard multiple interactions and parton emissions.

#### 4. Rapidity gap survival probability

The rapidity gap survival probability  $\langle |S|^2 \rangle$  was originally defined by Bjorken [1]. In a series of recent papers, Gotsman, Levin and Maor [21–23] use a eikonal

model to calculate the energy dependence of  $\langle |S|^2 \rangle$ . For example, they obtain in  $p\bar{p}$  collisions at 630 (1800) GeV values of 16.3% (5.6 %) [22]. The eikonal model used in PHOJET is a two-channel model which differs certainly from the one used by Gotsman et al., but the gap survival probability as contained in the PHOJET Monte Carlo events is calculated in a rather analogous way. We can use the JgJ events and JJ events obtained from PHOJET for given trigger conditions to give the gap survival probability according to PHOJET.

In the PHOJET Monte Carlo we can subdivide the hard scattering events into g-g, g-q and q-q scatterings. We calculate (not shown here) for the D0-h and D0-l triggers the fractions or weights  $W_{JJ}^i$  for  $i = g-g, g-q$  and  $q-q$  events for JJ events (without gap trigger),  $W_{JgJ}^i$  for JgJ events obtained with SCR and  $W_{JgJbg}^i$  for background JgJ events (obtained without SCR). We find, that q-q scattering dominates the JgJ events, but g-q and g-g scattering contributes also.

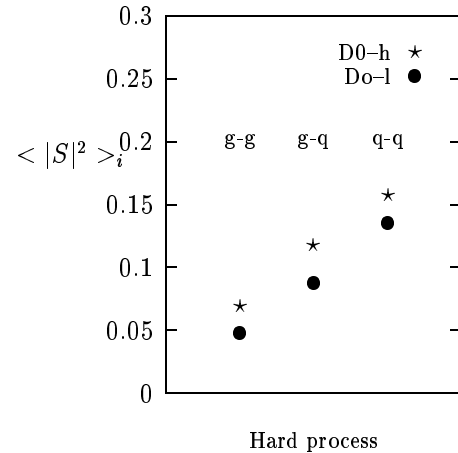


Figure 2. The gap survival probabilities  $\langle |S|^2 \rangle_i$  according to PHOJET given separately for  $i = g-g, g-q$  and  $q-q$  events and for the D0-h and D0-l triggers.

Starting from the JJ and JgJ weights  $W_{JJ}^i$  and  $W_{JgJ}^i$  ( $i = g-g, g-q$  and  $q-q$ ) and the SCR probabilities  $F_i$  we work out the gap survival probabilities according to PHOJET. We obtain the gap survival probabilities as follows

$$\langle |S|^2 \rangle_i = \frac{W_{JgJ}^i}{W_{JJ}^i F_i}. \quad (1)$$

$W_{JJ}^i F_i$  is the probability to have two jets corresponding to the given trigger without gaps and furthermore a gap between the two jets due to SCR. Most of the

gaps are filled by soft or hard multiple interactions and or parton showering, therefore  $W_{JgJ}^i$  is considerably smaller than  $W_{JJ}^i F_i$ . In Fig. 2 we plot for the D0-h and D0-l triggers at  $\sqrt{s} = 1800$  GeV the  $\langle |S|^2 \rangle_i$  obtained. We find values larger than but roughly consistent to the calculation by Gotsman et al. [22]. However, in contrast to the assumptions used in [1,22], we find a slight dependence of the gap survival probability on the trigger conditions resulting in a smaller  $\langle |S|^2 \rangle_i$  for the D0-l trigger. Furthermore, we find  $\langle |S|^2 \rangle_i$  to depend on the hard scattering process with  $\langle |S|^2 \rangle_{q-q}$  larger than  $\langle |S|^2 \rangle_{g-g}$  and  $\langle |S|^2 \rangle_{g-q}$ .

## 5. Concluding remarks

The processes implemented in PHOJET allow us to study hard and soft diffraction in many channels. Here we have been able to demonstrate, that the PHOJET model supplemented with the soft color recombination mechanism describes remarkably well the data from the TEVATRON on color singlet exchange between jets. Besides of finding a good agreement with the D0 and CDF data we are able in addition to study many features of the model, which would be useful to verify in the experiments.

We hope that the PHOJET tool and more TEVATRON data in Run II on color singlet exchange and on hard and soft single diffraction and central diffraction could help to answer important questions: (i) Is soft color recombination the correct mechanism to describe color singlet exchange processes between jets? Could this mechanism be responsible for other features of diffractive processes as well? (ii) Can hard diffraction consistently be described by pomeron structure functions? What is the best pomeron structure function?

## Acknowledgements

One of the authors (R.E.) is supported by U.S. Department of Energy grant DE-FG02 91ER 40626.

## REFERENCES

1. J. D. Bjorken: Phys. Rev. D47 (1993) 101
2. A. H. Mueller and W. K. Tang: Phys. Lett. B284 (1992) 123
3. B. Cox, J. R. Forshaw and L. Lönnblad: JHEP 10 (1999) 023
4. O. J. P. Eboli, E. M. Gregores and F. Halzen: Phys. Rev. D58 (1998) 114005
5. O. J. P. Eboli, E. M. Gregores and F. Halzen: MADPH-99-1135, (hep-ph/9908374), 1999
6. R. Engel: Z. Phys. C66 (1995) 203
7. R. Engel and J. Ranft: Phys. Rev. D54 (1996) 4244
8. A. Capella, U. Sukhatme, C. I. Tan and J. Trân Thanh Vân: Phys. Rep. 236 (1994) 225
9. P. Aurenche, F. W. Bopp, A. Capella, J. Kwieciński, M. Maire, J. Ranft and J. Trân Thanh Vân: Phys. Rev. D45 (1992) 92
10. J. F. Amundson, O. J. P. Eboli, E. M. Gregores and F. Halzen: Phys. Lett. B372 (1996) 127
11. D0 Collab.: S. Abachi et al.: Phys. Rev. Lett. 72 (1994) 2332
12. D0 Collab.: S. Abachi et al.: Phys. Rev. Lett. 76 (1996) 734
13. D0 Collab.: S. Abachi et al.: Phys. Rev. D53 (1996) 6000
14. D0 Collab.: B. Abbott et al.: Phys. Lett. B440 (1998) 189
15. CDF Collab.: F. Abe et al.: Phys. Rev. Lett. 74 (1995) 855
16. CDF Collab.: F. Abe et al.: Phys. Rev. Lett. 80 (1998) 1156
17. CDF Collab.: F. Abe et al.: Phys. Rev. Lett. 81 (1998) 5278
18. R. Engel and J. Ranft: (hep-ph/9711383), in Proceedings of The Int. Symposium on Near Beam Physics, Fermilab, Sept. 22-24, 1997, 1997
19. F. W. Bopp, R. Engel and J. Ranft: (hep-ph/9803437), Proceedings of LAFEX Int. School on High-Energy Physics (LISHEP98), Session C: Workshop on Diffractive Physics, Rio de Janeiro, Brazil, 16-20 Feb. 1998, 1998
20. R. Engel and J. Ranft: Proceedings of the 4th Workshop on Small- $x$  and Diffractive Physics, Fermilab Sept. 1998, p. 255, 1998
21. E. Gotsman, E. M. Levin and U. Maor: Phys. Lett. B309 (1993) 199
22. E. Gotsman, E. Levin and U. Maor: Phys. Lett. B438 (1998) 229
23. E. Gotsman, E. Levin and U. Maor: Phys. Rev. D60 (1999) 094011

# Hard Color Coherent Phenomena

M. Strikman<sup>a</sup>

<sup>a</sup>PSU, University Park, PA16802

We consider hard color coherent phenomena which can be probed at FNAL collider.

## 1. Introduction

During the last few years a number of hard color coherent phenomena was discovered which can be legitimately calculated in QCD: pion dissociation into 2 jets observed in [1] is consistent with predictions of [2], HERA data for exclusive production of mesons in DIS initiated by longitudinally polarized photons are consistent with predictions of [3]. These processes allow both to study the interaction of small color dipoles with hadrons at high energies and hence probe break down of the DGLAP approximation as well as to study hadron wave functions in the minimal Fock space configurations.

## 2. Hard exclusive diffraction

### 2.1. Diffraction into three jets

It is possible that a nucleon (meson) has a significant amplitude to be in a configuration where valence partons are localized in a small transverse area together with the rest of the partons. These configurations are usually referred to as *minimal* Fock space configurations -  $|3q\rangle$  ( $|q\bar{q}\rangle$ ). Hadrons in such a configuration occupy a small transverse area with a larger probability than in the case of non-minimal configurations, because, e.g. the long range pion field is very weak. Therefore, such initial configurations are expected to interact with other hadrons, even at high energy, with a small cross-section. However for the fixed transverse size,  $b$ , this cross section is proportional to the gluon density at  $Q^2 \sim 10/b^2$  and hence rapidly increases with increase of energy. At sufficiently high energies this growth should be tamed not to violate unitarity constraints, for the recent discussion see [4].

In the case of the “elastic scattering” of such a proton configuration off another proton, this three-quark system with large relative momenta should preferentially diffractively dissociate into a system of three jets with large transverse momenta  $p_{T_i} \sim \pi b^{-1}$ , where  $b$  is the transverse size of the minimal configuration. Kinematics of the process is presented at the lego plot of Fig.1.

The production cross-section for the three jets can be estimated to leading order in  $(\alpha_s \ln M_{3jet}^2)$ . As in

the case of diffractive vector meson production in deep inelastic scattering, the cross-section is proportional to the square of the gluon density in the nucleon at  $x \approx M_{3jets}^2/s$ , and virtuality  $\sim p_{T\ jet}^2$ [5]. The distribution over the fractions of the momentum carried by the jets is proportional to the square of the light cone wave function of the  $|3q\rangle$  configuration. Hence the diffraction of a proton into three jets provides important information about the short-distance quark structure of the proton, and also provides unique information about the longitudinal momentum distribution in the  $|3q\rangle$  configuration. From an analysis of diffraction data [5,6], numerical estimates for  $\sqrt{s} = 2$  TeV lead to a value of the cross-section integrated over everything except a  $p_{T\ jet}$  threshold for one jet,

$$\sigma_{3\ jets} \sim (10^{-5} - 10^{-6}) \left( \frac{5\ \text{GeV}}{p_{T\ jet}} \right)^8 \text{ mb.} \quad (1)$$

The probability of the  $|3q\rangle$  configuration is estimated using a phenomenological fit to the probability of configurations of different interaction strengths in a nucleon (cf. [5,6]).

Another interesting group of hard processes is proton diffraction into 2 high  $p_T$  jets and one collinear jet. These processes are dominated by parton configurations when only 2 quarks in the projectile proton are close to each other, i.e., have large transverse momenta. Such quark configurations are relevant for estimates of proton decay rates. The wave function describing such a configuration can be measured in the double-diffraction process where each of the protons fragments into 3 high  $p_t$  jets:  $pp \rightarrow jet(k_t) + jet(-k_t - q_t) + jet(q_t) + jet(l_t) + jet(-l_t - r_t) + jet(r_t)$ .

### 2.2. Tagged-pion diffraction dissociation

Reactions containing a very forward neutron or a  $\Delta$ -isobar can be dominated by the scattering off the pion cloud of the nucleon. In this way the proton beam is effectively converted into a pion beam; the leading baryon is effectively a pion tag. A necessary condition that one-pion exchange dominates this process is that the transverse momentum of the forward baryon be small compared to 300 MeV and, in the case of the  $\Delta$ , that its  $x_F$  exceed 0.9. The precise condition is

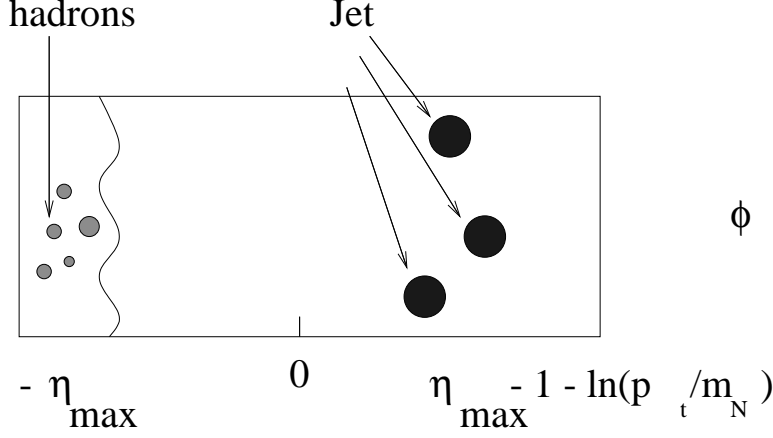


Figure 1. LEGO plot for diffraction of proton into three jets

$$|t| = \left( \frac{M_B^2}{x_F} - m_N^2 \right) (1 - x_F) + \frac{k_t^2}{x_F} \leq 0.1 \text{ GeV}^2. \quad (2)$$

One must still deal with absorptive corrections due to the simultaneous interactions of the projectile with a nucleon and a pion. These are expected to be corrections no larger than a factor two.

Two types of processes would be of special interest:

#### Pion diffraction into two jets:

In analogy with the process of nucleon diffraction into three jets it is expected that a pion can dissociate into two jets in the process  $\pi + p \rightarrow jet_1 + jet_2 + p$  [7,2] (Fig. 2).

The cross-section for this process has a similar structure [2]: due to the rapid increase of the gluon density with energy one expects the cross-section for pion diffraction into two jets to be much larger than in the case of the fixed target experiment E791 at FNAL which has just reported first evidence for this effect [1].

#### Two $\rightarrow$ three hard reactions:

It is also interesting to study large  $|t|$  elastic scattering off the pion cloud in a number of reactions [8].

$$pp \rightarrow B(p_{T B}) + \pi(p_{T \pi}) + p(p_{T p}), \quad (3)$$

for  $B = N, \Delta$ ,  $x_F(B) \geq 0.9$ ,  $p_{T B} \sim 0$ , and  $p_{T \pi} \sim -p_{T p} \gg 1 \text{ GeV}$ , which corresponds to the proton elastic scattering off the pion cloud. Although the flux of such pions in the proton is only  $\sim 1\%$ , at large  $|t| \approx p_{T p}^2$  the cross-section for elastic  $\pi p$  scattering is expected to be substantially larger than the

cross-section for elastic  $pp$  scattering. \* Hence the cross-sections for reaction (3) and elastic  $pp$  scattering at  $|t|$  larger than  $10 \text{ GeV}^2$  should be comparable.

One may also consider elastic scattering of two pions in processes like

$$pp \rightarrow B(p_{T B}) + \pi(p_{T \pi}) + \pi(p_{T \pi'}) + B'(p_{T B'}) \quad (4)$$

for  $B, B' = N, \Delta$ ,  $x_B, x_{B'} \geq 0.9$ ,  $p_{T B} \sim p_{T B'} \sim 0$ , and  $p_{T \pi} \sim -p_{T \pi'} \gg 1 \text{ GeV}$ . Again the much slower decrease of the  $\pi\pi$  elastic scattering with  $|t|$  helps to compensate the small probability of finding both nucleons in configurations with pions.

Many generalizations of such processes can be estimated. These include channels with strange particles in the final state like

$$pp \rightarrow (\Lambda K^+, \Sigma^+ K^0) + p$$

as well as kinematics for which the transverse momentum of the proton is balanced by a baryon, not a meson. Such processes are of interest, both for the study of high-energy scattering and for the structure of color correlations in hadrons, especially in relation to the question of intrinsic strangeness in nucleons, see e.g. [10]. Note that at sufficiently large  $|t|$ , where the colliding-hadron configurations are sufficiently small for the applicability of perturbative QCD, new factorization relations are expected to be valid relating these processes with analogous exclusive DIS processes.

### 3. Diffractive hard factorization

In difference from the case of deep inelastic scattering there is no reason for applicability of the factor-

\*The high-energy data on large  $|t|$   $\pi p$  elastic scattering [9] are consistent with this expectation.



# Double Pomeron Physics in Run II

Jon Pumplin<sup>a</sup>

<sup>a</sup>Department of Physics and Astronomy, Michigan State University, East Lansing, MI 48824

A “normal” event at the Tevatron produces  $\sim 0.3$  hadron resonances per unit of  $\Delta\eta \times \Delta\phi$ . Hence in a region of length  $\Delta y$ , one expects  $\sim 0.3 \times 2\pi \times \Delta y$  of them. Naively assuming no correlations, i.e., a Poisson distribution in the number, leads to the probability  $\approx e^{-2.0\Delta y}$  of zero particles: a rapidity gap. A much more sophisticated argument from Regge theory also predicts the gap probability to be suppressed exponentially, albeit with a smaller coefficient:  $\sigma_{\text{gap}} \approx e^{2(\alpha_R-1)\Delta y} \approx e^{-1.0\Delta y}$  based on the vector meson Regge intercepts  $\alpha_\rho, \alpha_\omega$  near 0.5.

But rapidity gap cross sections are actually *not* suppressed exponentially in this way. Fitting the multiplicity distribution in a region  $> 2-3$  units in rapidity, using a smooth distribution such as negative binomial or generalizations thereof, reveals an excess at zero multiplicity which is the rapidity gap cross section. The pomeron can be defined operationally as the thing that makes rapidity gaps. We must keep our minds open, however, to the possibility that there may be more than one kind of pomeron — e.g., the classical “soft” pomeron may be different from the pomeron that operates when there is a large momentum transfer  $t$  at one end of the gap; or when there is a large momentum transfer  $p_\perp$  across the gap.

Roman pots that detect  $p$  or  $\bar{p}$  very close to the beam directions can be used to study rapidity gaps according to the kinematic relation

$$\xi = 1 - x_p = \sum \sqrt{p_\perp^2 + m^2} e^y / \sqrt{s}.$$

For example if a  $\bar{p}$  is observed with a momentum fraction  $x_p = 0.98$ , no pions with  $p_\perp > 0.3$  GeV can appear at  $y > 4.7$ , so there is a gap  $> 2.8$  between any such pion and the leading proton which is at  $y = 7.5$ . The Roman pot method of observing gaps has several advantages: it allows us to study pure  $\bar{p}$  going in the beam direction instead of an unknown mixture of  $\bar{p}$  and  $\bar{p}^*$ ; it allows measurement of the momentum transfer squared  $t$ ; and if Roman pots can be placed both forward and backward, important azimuthal angular correlations between the forward and backward  $p$  and  $\bar{p}$  can be observed. It will be important to see if final state properties change with  $t$  (or  $t_{\text{forward}}$  and  $t_{\text{backward}}$ ). It is also important to study how large the non-diffractive

contamination is for, say,  $x < 0.95$ . Perhaps one could also get a handle on this by comparing forward protons with forward neutrons as HERA, using the Zeus forward neutron detector.

Double pomeron exchange (DPE) will be studied in Tevatron Run II in reactions of the form  $p\bar{p} \rightarrow pX\bar{p}$ . A variety of centrally produced systems  $X$  are worthy of study:

1. **X = soft, inclusive:** The fully differential cross section is  $d\sigma/dt_1 dt_2 dy_1 dy_2$ , where  $t_1, t_2$  are the 4-momentum transfers to the quasi-elastically scattered  $p$  and  $\bar{p}$ , and  $y_1, y_2$  are the inside edges of the gaps. This cross section is integrated over  $t_1$  and  $t_2$  in the absence of Roman pots. The measurement can be compared with predictions based on measurements of single diffractive scattering by assuming Regge factorization.
2. **X = soft, exclusive:** Low multiplicity final states in DPE are a prime hunting ground for glueball states, since  $X$  automatically has isospin 0 and is made more-or-less from gluons [1]. In this case, azimuthal correlations with the quasi-elastic  $p$  and  $\bar{p}$  can be particularly significant [2]. The absence of large  $p_\perp$  presents a challenge for triggering on these final states, but low multiplicity and the presence of the gaps and/or Roman pot triggers should make it possible.
3. **X = hard, inclusive:** Dijet production in DPE [4] has already been measured in Run I; but Run II offers, along with improved accuracy and the push to higher jet  $p_t$ , the possibility to study the dependence on momentum transfers to the  $p$  and  $\bar{p}$ . It should also be possible to measure the fraction of the jets that are  $b\bar{b}$ .
4. **X = hard, exclusive:** It is possible that some simple heavy quark systems can be produced exclusively in DPE [3]. A promising candidate to search for is the  $b\bar{b}$  state  $\chi_{b1}(1P)$ , which has a mass of 9.892 GeV. It decays with a 35% branching ratio to  $\gamma \Upsilon(1S)$ , with subsequent decay  $\Upsilon \rightarrow \ell^+\ell^-$  with 10% branching ratio ( $\ell = e$  or  $\mu$ ). This would have a remarkable signature:

nothing but  $\ell^+\ell^-\gamma$  in the entire central detector. Although the rate will surely be small, the transverse momenta of several GeV along with the large quiet regions in the detector should be sufficient to make triggering possible. Meanwhile the large  $Q^2$  scale offers the hope of attempting to calculate the cross section in pQCD. Depending on how the pomeron really works, exclusive processes may turn out to be very strongly suppressed by the condition that in spite of the large  $Q^2$  scale, no extra soft gluons are radiated.

The quantum number selection rules for the production of exclusive  $b\bar{b}$  states are as follows. The pomeron is believed to have the same internal quantum numbers as the vacuum, so the state  $X$  produced by the “collision” of two pomerons must have  $I = 0$  and  $C = +$ . The pomeron is an even-signature Regge trajectory, so it has spin and parity  $J^P = 0^+, 2^+, 4^+, \dots$ ; but when two of these are combined with the orbital angular momentum of the collision, all  $J^P$  values become allowed for  $X$ . For the purposes of a DPE experiment,  $\chi_{b1}(1P)$  ( $m = 9.892$ ,  $J^{PC} = 1^{++}$ ) and  $\chi_{b2}(1P)$  ( $m = 9.913$ ,  $J^{PC} = 2^{++}$ ) are the most promising because of their large (35%, 22%) branching ratios into  $\gamma\Upsilon(1S)$ . As a control experiment, the states  $\Upsilon(1S)$  and  $\Upsilon(2S)$  should not be produced in DPE, because they have odd charge conjugation.

One could also look for  $\Upsilon\Upsilon$  or  $\psi\psi$  exclusive states, or even  $\gamma\psi$  [5], in DPE.

Finally, an important experimental problem to be addressed is how to study gap physics in the presence of multiple  $p\bar{p}$  collisions at the higher luminosity of Run II. Presumably the main tool will be to make use of scheduled or unscheduled running in which the luminosity is not in fact very high. For jet physics, the Roman pot method permits gap studies even when the gap cannot be observed directly because it is filled in by multiple interactions.

At the LHC, very high luminosity will make conventional rapidity gap physics impossible. With the help of Tevatron Run II, we should begin to think about whether similar physics can be done by a looser but more enforceable criterion of no *minijets* instead of no particles in a “gap” region. Since jet multiplicities are much less than particle multiplicities, this can only work if the required length  $\Delta y$  to define a gap is made larger.

As a final comment, backgrounds to DPE — along with some important questions regarding underlying events in jet physics — would benefit from an improved study of “minimum bias” physics, along the lines of

what was done long ago and at a lower energy in the UA(5) experiment. Results from that experiment are still being used in the absence of measurements at  $\sqrt{s} = 1.8$  TeV. This is another important topic to clean up before the LHC, where fluctuations from a large number of multiple interactions will be important.

## REFERENCES

1. F.E. Close and G.A. Schuler, hep-ph/9905305; WA102 Collaboration, hep-ph/9908253, hep-ex/9909013, hep-ph/9907302.
2. N. Kochelev, hep-ph/9902203; N.I. Kochelev, T. Morii, A.V. Vinnikov, hep-ph/9903279; A. Kirk, O. Villalobos Baillie, hep-ph/9811230.
3. J. Pumplin, Phys. Rev. D47, 4820 (1993) (hep-ph/9301216).
4. J. Pumplin, Phys. Rev. D52, 1477 (1995) (hep-ph/9412381); A. Berera and J. C. Collins, Nucl. Phys. B474, 183 (1996) (hep-ph/9509258); A.D. Martin, M.G. Ryskin, and V.A. Khoze, Phys. Rev. D56, 5867 (1997) (hep-ph/9705258); A. Berera hep-ph/9910405.
5. Jia-Sheng Xu and Hong-An Peng, hep-ph/9811416.

# Higgs and Heavy Quarks Diffractive Production

Eugene Levin <sup>a b</sup>

<sup>a</sup> HEP Department, School of Physics, Tel Aviv University, Tel Aviv 69978, ISRAEL

<sup>b</sup> Physics Department, Brookhaven National Laboratory, Upton, NY 11973 - 5000, USA

In this note we give the highest of reasonable estimates for the value of cross section of the double Pomeron Higgs meson production and suggest a new mechanism for heavy quark diffractive production which will dominate at the Tevatron energies.

## 1. INTRODUCTION

In this note we consider three reactions

$$p + p \longrightarrow p + [LRG] + H + [LRG] + p ; \quad (1)$$

$$p + p \longrightarrow X_1 + [LRG] + H + [LRG] + X_2 ; \quad (2)$$

$$p + p \longrightarrow b + \bar{b} + X + [LRG] + p ; \quad (3)$$

where LRG denotes the large rapidity gap between produced particles and  $X$  corresponds to a system of hadrons with masses much smaller than the total energy. The first two reactions are so called double Pomeron production of Higgs meson while the third is the single diffraction production of bottom - antibottom pair.

The goals of this note are the following:

1. To give the highest from reasonable estimates for the cross sections of reactions Eq. (1) and Eq. (2) ;
2. To summarize all uncertainties which we see in doing these estimates ;
3. To show that there is a new mechanism of diffractive heavy quark production ( Eq. (3) ) which is suppressed in DIS and dominates in hadron-hadron collision at the Tevatron ;
4. To estimate the value of the cross section of reaction Eq. (3) due to this new mechanism and to show that all attempts to compare the diffraction dissociation in hadron-hadron collisions and DIS[1] look unreliable without a detail experimental study of this process at Fermilab.

## 2. DOUBLE POMERON HIGGS PRODUCTION

### 2.1. Inclusive Higgs production

Inclusive Higgs production has been studied in many details [2-4] for the Tevatron energies. The main

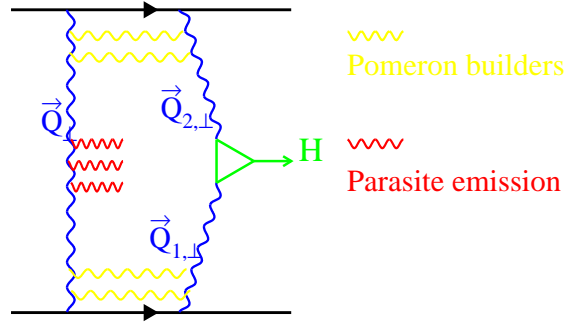


Figure 1. *Double Pomeron Higgs production in QCD*

source for Higgs is gluon-gluon fusion which gives  $\sigma(GG \rightarrow H) = 1pb$  for Higgs with mass  $M_H = 10 GeV$  [4]. The reference point for our estimates is the cross section of Higgs production due to W and Z fusion which is equal to  $\sigma(WW(ZZ) \rightarrow H) = 0.1pb$  [4]. In this process we also expect the two LRG [3] and in some sense this is a competing process for reactions of Eq. (1) and Eq. (2).

### 2.2. Double Pomeron Higgs production is a “soft” process !!!

Let us estimate the simplest digram for the DP Higgs production, namely, Fig.1 without any of s-channel gluons. This diagram leads to the amplitude

$$M(qq \rightarrow qHq) = \quad (4)$$

$$\frac{2}{9} 2 g_H \int \frac{d^2 Q_\perp}{Q_\perp^2 Q_{1,\perp}^2 Q_{2,\perp}^2} 4\alpha_S(Q_\perp^2) (\vec{Q}_{1,\perp} \cdot \vec{Q}_{2,\perp}).$$

For reaction of Eq. (1),  $|t_1| = |\vec{Q}_\perp - \vec{Q}_{1,\perp}| \approx |t_2| = |\vec{Q}_\perp - \vec{Q}_{2,\perp}| \approx 2/B_{el}$  and therefore,

$$M(q + q \rightarrow q + H + q) \propto \int \frac{d^2 Q_\perp}{Q_\perp^4}. \quad (5)$$

Eq. (5) has an infrared divergence that is regularized by the size of the colliding hadrons. In other words, one can see that the simplest diagrams shows that DP Higgs production is a typical “soft” process.

### 2.3. The more the gluons the more the problems...

In Fig.1 one can see that we have two sets of gluon which play a different role. The first one is the gluons that connect  $t$ -channel lines. Their contribution increases the value of cross section [5–8]

$$\frac{d\sigma_P(pp \rightarrow ppH)}{dy}\Big|_{y=0} = \quad (6)$$

$$\frac{4g_H^2}{16^2\pi^3} \int dt_1 dt_2 g_{Pp}^2 g_{Pp}^2 e^{\frac{B_{el}(s/M_H^2)}{2}(t_1+t_2)} \left(\frac{s}{M_H^2}\right)^{2\Delta_P}$$

Eq. (6) can be rewritten in the form

$$\frac{d\sigma_P(pp \rightarrow ppH)}{dy}\Big|_{y=0} = \quad (7)$$

$$\frac{16}{\pi} \sigma(GG \rightarrow H) \left(\frac{\sigma_{el}(s/M_H^2)}{\sigma_{tot}(s/M_H^2)}\right)^2$$

which is convenient for numeric estimates. However, first we need to find the value of  $\sigma(GG \rightarrow H) = g_H^2$ . In inclusive production the value of  $g_H^2$  has been calculated [9]

$$g_H^2 = \sqrt{2}G_F\alpha_S^2(M_H^2)N^2/9\pi^2. \quad (8)$$

However, I think that the scale of  $\alpha_S$  for our process is not the mass of Higgs but the “soft” scale ( $\alpha_S(Q_0^2)$  with  $Q_0^2 \approx 1 GeV^2$ ). Indeed, using BLM procedure [10] we can include the bubbles with large number of light quarks only in  $t$ -channel gluon line which carry the “soft” transverse momenta. This gives a sizable effect in numbers, since  $\sigma(GG \rightarrow H)$  for  $M_H = 100 GeV$  is equal to 1.16 pb ( $\alpha_S(M_H^2)$ ) and to 20 pb ( $\alpha_S(Q_0^2)$ ). Taking the last value we have

$$\frac{d\sigma_P(pp \rightarrow ppH)}{dy}\Big|_{y=0} = 2pb \quad (9)$$

This is our maximal value since all other effects related to gluon emission suppressed the value of the cross section.

### 2.4. Cost of survival

Actually, we have to multiply the cross section of Eq. (9) by two factors to obtain the estimate for the experimental cross section

$$\frac{d}{\sigma}(pp \rightarrow ppH)dy\Big|_{y=0} \quad (10)$$

$$= S_{spect}^2 S_{par}^2 \frac{d\sigma_P(pp \rightarrow ppH)}{dy}\Big|_{y=0}$$

The first factor is the probability that there is no inelastic interaction of the spectators in our process. I The situation with calculation of this factor has been reported in this workshop [11] and the conclusion is that this factor  $S_{spect}^2 = 0.07 \div 0.13$  at the Tevatron energies. The discussion for double Pomeron processes you can find in Ref. [12]

The second factor in Eq. (10) describe the probability that there is no parasite emission in Fig.1 which leads to a process with hadrons in central rapidity region which do not come from the Higgs decay. The generic formula for  $S_{par}^2$  is

$$S_{spect}^2 = e^{-\langle N_G(\Delta y = \ln(M_H^2/s_0)) \rangle} \quad (11)$$

where  $\langle N_G(\Delta y) \rangle$  is the mean number of gluon in interval  $\Delta y$ . In pQCD this number is large [13]  $\langle N_G(\Delta y) \approx 8$  which leads to very small cross section for Higgs production. For “soft” double Pomeron production we can estimate the value of  $\langle N_G(\Delta y) \rangle$  assuming that the hadron production is two stage process: (i) production of mini jet with  $p_t \approx 2 - 3 GeV$  and (ii) minijet decay in hadrons which can be taken from  $e^+e^- \rightarrow hadrons$  process. Finally,

$$\langle N_G(\Delta y) \rangle = \frac{N_{hadrons}}{N(one\ minijet)} \approx 2 \div 3, \quad (12)$$

which gives  $S_{parasite\ emission}^2 \approx 0.1$ .

### 2.5. God loves the brave !!!

Finally, we have

$$\frac{d\sigma(pp \rightarrow ppH)}{dy}\Big|_{y=0} = 0.02pb \quad (13)$$

We can increase the cross section, measuring reaction of Eq. (2). Its cross section is equal to

$$\frac{d\sigma(pp \rightarrow X_1 X_2 H)}{dy}\Big|_{y=0} = \quad (14)$$

$$\frac{d\sigma(pp \rightarrow ppH)}{dy}\Big|_{y=0} \left(\frac{\sigma^{SD} \cdot B_{el}(\sqrt{s}/M_H)}{4\sigma_{el} \cdot B_{DD}(\sqrt{s}/M_H)}\right)^2 =$$

$$3 - 4 \frac{d\sigma(pp \rightarrow ppH)}{dy}\Big|_{y=0} = 0.06 \div 0.08pb$$

### 2.6. Sensitive issues

Eq. (13) and Eq. (14) are our results. I firmly believe that they give the maximum values of the cross sections which we could obtain from reasonable estimates. However, I would like to summarize the most sensitive points in our estimates:

1. The scale for running coupling QCD constant in cross section of Higgs production. We took the “soft” scale for our estimates. However, it is a point which needs more discussion and even more it looks in contradiction with our feeling, as I have realized during our last meeting. My argument is the BLM procedure but more discussions are needed;
2. We took  $S_{spect}^2$  for double Pomeron processes the same as for “hard” LRG process. The justification for this is eikonal type model [12], but it could be different opinions as well as direct experimental data;
3. The estimates for  $S_{par}^2$  is very approximate and we need to work out better theory for this suppression.

### 3. DIFFRACTIVE HEAVY QUARK PRODUCTION

The main observation is that there are two contributions for heavy quark diffractive production (see Eq. (3)): (i) the first is so called Ingelman-Schlein mechanism [15] which described by Fig.2-a and (ii) the second one is closely related to coherent diffraction suggested in Ref. [16] and which corresponds to Fig. 2-b. The estimates of both of them have been discussed in Ref. [14]. The main conclusion is that the main contribution for the Tevatron energies stems from CD (see also [17,18] while the IS mechanism leads to the value of the cross section in one order [14,19] less than CD one. on the other hand in DIS the CD contribution belongs to the high twist and because of that it is rather small [14,17].

Our conclusion is very simple. At the Tevatron we has a good chance to measure a new contribution to “hard” diffraction which is small in DIS. The typical values of the cross section is

$$\frac{d\sigma}{dY} = \int_{p_t^{min}}^{\infty} dp_t^2 \int_{-\infty}^{+\infty} d\Delta y \int_0^{\infty} dq_t^2 \frac{d\sigma}{dY d\Delta y dq_t^2 dp_t^2}$$

$$\approx 10^{-4} \div 10^{-10} \quad \text{for } p_{t,min} = 5 \div 50 \text{ GeV} \quad (15)$$

One can find all details in Ref. [14].

### REFERENCES

1. L. Alvero, J.C. Collins and J.J. Whitmore, PSU-TH-200, hep-ph/9806340;  
L. Alvero, J.C. Collins, J. Terron and J.J. Whitmore, Phys. Rev. D59 (1999) 074022.

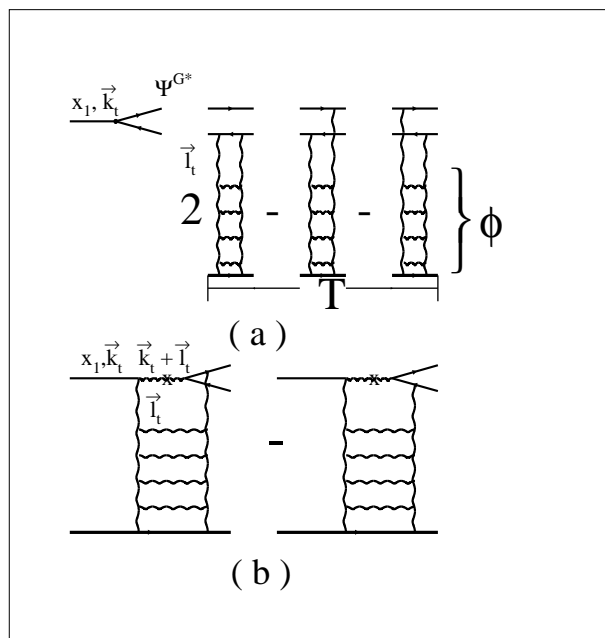


Figure 2. *The contributions for diffractive Higgs production: (a) Ingelman-Schlein mechanism and (b) Coherent diffraction*

2. Z. Kunszt and W.J. Stirling, Aachen ECFA WS, p.428, 1990.
3. Yu.L. Dokshitzer, V.A. Khoze and T. Sjostrand, Phys. Lett. B274 (1992) 116.
4. A.Strange, W. Marciano and S. Willenbrock, Phys. Rev. D49 (1994) 1354.
5. A. Bialas and P.V. Landshoff, Phys. Lett. B256 (1991) 540.
6. B. Muller and Alec J. Schramm, Nucl. Phys. A523 (1991) 677.
7. J-R Cudell and Oscar F. Hernandez, Nucl. Phys. B471 (1996) 471.
8. V. Barger, R.J.N.Phillips and D.Zeppenfeld, Phys. Lett. B346 (1995) 106.
9. S. Dawson, Nucl. Phys. B359 (1991) 283; A. Djouadi, M. Spira and P. Zerwas, Phys. Lett. B264 (1991) 440.
10. S.J. Brodsky, P. Lepage and P. B. Mackenzie, Phys.Rev. D28 (1983) 228.
11. E. Levin, talk at this WS.
12. E. Gotsman, E. Levin and U. Maor, Phys.Lett. B353 (1995) 526.
13. A.D. Martin, M.G. Ryskin and V.A. Khoze, Phys.Rev. D56 (1997) 5867; Phys.Lett. B401 (1997) 330.

14. G. Alves, E. Levin and A. Santoro, Phys. Rev. DD55 (1997) 2683.
15. G. Ingelman and P. Schlein, Phys. Lett. B152 (1985) 256.
16. J. Collins, L. Frankfurt and M. Strikman, Phys. Lett. B307 (1993) 161.
17. D. E. Soper, Talk at DIS'97, hep-ph/9707384.
18. M. Wüsthoff and A.D. Martin, hep-ph/9909362.
19. F. Yuan and K.-T. Chao, hep-ph/9810340; hep-ph/9811285.

# Diffractive Production of Glueballs

Dmitri Kharzeev<sup>a</sup>

<sup>a</sup>Physics Department and RIKEN-BNL Research Center, Brookhaven National Laboratory, Upton NY 11973, USA

This contribution is based on the work with John Ellis [1], in which we link the unexpected azimuthal dependence of the production of scalar glueball candidate observed recently by the WA91 and WA102 Collaborations to the broken scale invariance of QCD.

Confinement and the non-Abelian structure of QCD imply the existence of bound states of gluons. Clearly, finding and recognizing such glueball states is very important. One intriguing possibility is to identify the observed  $f_0(1500)$  state with the lightest scalar glueball [2]. To verify the gluonic nature of this state, one has to check in particular if the mechanisms of its production are consistent with those expected for glueball states. This suggests in particular that one looks for its production in gluon-rich environments. It was suggested long time ago [3] that the glueballs should be produced copiously in the central production process

$$pp \rightarrow p_f X p_s \quad (1)$$

This may be dominated by double-Pomeron exchange when the final-state protons carry large fractions of the initial-state proton momenta in the centre-of-mass frame. In fixed-target experiments, this requires the presence of fast ( $p_f$ ) and slow ( $p_s$ ) protons in the final state.

Recently, a big step in the investigation of this process has been taken by the WA91 and WA102 Collaborations, which have reported remarkable kinematical dependences of central meson production [4,5]. Specifically, it was observed [5] that the production of glueball candidates depends strongly on the relative transverse momenta of the final-state protons  $p_f$  and  $p_s$ . The variable suggested in [5,6] was the difference between the transverse momenta  $\vec{p}'_t$  and  $\vec{q}'_t$  of the final-state protons:

$$dP_t = |\vec{p}'_t - \vec{q}'_t|. \quad (2)$$

The dependence of central meson production on this variable appears to be very non-trivial: namely, it was found that at small  $dP_t$  the production of glueball candidates, in particular the  $f_0(1500)$ , was significantly enhanced over the production of conventional  $\bar{q}q$  mesons. It was proposed [6] that this remarkable feature of central production could be related to the intrinsic structure of glueball states, and that the selection of events with small  $dP_t$  could act effectively as a

glueball filter. So far, no dynamical explanation of this important empirical observation has been suggested, so the challenge for theory is to understand the dynamics behind this glueball filter.

We have proposed [1] the following form for the coupling responsible for scalar glueball production in Pomeron-Pomeron collisions:

$$\mathbb{L} \sim \Theta(x) G_a^{\mu\nu}(x) G_{\mu\nu}^a(x), \quad (3)$$

In momentum space, this coupling leads to an amplitude that is proportional to the square of the scalar product of the four-momenta of the colliding gluons  $g_1$  and  $g_2$ :

$$\begin{aligned} \mathcal{M} &\sim (g_1 \cdot g_2 g^{\mu\nu} - g_1^\mu g_2^\nu)(g_1 \cdot g_2 g_{\mu\nu} - g_{1\mu} g_{2\nu}) \\ &\sim (g_1 \cdot g_2)^2. \end{aligned} \quad (4)$$

This form of the coupling, and the Pomeron flux factors, imply [1] that the production of the scalar glueball should be most efficient when the two protons scatter in parallel directions in the transverse plane, in agreement with the experimental observations.

Our findings support the idea that the azimuthal dependence in double diffractive production provides a valuable way to single out the scalar glueballs and to understand their properties. It would be extremely interesting to extend these studies to collider energies, where the dominance of the Pomeron exchange is much better justified.

## REFERENCES

1. J. Ellis and D. Kharzeev, hep-ph/9811222.
2. For a review, see R. Landua, Ann. Rev. Nucl. Part. Sc. 46 (1997) 351.
3. D. Robson, Nucl. Phys. B 130 (1977) 328; Phys. Lett. B66 (1977) 267.
4. D. Barberis et al., WA91 Collaboration, Phys. Lett. B388 (1996) 853.
5. D. Barberis et al., WA102 Collaboration, Phys. Lett. B397 (1997) 339; A. Kirk et al., WA102 Collaboration, hep-ph/9810221.

6. F.E. Close and A. Kirk, Phys. Lett. B397 (1997) 333.

# Glueballs and Exclusive Hadron Production at the Tevatron

Michael G. Albrow<sup>a</sup>

<sup>a</sup>Fermilab, USA

The study of *low mass* hadronic systems in double pomeron exchange processes is completely virgin territory at the Tevatron. These are events with the  $p$  and  $\bar{p}$  at Feynman  $x_F \geq 0.997$  or so, with central masses less than a few GeV and large rapidity gaps in both forward directions. Important physics topics are (a) to search for glueball states  $G$  by the exclusive process  $p\bar{p} \rightarrow pG\bar{p}$  (b) to measure exclusive hyperon-antihyperon production up to  $\Omega^-\bar{\Omega}^+$  (c) to search for exclusive  $\chi_c$  and  $\chi_b$  production (d) to search for events with an unusually large or small ratio of charged hadrons to  $\pi^0$  (DCC = disoriented chiral condensate?). These studies would all extend our understanding of QCD to the low- $Q^2$  domain. I discuss briefly how they could be carried out in CDF and DØ .

## 1. DOUBLE POMERON EXCHANGE

Double pomeron exchange, DPE, events [1] contain two large rapidity gaps, where by “large” is meant not exponentially damped on a scale of order one unit of rapidity. A region  $\Delta\eta$  (or better  $\Delta y$ ) as large as (say) 4 units with no hadrons is dominated by pomeron,  $P$ , exchange in the t-channel, with little background from other processes (non-diffractive or reggeon exchange). The “pomeron” is a colorless but strongly interacting entity with the quantum numbers of the vacuum: No charge, no isospin, positive parity, C-parity and G-parity. Probably at low  $|t|$  and  $Q^2$  it is predominantly two or more gluons in a colorless combination. Probing it with virtual photons at HERA [2], and observing diffractive  $W$  production at the Tevatron [3], demonstrate a  $q\bar{q}$  component at large  $Q^2$ .

The total rapidity range of a  $p\bar{p}$  collision is  $\Delta y = \ln \frac{s}{m_p^2}$ , which was 8.4 at the CERN ISR ( $\sqrt{s} = 63$  GeV), 13.0 at the  $Spp\bar{p}S$  ( $\sqrt{s} = 630$  GeV), and is 15.3 at the Tevatron ( $\sqrt{s} = 2000$  GeV).  $\Delta y = 6.9$  (7.4) at the fixed target experiments WA102 [4] (E690 [5]) with  $p_{beam} = 450$  (800) GeV/c. At the colliders if we restrict ourselves to events with all central hadrons in  $|\eta| \leq 1.5$  ( $155^\circ \geq \theta \geq 25^\circ$ ) where they can be well measured, the forward rapidity gaps exceed 2.7 at the ISR and 6.1 at the Tevatron. The AFS experiment at the ISR [6] showed very little non-DPE background in central  $\pi^+\pi^-$  production. Gaps exceeding 6 units at the Tevatron will have negligible background from non-pomeron exchange\*.

## 2. GLUEBALL PHYSICS

At this workshop Barnes [7], Kharzeev [10] and Pumplin [11] also discussed hadron spectroscopy in double pomeron exchange processes. There are differ-

ent ways of thinking about the *exclusive* process  $p\bar{p} \rightarrow pG\bar{p}$  with  $G$  a central gluonium or glueball state. (D.Robson [12] first suggested this channel.) One is to note that any hadrons or hadron pairs with the quantum numbers of the vacuum will be present as virtual states in the vacuum and they can be made real by the collision of two hadrons, whose role is essentially to allow 4-momentum to be conserved. (What is the spectrum of these states, for specific quantum numbers?) Another is to consider the fusion of a colorless pair (or triplet) of gluons from each beam particle, noting that the gluon density rises rapidly as  $x_{Bjorken}$  becomes very small. Yet another is to note that glueball states, like all hadrons, must couple to the pomeron and if the quantum numbers are right the process will proceed by  $PP \rightarrow G$ . Allowed quantum numbers are  $I = 0, C = +$  but any  $J^P$  [11]. The advantage of the *exclusive* process is clear: Glueballs are probably being produced with a high cross section in inelastic collisions but when the multiplicity is high the combinatorial background is overwhelming. In exclusive production there is **no** combinatorial background.

For this physics one would like to select events with 2, 4 or possibly 6 well measured charged particles in the central detectors. Particle identification ( $\pi, K, p$ ) is important both for reconstructing the mass and checking that the overall charge, strangeness, and baryon number are zero. Additional neutral particles ( $\gamma, \pi^0, K_L^0, n$ ) may be looked for and either used in the final state combination or used to reject non-exclusive events. The list of interesting final states is long and fairly obvious, including  $\pi^+\pi^-, K^+K^-, K_S^0K_S^0, p\bar{p}, \Lambda\bar{\Lambda}, \phi\phi, 4\pi, \pi\pi KK, KKKK$ , etc. The mass resolution when the charged tracks are all measured is very good, typically 10 MeV. It would be good to be able to use the electromagnetic calorimetry to measure neutral states like  $\eta\eta \rightarrow 4\gamma$  but I suspect this is very difficult to trigger on, the

\*I assume no *Odderon* exchange. That could be looked for by the exclusive production of a central  $\omega$  or  $\phi$  with  $I^G J^{PC} = 0^- 1^{--}$ .

backgrounds would be high and the mass resolution poor. However I have not done a study of this.

### 3. HYPERON AND OTHER PAIRS

At the Axial Field Spectrometer at the ISR exclusive central  $p\bar{p}$  pairs were observed [6] with masses from 2 GeV to 2.8 GeV. With only 64 events there were no significant structures. (WA102 [4] also reported no significant structures with more events but more non-DPE background.) The total cross section for  $pp \rightarrow pp\bar{p}p$  with the central  $p$  and  $\bar{p}$  having  $|\eta| \leq 1.5$  is  $40 \pm 20$  nb which, if  $s$ -independent<sup>†</sup>, would correspond to a rate of 4 Hz at  $L = 10^{32} \text{cm}^{-2} \text{s}^{-1}$ . Actually with that luminosity and 36 bunches ( $\Delta t = 396 \text{ns}$ ) the fraction of inelastic collisions that occur in isolation (therefore useful for gap physics) is only about 13%. The optimum luminosity for gap physics is when  $\langle n \rangle = 1$ , at  $L \approx 5 \times 10^{31} \text{cm}^{-2} \text{s}^{-1}$ , and the fraction of events that occur singly is then 37%. So perhaps one could get thousands of events in an hour of special running, along with other channels that could come with the same trigger (say 2 or 4 central charged particles). This estimate is assuming full  $|t|$  coverage and should be multiplied by the  $t$ -acceptance if it is limited.

If proton pairs are produced by DPE we must also have hyperon pairs  $Y\bar{Y}$  produced. Just using charged particles, and allowing for displaced vertices, one can measure pairs of  $\Lambda, \Xi^-, \Xi(1530), \Omega^-$  and maybe even  $\Lambda_c$ . Using  $\gamma$  and  $\pi^0$  other pairs like  $\Sigma^0, \Sigma^+$  and  $\Xi^0$  become accessible. Why would one want to do this? The wealth of data possible can be used to measure the coupling of all these baryons to the pomeron, and relate them to elastic and total cross sections ... does the phenomenology hang together? How do the  $Y\bar{Y}$  mass spectra depend on  $Y$ , and on  $t_1, t_2$  if they are measured. If one measures also meson pair production ( $\phi\phi$ ) how do the cross sections compare at the same mass (2-quarks vs 3-quarks)? With hyperon pairs one can measure polarizations and hence study spin-spin correlations which might reveal interesting things about the spin of the pomeron (are there correlations with  $t_1, t_2, \Delta\phi(p\bar{p})$ )? When  $K^0\bar{K}^0$  pairs are produced are they  $K_s^0 K_s^0$  and  $K_L^0 K_L^0$  or sometimes  $K_S^0 K_L^0$ , and is the answer dependent on  $M_{K\bar{K}}$ ? If both kaons were to decay to  $\pi^+\pi^-$  is there a correlation between their decay times as there is in  $\phi$  decay?

<sup>†</sup>The cross section should be  $s$ -independent for  $\alpha_P(0) = 1.0$ , whereas it falls with  $s$  for reggeon exchange  $\alpha_R(0) < 1.0$ .

### 4. HYBRIDS, HEAVY MESONS, AND HIGGS

There can be a very interesting spectroscopy of, possibly narrow, hybrid states  $b\bar{b}g$  [7] [13]. Those with the allowed quantum numbers (DPE is a *Quantum Number Filter*) will be produced exclusively; e.g. one gluon from each beam proton fuse  $gg \rightarrow g$  and another make  $gg \rightarrow b\bar{b}$ .

Also we should search for the  $0^+0^{++}$   $\chi_c$  and  $\chi_b$  states; the latter decays to  $\Upsilon\gamma$  to  $\mu^+\mu^-\gamma$ . One very interesting reason to study isolated central  $\chi_b$  production is because it may instruct us about a possible *Higgs* production (discovery?) channel [8]. In the former case two gluons fuse to form the  $\chi_b$ , and another soft gluon is exchanged between the two beam particles to leave them colorless and unexcited. (This is called non-factorisable double pomeron exchange, NFDP.) Measuring this cross section will enable us to better estimate the similar process where the two gluons (low  $p_T$  but  $p_L \approx p_{beam} - \frac{M_H}{2}$ ) make a Higgs via a top-quark loop, and another soft gluon sorts out the color. The process is then  $p\bar{p} \rightarrow pH\bar{p}$ . Measuring the outgoing  $x_F \approx 0.94$  beam particles in precision roman pot detectors (this requires dipole spectrometers on both sides to get to  $|t| = t_{min}$ ) the missing mass resolution can be much better than the effective mass resolution of the  $H \rightarrow b\bar{b}$  jet pair. . Neither CDF nor DØ have the apparatus for this but if the signal estimates and (DPE/QCD  $b - \bar{b}$  dijet) backgrounds are encouraging then it could be done [9].

Studies of meson pairs may be extendable to the charm sector; the masses of  $D$  and  $D_s$  are little above the  $\Omega$  mass, and there are exclusive decay modes e.g.  $KK\pi$  with branching fractions around 9% and 5% respectively. Unfortunately exclusive  $B\bar{B}$  pairs are probably unobtainable.

All these processes, systematically studied, will clearly tell us a lot about the nature of diffraction/pomerons, in addition to the hybrid or meson spectroscopy itself.

### 5. DISORIENTED CHIRAL CONDENSATES etc.

High energy cosmic ray events have been observed with either an anomalously large ratio of charged hadrons: $\gamma/e$  (Centaurus; one striking event has a ratio 49:1) or a very small ratio (Anticentaurus; one event has 1 charged track and 32  $\gamma$ 's in an  $\eta, \phi$  circle of radius 0.7). Such events have been interpreted [14] as manifestations of a "Disoriented Chiral Condensate". No accelerator experiments have seen anomalous tails on the charged:neutral ratio [15]. No searches have yet been made in the central region of DPE events.

It is worthwhile making a search, because as I have said for low- $t$ , low  $Q^2$  (no jets) events the pomeron might be dominated by just gluons. In that case this would be the first study of high mass ( $\approx 50$  GeV) “isotropic” events where the initial state is (to some degree) purely gluonic. One would trigger on gap-X-gap events, anti-select on jets, construct the ratio  $\Sigma_{p_T}(\text{charged tracks}) : \Sigma_{E_T}(\text{electromagnetic cal})$  and study the tails (with a single vertex, rejecting cosmics, etc.).

High charged multiplicity events, DCC candidates or not, can be analysed for Bose-Einstein correlations, which can be used to measure the radius of the particle emission (separately for pions and kaons, if identified ... also for  $K_s^0$  if there are enough of them per event) in both the longitudinal and transverse directions. The  $K/\pi$  ratio is another interesting quantity to study either in a sample of DCC candidate events or in other special classes of events. Note that the AFS experiment [6] found, for 2-central tracks,  $R[K^+K^-/\pi^+\pi^-]$  above 1.0 just above the  $K\bar{K}$  threshold, but this is probably a manifestation of the prominent  $f_0(970)$  resonance.

## 6. EXPERIMENTAL CONSIDERATIONS

CDF and DØ have some complementary aspects for this physics and it would be best to have both experiments producing results, for cross checks where they overlap. DØ will have the apparent advantage of having roman pots (quadrupole spectrometers) on both the  $p$  and the  $\bar{p}$  side, while CDF only has a dipole pot spectrometer on the  $\bar{p}$  side. So DØ can tag both beam particles and measure their  $t$  and  $\phi$ , which CDF cannot. Very interesting dependences of the central mass spectra ( $\pi^+\pi^-$ ) on the relative azimuth  $\Delta\phi$  have been observed [16] at  $\sqrt{s} = 28$  GeV/c. Are these dependences due to regge exchanges which will die away with  $\sqrt{s}$ ? DØ will pay a fairly severe rate penalty  $\approx 10^{-4}$  for double tagging, because  $|t_{min}| \approx 0.5 - 0.6$  GeV<sup>2</sup> on each side. Even when both  $p$  and  $\bar{p}$  are detected, the *missing mass* resolution is O(GeV); the spectroscopy is done by reconstructing the effective mass of the central system. The CDF approach is to ignore the forward  $p$  and  $\bar{p}$ , allowing them to go down the beam pipe, which gives acceptance for all  $|t|$ . CDF can trigger on rapidity gaps on both sides, and to make this possible have installed *Beam Shower Counters (BSC)* where possible around the beam pipe (just in front of the low- $\beta$  quadrupoles, before and after the electrostatic separators, and on the  $\bar{p}$  side just before the Roman Pots at 56 m). CDF hopes to install also *Miniplug Calorimeters* for  $3.5 \leq |\eta| \leq 5.5$  ( $\theta \leq 3^\circ$ ) and in this region there are also the *Cerenkov Luminosity*

*Counters (CLC)* which count charged particles from the interaction region. All of these in veto will give rapidity gaps of 4 units on each side. It might be advantageous to require even larger gaps by (in CDF) vetoing on energy in the plug calorimeter (which has an  $\eta\phi$  geometry) with  $|\eta| \geq 2.0$  ... after all one cannot measure tracks well there. DØ could, I believe, make a similar trigger. These “2-gap” triggers will be *very* effective at vetoing multiple interactions. Of course some positive requirement (more than the beam crossing signal  $X_0$ ) is also needed. This could be made in principal, in CDF or DØ, by requiring a minimal energy  $E$  in the complementary central region; above noise levels but as low as possible. CDF has the more attractive possibility of using its time-of-flight (*TOF*) barrel (216  $\phi$ -segments of fast scintillator) to trigger on a central charged particle multiplicity of 2,4 or 6 particles. (Actually the trigger would probably be only able to use  $\phi$  segments of  $15^\circ$  for technical reasons.) The tracks which hit the *TOF* barrel are full length and very well measured. Most will also be identified: The *TOF* gives  $2\sigma$  separation of  $\pi$  and  $K$  to 1.6 GeV/c, and the *Central Outer Tracker (COT)* will measure  $dE/dx$  to 10% which will provide further information on  $\pi, K, p$  identification.

The best way of implementing this physics program in CDF and DØ is probably to set up a trigger table based on two forward gaps and the various central requirements. One wants in addition the same central requirements with one or no forward gaps required, but with large prescaling factors to compensate for the much higher rates. These samples are used to measure cross sections and estimate the signal:background (multiplicity = 0 tails of non-diffractive events). Ideally one would like this trigger table to give a rate of about 50 Hz at  $L = 5.10^{31} \text{cm}^{-2} \text{s}^{-1}$ , and to take 3-4 hours of test data at such a luminosity (or at a lower luminosity if the trigger cross section is higher). These 0.5-1.0 million events should be analysed both for their own physics and to refine triggers. This should be enough to whet our appetite for the most promising and interesting channels, and either to take more dedicated running towards the end of stores or to include this as a fraction of the “QCD bandwidth”.

## 7. CONCLUSION

There is a great deal of new physics to study with low mass exclusive central states in DPE at the Tevatron. The hardware should exist (the CDF Miniplugs should be approved!) and the fraction of additional integrated dead-time needed is negligible.

## REFERENCES

1. See e.g. M.G. Albrow, Double Pomeron Exchange from the ISR to the SSC, Nucl. Phys. B (Proc.Supp.) **12**, 291 (1990) and references therein.
2. M. Derrick et al. (ZEUS), Phys. Lett. **B315**, 481 (1993); T. Ahmed et al.(H1), Nucl. Phys. **B429**, 477 (1994).
3. F. Abe et al. (CDF), Phys. Rev. Lett. **78**, 2698 (1997); L. Coney (DØ), Observation of Diffractive  $W$  Production at DØ, APS Meeting, Atlanta GA, March 1999.
4. See e.g. D. Barberis et al. (WA102), Phys. Lett. **B432**, 436 (1998) for  $DPE \rightarrow \phi\phi$ ; D.Barberis et al., Phys. Lett. **B446**, 342 (1999) for  $p\bar{p}$  and  $\Lambda\bar{\Lambda}$ , and other WA102 papers.
5. M.A. Reyes et al., Phys. Rev. Lett. **81**, 4079 (1998); M. Sosa et al., Phys. Rev. Lett. **83**, 913 (1999) (E690).
6. T. Akesson et al. (AFS,R807), Nucl.Phys. **B264**, 154 (1986).
7. Ted Barnes, Glueballs and Exotics in QCD, talk at this workshop.
8. A. Bialas and P.V. Landshoff, Phys. Lett. **B256**, 540 (1991); D. Kharzeev and E. Levin, hep-ph/0005311 and references therein.
9. M. Albrow, D. Litvintsev, P. Murat and A. Rostovtsev, Run II SUSY Higgs Workshop proc. (<http://fnth37.fnal.gov/susy.html>) pp 87-89.
10. Dmitri Kharzeev, Diffractive Production of Glueballs, these proceedings.
11. Jon Pumplin, Double Pomeron Physics in Run II, these proceedings.
12. D. Robson, Nucl. Phys. **B130**, 328 (1977).
13. See e.g. P.R. Page, E.S. Swanson and A.P. Szczepaniak, Phys. Rev. **D59**:034016 (1999).
14. J.D. Bjorken, Int. J. Mod. Phys. **A7**, 4189 (1992).
15. For a CDF limit, see P. Melese, Proc.XI Topical Workshop on  $p\bar{p}$  Collider Physics, Padova, Italy (1996). FERMILAB-Conf-96/205-E.
16. D. Barberis et al. (WA102), Phys. Lett. **B397**, 339 (1997), F. Close, A. Kirk and G. Schuler, Phys. Lett. **B477**, 13 (2000).

# A Determination of Pomeron Intercepts at Colliders

R. Peschanski <sup>a</sup> C. Royon <sup>b</sup>

<sup>a</sup>CEA, Service de Physique Theorique, CE-Saclay, F-91191 Gif-sur-Yvette Cedex

<sup>b</sup>DAPNIA/SPP, Commissariat à l’Energie Atomique, Saclay, F-91191 Gif-sur-Yvette Cedex

A method allowing for a direct comparison of data with theoretical predictions is proposed for forward jet production at HERA and Mueller-Navelet jets at Tevatron. An application to the determination of the *effective* Pomeron intercept in the BFKL-LO parameterization from  $d\sigma/dx$  data at HERA leads to a good fit with a significantly higher *effective* intercept,  $\alpha_P = 1.43 \pm 0.025(stat.) \pm 0.025(syst.)$ , than for proton (total and diffractive) structure functions. It is however less than the value of the pomeron intercept using dijets with large rapidity intervals obtained at Tevatron. We also evaluate the rapidity veto contribution to the higher order BFKL corrections. We suggest to measure the dependence of the dijet cross-sections as a function of the jet transverse energies as a signal for BFKL pomeron at Tevatron.

## 1. Forward jet cross-section at HERA

The study of forward jets at colliders is considered as the milestone of QCD studies at high energies, since it provides a direct way of testing the perturbative resummations of soft gluon radiation. More precisely, the study of one forward jet (w.r.t. the proton) in an electron-proton collider [1] seems to be a good candidate to test the energy dependence of hard QCD cross-sections. It is similar to the previous proposal of studying two jets separated by a large rapidity interval in hadronic colliders [2], for which only preliminary results are available [3]. This test is also possible in  $\gamma^*\text{-}\gamma^*$  scattering [4] but here the statistics and the energy range are still insufficient to get a reliable determination of the physical parameters for hard QCD cross-sections. Indeed, the proposed (and favored for the moment being) set-up [1] is to consider jets with transverse momentum  $k_T$  of the order of the photon virtuality  $Q$  allowing to damp the QCD evolution as a function of  $k_T$  (DGLAP evolution [5]) in favor of the evolution in energy at fixed  $k_T$  (BFKL evolution [6]).

In contrast to full Monte-Carlo studies we want to focus on the jet cross section  $d\sigma/dx$  observable itself, by a consistent treatment of the experimental cuts and minimizing the uncertainties for that particular observable. Let us remark that our approach is not intended to provide a substitution to the other methods, since the Monte-Carlo simulations have the great merit of making a set of predictions for various observables. Hence, our method has to be considered as complementary to the others and dedicated to a better determination of the *effective* Pomeron intercept using the  $d\sigma/dx$  data. As we shall see, it will fix more precisely this parameter, but it will leave less constrained other interesting parameters, such as the cross-section

normalization.

The cross-section for forward jet production at HERA in the dipole model reads [10]:

$$\frac{d^{(4)}\sigma}{dx dQ^2 dx_J dk_T^2 d\Phi} = \frac{\pi N_C \alpha^2 \alpha_S(k_T^2)}{Q^4 k_T^2} f_{eff}(x, \mu_f^2) \Sigma e_Q^2 \int_{\frac{1}{2}-i\infty}^{\frac{1}{2}+i\infty} \frac{d\gamma}{2i\pi} \left(\frac{Q^2}{k_T^2}\right)^\gamma \exp\{\epsilon(\gamma, 0)Y\} \times \left[ \frac{h_T(\gamma) + h_L(\gamma)}{\gamma} (1-y) + \frac{h_T(\gamma)}{\gamma} \frac{y^2}{2} \right] \quad (1)$$

where

$$Y = \ln \frac{x_J}{x} \quad (2)$$

$$\epsilon(\gamma, p) = \bar{\alpha} [2\psi(1) - \psi(p+1-\gamma) - \psi(p+\gamma)] \quad (3)$$

$$f_{eff}(x, \mu_f^2) = G(x, \mu_f^2) + \frac{4}{9} \Sigma(Q_f + \bar{Q}_f) \quad (4)$$

$$\mu_f^2 \sim k_T^2, \quad (5)$$

are, respectively,  $Y$  the rapidity interval between the photon probe and the jet,  $\epsilon(\gamma, p)$  the BFKL kernel eigenvalues,  $f_{eff}$  the effective structure function combination, and  $\mu_f$  the corresponding factorization scale. The main BFKL parameter is  $\bar{\alpha}$ , which is the (fixed) value of the effective strong coupling constant in LO-BFKL formulae. Note that we gave the BFKL formula not including the azimuthal dependence as we will stick to the azimuth-independent contribution with the dominant  $\exp\{\epsilon(\gamma, 0)Y\}$  factor.

The so-called “impact factors”  $h_T, h_L$

$$\begin{pmatrix} h_T \\ h_L \end{pmatrix} = \frac{\alpha_S(k_T^2)}{3\pi\gamma} \frac{(\Gamma(1-\gamma)\Gamma(1+\gamma))^3}{\Gamma(2-2\gamma)\Gamma(2+2\gamma)} \frac{1}{1-\frac{2}{3}\gamma} \begin{pmatrix} (1+\gamma)(1-\frac{\gamma}{2}) \\ \gamma(1-\gamma) \end{pmatrix}, \quad (6)$$

are obtained from the  $k_T$  factorization properties [15] of the coupling of the BFKL amplitudes to external hard probes. The same factors can be related to the photon wave functions [16,14] within the equivalent context of the QCD dipole model [17].

Our goal is to compare as directly as possible the theoretical parameterization (1) to the data which are collected in experiments [7,8]. The crucial point is how to take into account the experimentally defined kinematic cuts [7,8].

The main problem to solve is to investigate the effect of these cuts on the determination of the integration variables leading to a prediction for  $d\sigma/dx$  from the given theoretical formula for  $d^{(4)}\sigma$  as given in formula (1). The effect is expected to appear as bin-per-bin *correction factors* to be multiplied to the theoretical cross-sections for average values of the kinematic variables for a given  $x$ -bin before comparing to data (e.g. fitting the cross-sections) [9].

The experimental correction factors have been determined using a toy Monte-Carlo designed as follows. We generate flat distributions in the variables  $k_T^2/Q^2$ ,  $1/Q^2$ ,  $x_J$ , using reference intervals which include the whole of the experimental phase-space (the  $\Phi$  variable is not used in the generation since all the cross-section measurements are  $\phi$  independent). In practice, we get the correction factors by counting the numbers of events which fulfill the experimental cuts given in Table I for each  $x$ -bin. The correction factor is obtained by the ratio to the number of events which pass the experimental cuts and the kinematic constraints, and the number of events which fulfill only the kinematic constraints, i.e. the so-called reference bin. The correction factors are given in reference [9].

We perform a fit to the H1 and ZEUS data with only two free parameters. these are the *effective* strong coupling constant in LO BFKL formulae  $\bar{\alpha}$  corresponding to the *effective* Lipatov intercept  $\alpha_P = 1 + 4 \log 2\bar{\alpha}N_C/\pi$ , and the cross-section normalization. The obtained values of the parameters and the  $\chi^2$  of the fit are given in Table III for a fit to the H1 and ZEUS data separately, and then to the H1 + ZEUS data together.

The  $\chi^2$  of the fits have been calculated using statistical error only and are very satisfactory (about 0.6 *per point* for H1 data, and 1. *per point* for ZEUS data). We give both statistical and systematic errors for the fit parameters. The values of the Lipatov intercept are close to one another and compatible within errors for the H1 and ZEUS sets of data, and indicate a preferable medium value ( $\alpha_P = 1.4 - 1.5$ ). We also notice that the ZEUS data have the tendency to favour a higher exponent, but the number of data points used in the fit is much smaller than for H1, and the H1

Table 1  
Fit results.

fit	$\bar{\alpha}$	$\alpha_P$
H1	$0.17 \pm 0.02 \pm 0.01$	$1.44 \pm 0.05 \pm 0.025$
ZEUS	$0.20 \pm 0.02 \pm 0.01$	$1.52 \pm 0.05 \pm 0.025$
H1+ZEUS	$0.16 \pm 0.01 \pm 0.01$	$1.43 \pm 0.025 \pm 0.025$
D0	$0.24 \pm 0.02 \pm 0.02$	$1.65 \pm 0.05 \pm 0.05$
fit	Norm.	$\chi^2/(dof)$
H1	$29.4 \pm 4.8 \pm 5.2$	5.7 (/9)
ZEUS	$26.4 \pm 3.9 \pm 4.7$	2.0 (/2)
H1+ZEUS	$30.7 \pm 2.9 \pm 3.5$	12.0 (/13)

data are also at lower  $x$ . The normalization is also compatible between ZEUS and H1. The fit results are shown in Figure 1 and compared with the H1 and ZEUS measurements.

## 2. Comparison with Tevatron results

The final result of our new determination of the effective pomeron intercept is  $\alpha_P = 1.43 \pm 0.025$  (stat.)  $\pm 0.025$  (syst.). Our method allows a direct comparison of the intercept values with those obtained in other experimental processes, i.e.  $\gamma^*\gamma^*$  cross-sections at LEP [4], jet-jet cross-sections at Tevatron at large rapidity intervals [3],  $F_2$  and  $F_2^D$  proton structure function measurements [12–14].

Let us compare our results with the effective intercept we obtain from recent preliminary dijet data obtained by the D0 Collaboration at Tevatron [3]. The measurement consists in the ratio  $R = \sigma_{1800}/\sigma_{630}$  where  $\sigma$  is the dijet cross-section at large rapidity interval  $Y \sim \Delta\eta$  for two center-of-mass energies (630 and 1800 GeV),  $\Delta\eta_{1800} = 4.6$ ,  $\Delta\eta_{630} = 2.4$ . The experimental measurement is  $R = 2.9 \pm 0.3$  (stat.)  $\pm 0.3$  (syst.). Using the Mueller-Navelet formula [2], this measurement allows us to get a value of the effective intercept for this process

$$R = \frac{\int_{\frac{1}{2}-i\infty}^{\frac{1}{2}+i\infty} \frac{d\gamma}{2i\pi\gamma(1-\gamma)} e^{\epsilon(\gamma,0)\Delta\eta_{1800}}}{\int_{\frac{1}{2}-i\infty}^{\frac{1}{2}+i\infty} \frac{d\gamma}{2i\pi\gamma(1-\gamma)} e^{\epsilon(\gamma,0)\Delta\eta_{630}}}. \quad (7)$$

We get  $\alpha_P = 1.65 \pm 0.05$  (stat.)  $\pm 0.05$  (syst.), in agreement with the value obtained by D0 using a saddle-point approximation [3] (see Table 1). This intercept is higher than the one obtained in the forward jet study.

Formula (7) is obtained after integration over the jet transverse energies at 630 and 1800 GeV,  $E_{T_1}$ ,  $E_{T_2}$ . We

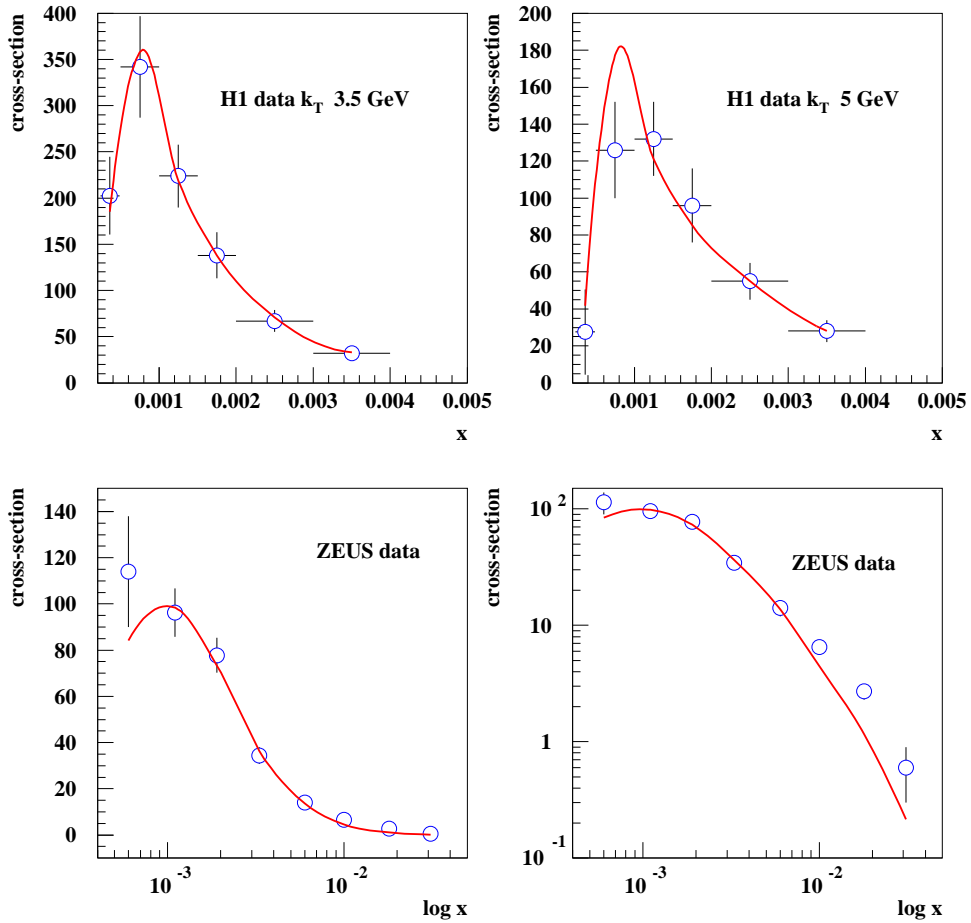


Figure 1. The H1 data ( $k_T > 3.5$  GeV,  $k_T > 5$  GeV), and the ZEUS data are compared with the result of the fit. ZEUS data are also displayed in logarithmic scales in vertical coordinates to show the discrepancy at high  $x$  values.

note that the non integrated formula

$$R(E_{T_1}/E_{T_2}) = \frac{\int_{\frac{1}{2}-i\infty}^{\frac{1}{2}+i\infty} \frac{d\gamma}{2i\pi} \left(\frac{E_{T_1}}{E_{T_2}}\right)^{2\gamma} e^{\epsilon(\gamma,0)\Delta\eta_{1800}}}{\int_{\frac{1}{2}-i\infty}^{\frac{1}{2}+i\infty} \frac{d\gamma}{2i\pi} \left(\frac{E_{T_1}}{E_{T_2}}\right)^{2\gamma} e^{\epsilon(\gamma,0)\Delta\eta_{630}}} \quad (8)$$

shows a sizeable dependence on  $E_{T_1}/E_{T_2}$ , which could be confronted with experiment. Let us show both the integrated and  $E_{T_1}/E_{T_2}$  dependent cross-sections in Figure 2.

The question arises to interpret the different values of the effective intercept. It could reasonably come from the differences in higher order QCD corrections for the BFKL kernel and/or in the impact factors depending on the initial probes ( $\gamma^*$  vs. jets). In order to evaluate the approximate size of the higher order BFKL corrections, we will use their description in terms of rapidity veto effects [18]. In formula (1), we replace  $\exp(\epsilon(\gamma, 0)Y)$  by

$$\sum_{n=0}^{\infty} \theta(Y - (n+1)b) \frac{[\epsilon(\gamma, 0) (Y - (n+1)b)]^n}{\Gamma(n+1)}. \quad (9)$$

The Heaviside function  $\theta$  ensures that a BFKL ladder of  $n$  gluons occupies  $(n+1)b$  rapidity interval where  $b$  parametrises the strength of NLO BFKL corrections. The value of the leading order intercept is fixed to  $\alpha_p = 1.75(\alpha_S(Q^2 = 10) = 0.28)$ , where  $Q^2 = 10$  GeV<sup>2</sup> is inside the average range of  $Q^2$  in the forward jet measurement. The fitted value of the  $b$  parameter obtained using the forward jet data is found to be  $1.28 \pm 0.08$  (stat.)  $\pm 0.02$  (syst.). Imposing the same value of  $\alpha_P$  with Tevatron data gives  $b=0.21 \pm 0.11$  (stat.)  $\pm 0.11$  (syst.). Note that the theoretical value of  $b$  for the NLO BFKL kernel is expected to be of the order 2.4, which is also compatible with the result obtained for the  $\gamma^*\gamma^*$  cross-section. A contribution from the NLO impact factors is not yet known, and could perhaps explain the different values of  $b$ .

### 3. Conclusion

To summarize our results, using a new method to disentangle the effects of the kinematic cuts from the genuine dynamical values we find that the effective pomeron intercept of the forward jet cross-sections at HERA is  $\alpha_P = 1.43 \pm 0.025$  (stat.)  $\pm 0.025$  (syst.). It is much higher than the soft pomeron intercept, and, among those determined in hard processes, it is intermediate between  $\gamma^*\gamma^*$  interactions at LEP and dijet productions with large rapidity intervals at Tevatron, where we get  $\alpha_P=1.65 \pm 0.05$  (stat.)  $\pm 0.05$  (syst.).

Looking for an interpretation of our results in terms of higher order BFKL corrections expressed by rapidity gap vetoes  $b$  between emitted gluons, we find a value of  $b=1.3$  at HERA, and 0.21 at Tevatron. The HERA

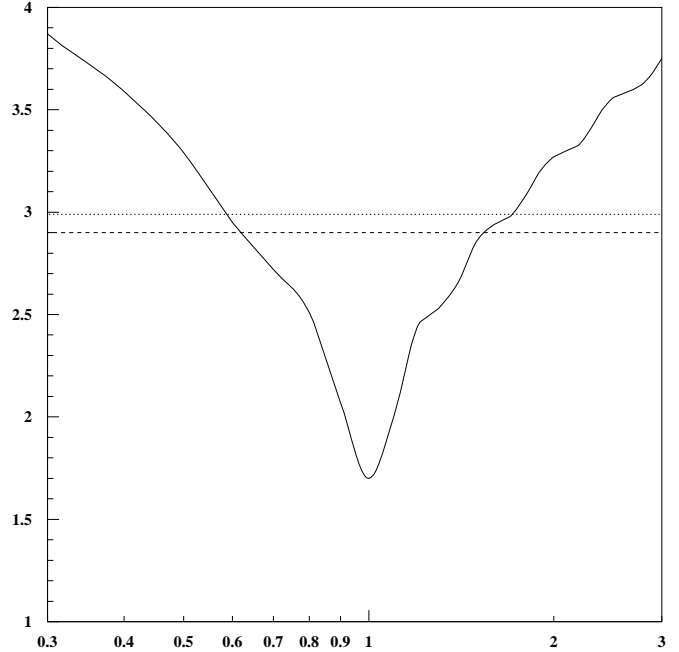


Figure 2.  $E_{T_1}/E_{T_2}$  dependence of the dijet cross-section ratio.  $E_{T_1}/E_{T_2}$  is given in the horizontal axis, and  $R$  in vertical axis. In full line is given the non integrated  $R(E_{T_1}/E_{T_2})$  (see formula (8)), in dotted line, the integrated  $R$  (formula (7)) and in dashed line, the saddle point approximation of  $R$  [2], for the fitted value of  $\alpha_P$  (see table 1).

value is sizeable but less than the theoretically predicted [11] value for the NLO BFKL kernel ( $b=2.4$ ). The Tevatron value is compatible with zero. The observed dependence in the process deserves further more precise studies [19].

We suggest to measure the dependence of the dijet cross-sections as a function of the jet transverse energies as a signal for BFKL pomeron at Tevatron run II. The Mueller Navelet jet study would also benefit from a lower energy run at the end of Run II to allow a normalization independence of the intercept determination and BFKL tests.

#### 4. Acknowledgments

R.P. acknowledges supports by the EU Fourth Framework Programme ‘Training and Mobility of Researchers’, Network ‘Quantum Chromodynamics and the Deep Structure of Elementary Particles’, contract FMRX-CT98-0194 (DG 12 - MIHT).

#### REFERENCES

1. A.H. Mueller, *Nucl. Phys. B* (Proc. Suppl.) **18C** (1991) 125.
2. A.H. Mueller and H. Navelet, *Nucl. Phys.* **B282** (1987) 107.
3. A. Goussiou, for the D0 collaboration, *Dijet Cross section at large  $s/Q^2$  in  $\bar{p}p$  Collisions*, presented at the ‘International Europhysics Conference On High-Energy Physics’ (EPS-HEP 99), Tampere, Finland, July, 1999.
4. S.Brodsky, V.S. Fadin, V.T. Kim, L.N. Lipatov, G.B. Pivovarov, *JETP Lett.* **70** (1999) 155; M. Boonekamp, A. De Roeck, C. Royon, S. Wallon, *Nucl.Phys.* **B555** (1999) 540, for a recent review and references, Ch. Royon, *BFKL signatures at a linear collider*, invited talk given at the International Workshop on Linear Colliders (LCWS99), April 28- May 5, Sitges (Spain), hep-ph/9909295.
5. G. Altarelli and G. Parisi, *Nucl. Phys.* **B126** 18C (1977) 298; V.N. Gribov and L.N. Lipatov, *Sov. Journ. Nucl. Phys.* (1972) 438 and 675; Yu.L. Dokshitzer, *Sov. Phys. JETP.* **46** (1977) 641.
6. L.N. Lipatov, *Sov. J. Nucl. Phys.* **23** (1976) 642; V.S. Fadin, E.A. Kuraev and L.N. Lipatov, *Phys. Lett.* **B60** (1975) 50; E.A. Kuraev, L.N. Lipatov and V.S. Fadin, *Sov. Phys. JETP* **44** (1976) 45, **45** (1977) 199; I.I. Balitsky and L.N. Lipatov, *Sov. J. Nucl. Phys.* **28** (1978) 822.
7. H1 Collaboration, C. Adloff et al. *Nucl. Phys.* **B538** (1999) 3.
8. ZEUS Collaboration, J. Breitweg et al. *Eur. Phys. J.* **C6** (1999) 239.
9. G. Contreras, R. Peschanski, C. Royon, hep-ph/0002057, to appear.
10. J. Bartels, A. De Roeck, M. Loewe, *Zeit. für Phys.* **C54** (1992) 921; W-K. Tung, *Phys. Lett.* **B278** (1992) 635; J. Kwiecinski, A.D. Martin, P.J. Sutton, *Phys.Rev.* **D46** (1992) 921.
11. V.S. Fadin and L.N. Lipatov *Phys. Lett.* **B429** (1998)127; M. Ciafaloni *Phys. Lett.* **B429** (1998) 363; M. Ciafaloni and G. Camici *Phys. Lett.* **B430** (1998) 349.
12. H. Abramowicz, *Diffraction and the Pomeron Contribution to the 19th International Symposium on Lepton and Photon Interactions at High-Energies (LP 99)*, Stanford, California, 9-14 Aug 1999, hep-ph/0001054.
13. H. Navelet, R. Peschanski, Ch. Royon, *Phys. Lett.* **B366** (1995) 329. H. Navelet, R. Peschanski, Ch. Royon, S. Wallon, *Phys. Lett.* **B385** (1996) 357.
14. S. Munier, R. Peschanski, Ch. Royon, *Nucl. Phys.* **B534** (1998) 297.
15. S. Catani, M. Ciafaloni, F. Hautmann, *Nucl. Phys.* **B366** (1991) 135. J.C. Collins, R.K. Ellis, *Nucl. Phys.* **B360** (1991) 3. E.M. Levin, M.G. Ryskin, Yu. M. Shabelskii, A.G. Shuvaev, *Sov. J. Nucl. Phys.* **53** (1991) 657.
16. J.D. Bjorken, J. Kogut and D. Soper, *Phys. Rev.* **D3** (1971) 1382. N.N. Nikolaev, B.G. Zakharov, *Zeit. für. Phys.* **C49** (1991) 607; *Phys. Lett.* **B332** (1994) 184.
17. A.H. Mueller, *Nucl. Phys.* **B415** (1994) 373; A.H. Mueller and B. Patel, *Nucl. Phys.* **B425** (1994) 471; A.H. Mueller, *Nucl. Phys.* **B437** (1995) 107.
18. L.N. Lipatov, talk presented at the 4th Workshop on Small-x and Diffractive Physics, FNAL, September 1998, C. Schmidt, *Phys. Rev.* **D60** (1999) 074003, J. Forshaw, D.A. Ross, A. Sabio Vera, *Phys. Lett.* **B455** (1999) 273-282.
19. V.T. Kim, L.N. Lipatov, R. Peschanski, G. Pivovarov, C. Royon, in progress.

# BFKL Monte Carlo for Dijet Production at Hadron Colliders

Lynne H. Orr<sup>a</sup> and W.J. Stirling<sup>b</sup>

<sup>a</sup>Department of Physics and Astronomy, University of Rochester  
Rochester NY 14627-0171

<sup>b</sup>Departments of Physics and Mathematical Sciences, University of Durham,  
Durham DH1 3LE, UK

The production of jet pairs at large rapidity difference at hadron colliders is potentially sensitive to BFKL physics. We present the results of a BFKL Monte Carlo calculation of dijets at the Tevatron. The Monte Carlo incorporates kinematic effects that are absent in analytic BFKL calculations; these effects significantly modify the behavior of dijet cross sections.

## 1. MONTE CARLO APPROACH TO BFKL

Fixed-order QCD perturbation theory fails in some asymptotic regimes where large logarithms multiply the coupling constant. In those regimes resummation of the perturbation series to all orders is necessary to describe many high-energy processes. The Balitsky-Fadin-Kuraev-Lipatov (BFKL) equation [1] performs such a resummation for virtual and real soft gluon emissions in such processes as dijet production at large rapidity difference in hadron-hadron collisions. BFKL resummation gives [2] a subprocess cross section that increases with rapidity difference as  $\hat{\sigma} \sim \exp(\lambda\Delta)$ , where  $\Delta$  is the rapidity difference of the two jets with comparable transverse momenta  $p_{T1}$  and  $p_{T2}$ .

Experimental studies of these processes have recently begun at the Tevatron  $p\bar{p}$  and HERA  $ep$  colliders. Tests so far have been inconclusive; the data tend to lie between fixed-order QCD and analytic BFKL predictions. However the applicability of analytic BFKL solutions is limited by the fact that they implicitly contain integrations over arbitrary numbers of emitted gluons with arbitrarily large transverse momentum: there are no kinematic constraints included. Furthermore, the implicit sum over emitted gluons leaves only leading-order kinematics, including only the momenta of the ‘external’ particles. The absence of kinematic constraints and energy-momentum conservation cannot, of course, be reproduced in experiments. While the effects of such constraints are in principle sub-leading, in fact they can be substantial and should be included in predictions to be compared with experimental results.

The solution is to unfold the implicit sum over gluons and to implement the result in a Monte Carlo event generator [3,4]. This is achieved as follows. The BFKL equation contains separate integrals over real and virtual emitted gluons. We can reorganize the equation by combining the ‘unresolved’ real emissions — those with

transverse momenta below some minimum value (chosen to be small compared to the momentum threshold for measured jets) — with the virtual emissions. Schematically, we have

$$\int_{virtual} + \int_{real} = \int_{virtual+real,unres.} + \int_{real,res.} \quad (1)$$

We perform the integration over virtual and unresolved real emissions analytically. The integral containing the resolvable real emissions is left explicit.

We then solve by iteration, and we obtain a differential cross section that contains a sum over emitted gluons along with the appropriate phase space factors. In addition, we obtain an overall form factor due to virtual and unresolved emissions. The subprocess cross section is

$$d\hat{\sigma} = d\hat{\sigma}_0 \times \sum_{n \geq 0} f_n \quad (2)$$

where  $f_n$  is the iterated solution for  $n$  real gluons emitted and contains the overall form factor. It is then straightforward to implement the result in a Monte Carlo event generator. Because emitted real (resolved) gluons appear explicitly, conservation of momentum and energy, as well as evaluation of parton distributions, is based on exact kinematics for each event. In addition, we include the running of the strong coupling constant. See [3] for further details.

## 2. DIJET PRODUCTION AT HADRON COLLIDERS

At hadron colliders, the BFKL increase in the dijet subprocess cross section with rapidity difference  $\Delta$  is unfortunately washed out by the falling parton distribution functions (pdfs). As a result, the BFKL prediction for the total cross section is simply a less steep falloff than obtained in fixed-order QCD, and tests of this prediction are sensitive to pdf uncertainties. A

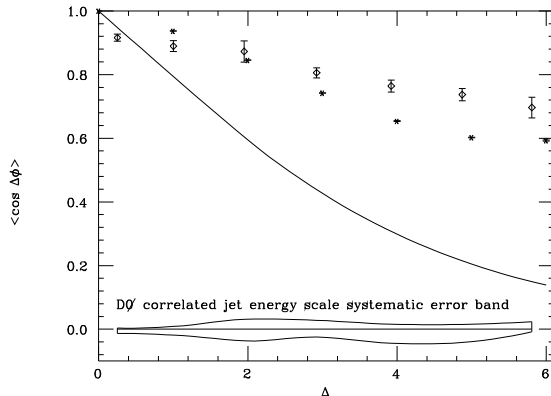


Figure 1. The azimuthal angle decorrelation in dijet production at the Tevatron as a function of dijet rapidity difference  $\Delta$ , for jet transverse momentum  $p_T > 20$  GeV. The analytic BFKL solution is shown as a solid curve and a preliminary  $D\phi$  measurement [6] is shown as diamonds. Error bars represent statistical and uncorrelated systematic errors; correlated jet energy scale systematics are shown as an error band.

more robust prediction is obtained by noting that the emitted gluons give rise to a decorrelation in azimuth between the two leading jets.[5,3] This decorrelation becomes stronger as  $\Delta$  increases and more gluons are emitted. In lowest order in QCD, in contrast, the jets are back-to-back in azimuth and the (subprocess) cross section is constant, independent of  $\Delta$ .

This azimuthal decorrelation is illustrated in Figure 1 for dijet production at the Tevatron  $p\bar{p}$  collider [3], with center of mass energy 1.8 TeV and jet transverse momentum  $p_T > 20$  GeV. The azimuthal angle difference  $\Delta\phi$  is defined such that  $\cos \Delta\phi = 1$  for back-to-back jets. The solid line shows the analytic BFKL prediction. The BFKL Monte Carlo prediction is shown as crosses. We see that the kinematic constraints result in a weaker decorrelation due to suppression of emitted gluons, and we obtain improved agreement with preliminary measurements by the  $D\phi$  collaboration [6], shown as diamonds in the figure.

In addition to studying the azimuthal decorrelation, one can look for the BFKL rise in dijet cross section with rapidity difference by considering ratios of cross sections at different center of mass energies at fixed  $\Delta$ . The idea is to cancel the pdf dependence, leaving the pure BFKL effect. This turns out to be rather tricky [8], because the desired cancellations occur only

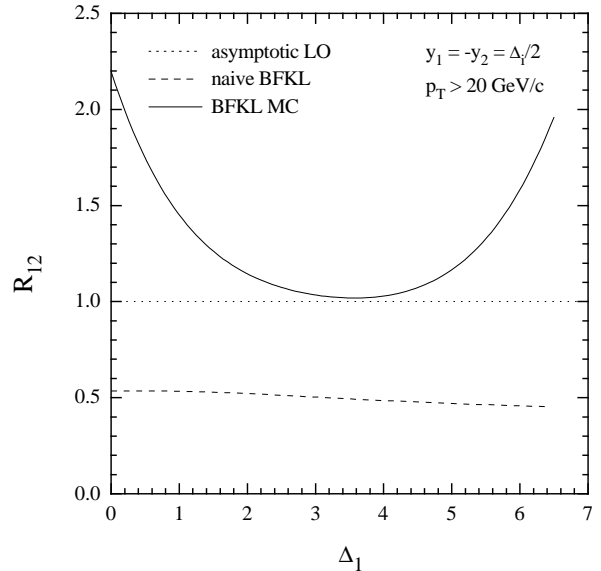


Figure 2. The ratio  $R_{12}$  of the dijet cross sections at the two collider energies  $\sqrt{s_1} = 630$  GeV and  $\sqrt{s_2} = 1800$  GeV, as defined in the text. The curves are: (i) the BFKL MC predictions (solid curve), (ii) the ‘naive’ BFKL prediction (dashed curve), and (iii) the asymptotic QCD leading-order prediction (dotted curve)  $R_{12} = 1$ .

at lowest order. Therefore we consider the ratio

$$R_{12} = \frac{d\sigma(\sqrt{s_1}, \Delta_1)}{d\sigma(\sqrt{s_2}, \Delta_2)} \quad (3)$$

with  $\Delta_2$  defined such that  $R_{12} = 1$  in QCD lowest-order. The result is shown in Figure 2, and we see that the kinematic constraints strongly affect the predicted behavior, not only quantitatively but sometimes qualitatively as well. More details can be found in [8].

### 3. CONCLUSIONS

In summary, we have developed a BFKL Monte Carlo event generator that allows us to include the subleading effects such as kinematic constraints and running of  $\alpha_s$ . We have applied this Monte Carlo to dijet production at large rapidity separation at the Tevatron. We found that kinematic constraints, though nominally subleading, can be very important. In particular they lead to suppression of gluon emission, which in turn suppresses some of the behavior that is considered to be characteristic of BFKL physics. It is clear therefore that reliable BFKL tests can only be performed using predictions that incorporate kinematic constraints.

## REFERENCES

1. L.N. Lipatov, Sov. J. Nucl. Phys. **23** (1976) 338; E.A. Kuraev, L.N. Lipatov and V.S. Fadin, Sov. Phys. JETP **45** (1977) 199; Ya.Ya. Balitsky and L.N. Lipatov, Sov. J. Nucl. Phys. **28** (1978) 822.
2. A.H. Mueller and H. Navelet, Nucl. Phys. **B282** (1987) 727.
3. L.H. Orr and W.J. Stirling, Phys. Rev. **D56** (1997) 5875.
4. C.R. Schmidt, Phys. Rev. Lett. **78** (1997) 4531.
5. V. Del Duca and C.R. Schmidt, Phys. Rev. **D49** (1994) 4510; W.J. Stirling, Nucl. Phys. **B423** (1994) 56; V. Del Duca and C.R. Schmidt, Phys. Rev. **D51** (1995) 215; V. Del Duca and C.R. Schmidt, Nucl. Phys. Proc. Suppl. **39BC** (1995) 137; preprint DESY 94-163 (1994), presented at the 6th Rencontres de Blois, Blois, France, June 1994.
6. D $\emptyset$  Collaboration: S. Abachi *et al.*, Phys. Rev. Lett. **77** (1996) 595; D $\emptyset$  Collaboration: presented by Soon Yung Jun at the Hadron Collider Physics XII Conference, Stony Brook, June 1997.
7. L.H. Orr and W.J. Stirling, Phys. Lett. **B436** (1998) 372.
8. L.H. Orr and W.J. Stirling, Phys. Lett. **B429** (1998) 135.

# Run 2 Plans for Hard Diffraction Studies in CDF

K. GOULIANOS, The Rockefeller University, 1230 York Avenue, New York, NY 10021, USA.

We summarize briefly the CDF proposal for “Further Studies in Hard Diffraction and Very Forward Physics with CDF in Run II” and discuss the present status of the proposed detectors.

A program has been proposed for studies of hard diffraction and very forward physics with CDF in Run 2, which requires adding to CDF three detector components (see Fig. 1):

**1) A Roman Pot Spectrometer (RPS)** to detect leading antiprotons.

**2) Two MiniPlug (MP)** calorimeters covering the pseudorapidity region  $3.5 < |\eta| < 5.5$  to detect particles and jets and measure their energies.

**3) A set of Beam Shower Counters (BSC)** positioned around the beam pipe at four (three) locations along the  $\bar{p}$  ( $p$ ) beam direction to tag rapidity gaps within  $5.5 < |\eta| < 7.5$ .

**The Roman Pot Spectrometer** will be the one used in Run 1C. It consists of  $X$ - $Y$  scintillation fiber detectors placed in three Roman Pots located at a distance of 57 m downstream in the  $\bar{p}$  direction. The detectors have a position resolution of  $\pm 100 \mu\text{m}$ , which makes possible a  $\sim 0.1\%$  measurement of the  $\bar{p}$  momentum. In Run 1C, the  $\bar{p}$ -beam was behind the proton beam, as viewed from the RPS side. An inverted polarity (with respect to Run I) of the electrostatic beam separators will enable us to move the RPS detectors closer to the  $\bar{p}$ -beam and thereby gain acceptance at small  $|t|$  down to  $\xi \equiv 1 - x_F(\bar{p}) = 0.03$  (at larger  $|t|$  lower  $\xi$  values can be reached with good acceptance).

**The MiniPlugs** will be placed within the holes of the muon toroids (see Fig. 2). They consist of layers of lead plates immersed in liquid scintillator (Fig. 3). The signal is guided by 1 mm dia. WLS fibers strung through holes in the plates, as shown, to be read out by multi-channel PMT's. The “tower” structure, defined by the way the fibers are grouped to be read out, is shown in Fig. 4. A full depth ( $\sim 30rl$ ) Mini-Plug prototype has been constructed and tested in high energy muon, electron and pion beams with excellent results [1,2]. As of December 1999, the final Miniplug design has been completed, the vessels and all mechanical parts have been fabricated, a prototype lead plate of the final design (laminated with reflective aluminum) has been procured, and several Hamamatsu R5900-M16 PMT's have been acquisitioned and tested.

**Beam Shower counters** are rings of scintillation counters “hugging” the beam pipe. In stations #1 the

rings are segmented into four quadrants, and in the other stations into two. As of December 1999, all 18 counters are ready for installation.

The physics topics to be addressed include:

### Hard single diffraction

$W$ ,  $b$ ,  $J/\psi$  and dijet production; dependence of the cross section on  $\xi$  and  $t$ ; third-jet activity in jet production; extraction of the pomeron structure function.

### Soft and hard double diffraction

(central rapidity gaps)

Dependence of cross section of dijet events with a rapidity gap between jets on jet  $E_T$  and jet  $\eta$  separation and comparison with predictions from BFKL and other models; measurement of the differential soft double diffraction cross section and comparison with phenomenological predictions; relationship between gap fractions in minimum bias and dijet events.

### Double pomeron exchange (DPE)

Measurement of dijet cross section in events with a DPE topology (pomeron-pomeron collisions); extraction of the diffractive proton structure function from DPE dijet events and comparison with the diffractive antiproton structure measured in single diffraction (test of factorization); measurement of soft DPE cross section (test of soft factorization); connection between soft and hard diffractive processes; opportunities for new physics in exclusive DPE channels.

### Small- $x$ /large- $x$ physics:

Measurement of proton parton distribution functions in the range  $4 \times 10^{-5} < x < 0.8$ ;  $x_{max}$  can be measured as a function of the  $E_T$  scale down to  $E_T$  of 5 GeV.

### Centauros and Disoriented Chiral Condensates

The signature for Centauros/ $D\chi$ Cs is multiparticle clusters of large  $dN/d\eta$  with abnormal charge to neutral ratios.

## REFERENCES

1. S. Bagdasarov, K. Goulios, A. Maghakian and Q. Wang, *Test-beam results of a prototype position sensitive towerless calorimeter*, Nucl. Instrum. Meth. **A 372** (1995) 117-124.
2. K. Goulios and S. Lami, *Performance of a prototype position sensitive towerless calorimeter*, Nucl. Instrum. Meth. **A 430** (1999) 34-47.

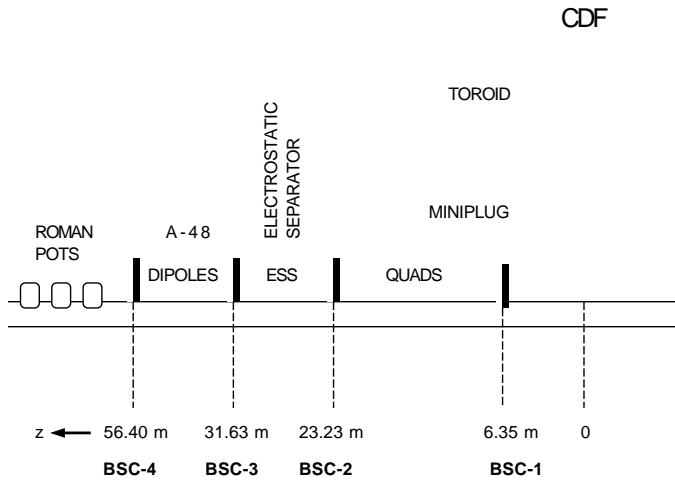


Figure 1. Location of the Beam Shower Counter stations along the  $\bar{p}$  direction on the West side of CDF (not to scale). On the East side only the first three BSC stations will be installed, as there is no room for BSC-4.

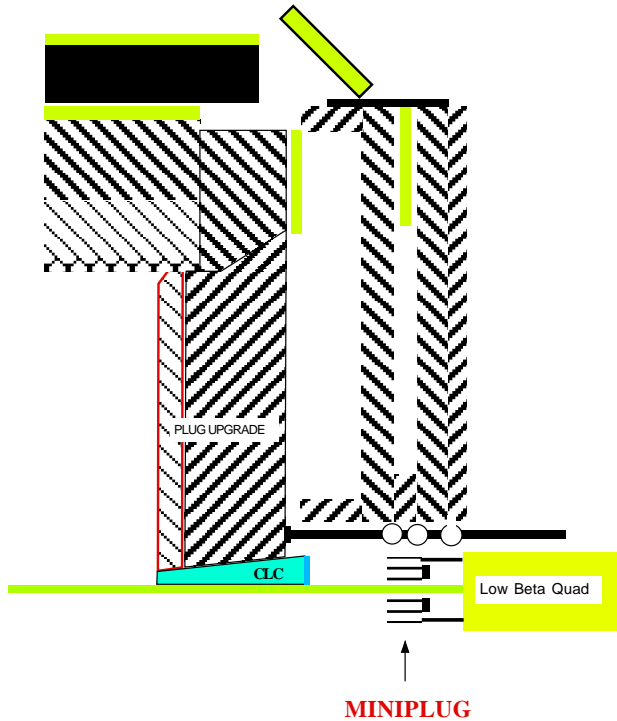


Figure 2. Schematic drawing showing a MiniPlug hanging from two beams supported on one end by the plug and on the other by the toroid (not to scale). This scheme allows for moving the toroids and/or the plug while the MiniPlug remains stationary.

### MINIPLUG SIDE VIEW (not to scale)

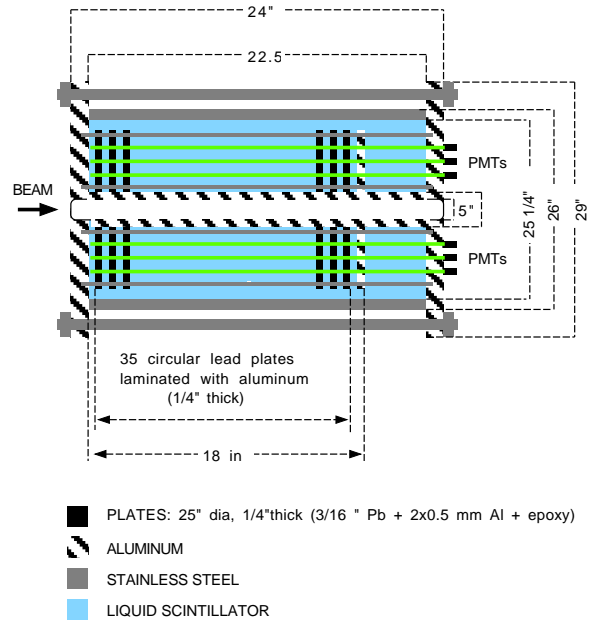


Figure 3. Schematic side view of a Miniplug.

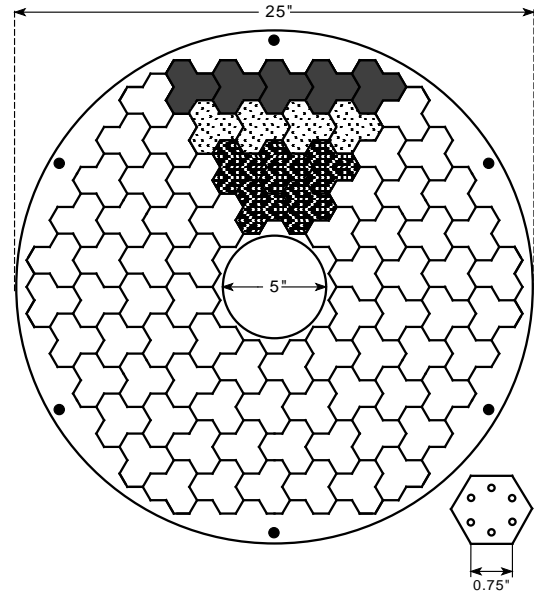


Figure 4. Proposed MiniPlug lead plate. The design is based on a hexagon geometry. Each hexagon has six holes, with a WLS fiber inserted in each hole. The six fibers of a hexagon are grouped together and are viewed by one MCPMT channel. There are 252 hexagons in each MiniPlug viewed by 18 16-channel MCPMTs. The MCPMT outputs are added in groups of 3 to form 84 calorimeter “towers”.

# The DØ Forward Proton Detector

Andrew Brandt (DØ Collaboration)<sup>a</sup>

<sup>a</sup>University of Texas at Arlington, P.O. Box 19059, Arlington, TX 76019

The Run II DØ Forward Proton Detector is described.

## 1. Hard Diffraction

One of the most interesting new results from Tevatron Run I was the existence of large rapidity gaps in events with a hard scattering. CDF and DØ published several papers on events with a central rapidity gap between jets [1,2] and have several more papers either published or in preparation on related topics, including diffractive production of jets [3,4],  $W$  and  $Z$  bosons [5,6], and  $b$  quarks [7]. Improved understanding of the new field of hard diffraction, which probes otherwise inaccessible details of the strong force and vacuum excitation, requires new detectors for tagging and measuring scattered protons.

## 2. The Forward Proton Detector

The DØ Forward Proton Detector (FPD) [8] consists of momentum spectrometers which make use of accelerator magnets along with points measured on the track of the scattered proton to calculate the proton's momentum and scattering angle. Tracks are measured using scintillating fiber detectors (a prototype detector is shown in Fig. 1) located in vacuum chambers positioned in the Tevatron tunnel 20–60 meters upstream and downstream of the central DØ detector. The vacuum chambers were built in Brazil and will be installed in the Tevatron in August 2000. One of the completed Roman pot castles is shown in Figure 2. The scintillating fiber detectors will be assembled at the University of Texas at Arlington.

Figure 3 shows the layout of the FPD. In the center of the diagram is the DØ detector (not to scale). The dipole spectrometer consists of two scintillating fiber detectors located after the Tevatron dipole magnets (D) about 57 meters downstream of the interaction point on the outgoing  $\bar{p}$  arm, and measures anti-protons that have lost a few per cent of the beam momentum (and are thus deflected out of the beam envelope and into the detector located on the radial inside of the Tevatron ring). The detectors comprising the quadrupole spectrometers are located adjacent to the electrostatic beam separators (S) on both the proton (P) and anti-proton (A) sides and use the low beta quadrupole magnets (Q) as the primary analyzing



Figure 1. A photograph of the prototype scintillating fiber detector.

magnets. They have acceptance for a large range of proton (anti-proton) momenta and angles.

Each of the nine independent spectrometers consists of a pair of detectors, both in the same plane: above, below, to the right, or to the left of the beam. This combination of spectrometers maximizes the acceptance for protons and anti-protons given the available space for locating the detectors. Particles traverse thin steel windows at the entrance and exit of each Roman pot (the stainless steel vessel that houses the detector). The pots are remotely controlled and can be moved close to the beam (within a few mm) during stable beam conditions and retracted otherwise. The scintillating fiber detectors are read out by multi-anode photomultiplier tubes and are incorporated into the standard DØ triggering and data acquisition system.

The FPD project has proceeded well and is expected to be ready for the start of Run II, although final funding for the phototubes and trigger electronics has not yet been secured. The FPD will allow new insight into an intriguing class of events that are not currently understood within the Standard Model. It allows us

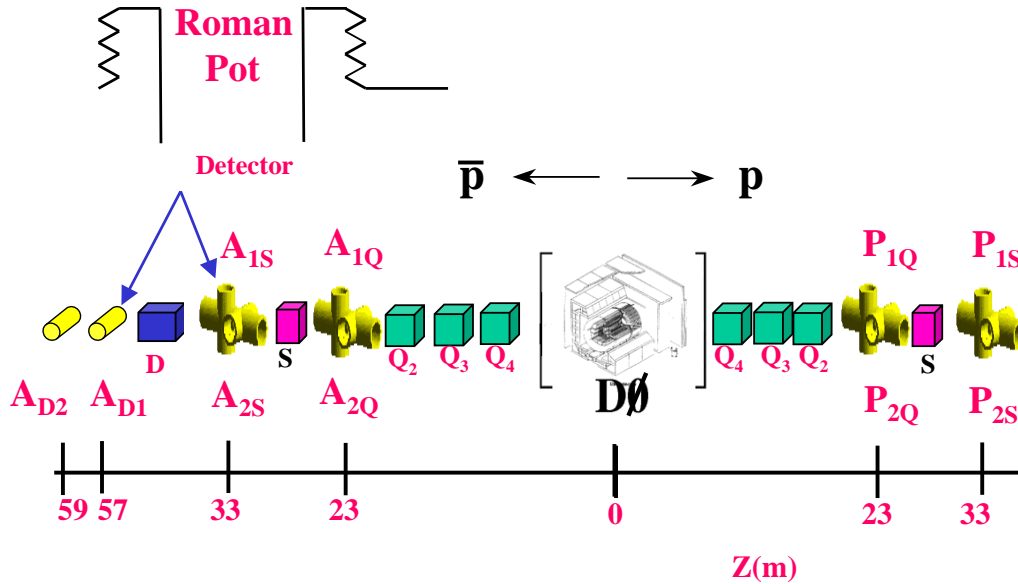


Figure 3. The layout of the Roman pot stations and Tevatron components comprising the Forward Proton Detector as described in the text (not drawn to scale).



Figure 2. A completed Roman pot castle at Fermilab along with project leaders Alberto Santoro (left) and Andrew Brandt.

to trigger directly on events with a scattered proton, anti-proton, or both, along with activity in the DØ detector. In addition to improved studies of recently discovered hard diffractive processes, the new detector will allow a search for glueballs and exotic phenomena. The FPD will also provide improved luminosity measurements, which are an important component to all DØ analyses.

## REFERENCES

1. S. Abachi *et al.* (DØ Collaboration), Phys. Rev. Lett. **72**, 2332 (1994); Phys. Rev. Lett. **76**, 734 (1996); B. Abbott *et al.* (DØ Collaboration), Phys. Lett. B **440** 189 (1998).
2. F. Abe *et al.* (CDF Collaboration), Phys. Rev. Lett. **74**, 855 (1995); Phys. Rev. Lett. **80**, 1156 (1998); Phys. Rev. Lett. **81**, 5278 (1998).
3. F. Abe *et al.* (CDF Collaboration), Phys. Rev. Lett. **79**, 2636 (1997); K. Hatakeyama (CDF Collaboration), *Proceedings of the XXXVth Rencontres de Moriond* (2000).
4. B. Abbott *et al.* (DØ Collaboration), Hep-ex 9912061, Submitted to Phys. Rev. Lett.
5. F. Abe *et al.* (CDF Collaboration), Phys. Rev. Lett. **78**, 2698 (1997).
6. L. Coney (DØ Collaboration), “Observation of Diffractive  $W$  Boson Production at DØ,” APS Meeting, Atlanta, Georgia, March 1999.
7. T. Affolder *et al.* (CDF Collaboration), Phys. Rev. Lett. **84**, 232 (2000).
8. DØ Collaboration, “Proposal for a Forward Proton Detector at DØ” (presented by A. Brandt to the Fermilab PAC, 1997); A. Brandt *et al.*, Fermilab PUB-97-377.